



Michael Runda, BSc

**Characterization and optimization of light-driven whole-cell  
hydroxylations catalyzed by Rieske non-heme iron  
oxygenases**

**MASTER'S THESIS**

to achieve the university degree of

Diplom-Ingenieur

Master's degree programme: Biotechnology

submitted to

**Graz University of Technology**

Supervisor

Dr. Sandy Schmidt

Prof. Dr. Robert Kourist

Institute for Molecular Biotechnology

Graz, October 2019

# Eidesstattliche Erklärung

Ich erkläre an Eides statt, dass ich die vorliegende Arbeit selbstständig verfasst, andere als die angegebenen Quellen/Hilfsmittel nicht benutzt, und die den benutzten Quellen wörtlich und inhaltlich entnommenen Stellen als solche kenntlich gemacht habe.

Graz, 04.08.2019

---

Unterschrift

# Acknowledgments

At this point, I would first like to thank Prof. Dr. Robert Kourist for giving me the opportunity to gain valuable insights into scientific research and to gather essential experience and knowledge which I consider very useful for my professional as well as personal future.

I wish to express my sincere appreciation to my thesis advisors Dr. Sandy Schmidt for agreeing to take me as one of her master students. Her comprehensive knowledge and professional support during the work on this thesis was a personal enrichment for my ongoing scientific carrier.

Furthermore, I would like to thank my colleagues of Prof. Dr. Kourist's working group, who made everyday work even more enjoyable and always had a sympathetic ear for me. Special thanks to Hanna Büchenschütz, Anna Schwaiger and Ivana Drienovska for their scientific advice and valuable feedback, which were an enormous help during the work on my thesis. I would also like to express my gratitude to Feyza Özgen and Peter Wied. Without their persistent help and guidance, this thesis would not have materialized.

Special thanks also to Clemens Farnleitner, Maria Schabhüttl and Simone Scharl, who have ensured smooth working conditions in the lab.

I would also like to thank the members of the master student "self-support" group: Kristin Bauer, Stefanie Hanreich, Andrea Nigl and Magdalena Wessely.

Last but not least, I would like to thank my parents, my sister and my girlfriend, who have always believed in my competences during my university carrier and for their as well mental as financial encouragement.

# Abstract

The demand for reliable strategies to utilize alternative and renewable energy sources gained increasing attention over the last few decades to overcome the dependency on depleting fossil fuels. Especially, the cost-effective transformation of abundant solar energy into accessible products is of great importance for a sustainable society. While considerable advances have been made to convert light energy into electrical energy by the use of photovoltaic cells, the rational and cost-efficient transformation of solar energy into chemical energy is still a major challenge in organic synthesis. However, recent developments in the field of photo-biocatalysis resulted in promising approaches towards the implementation of light-driven enzyme-catalyzed reactions exploiting the excitability of photoactive molecules induced by light irradiation. In particular, the implementation of light-driven systems for oxidoreductases is of great interest due to their broad reaction spectra. In the last few years, the focus has been especially on Rieske non-heme iron oxygenases (ROs) due to their ability to regio- and stereoselective oxidize olefins, thus having a great potential in organic syntheses. However, their applicability is hampered by their dependency on NAD(P)H, as well as their multicomponent nature and intrinsic instability in cell-free systems. Previous studies revealed the feasibility of a new light-driven whole-cell approach termed as artificial photosynthesis whereby alternative inorganic electron donors are able to shuttle electrons via different photosensitizers to the active site of the ROs. The aim of this thesis is a deeper characterization of the proposed light-driven whole-cell approach by extending the substrate, electron donor, and photosensitizer scope. Furthermore, the optimization of the system was tackled by varying catalyst concentrations and reaction conditions as well as by applying different RO variants to increase selectivity, activity, and product formation. Herein, an enhanced functionality of the described light-driven whole-cell approach could be verified by the use of rose bengal (RB) as photosensitizer and MOPS buffer as electron donor yielding in 89 % conversion.

# Zusammenfassung

Die Nachfrage nach effizienten Strategien zur Nutzung alternativer und erneuerbarer Energiequellen um den massiven Gebrauch von fossilen Brennstoffen entgegenzuwirken, hat in den letzten Jahrzehnten an großer Bedeutung gewonnen. Insbesondere die rentable Umwandlung von Sonnenenergie in nutzbare Produkte ist für eine nachhaltige Gesellschaft von großer Bedeutung. Während bei der Transformation von Lichtenergie in elektrische Energie durch die Verwendung von Photovoltaikzellen bereits große Fortschritte erzielt werden konnten, ist die gezielte und kostengünstige Umwandlung von Sonnenenergie in chemische Energie in Form von nützlichen Produkten nach wie vor eine große Herausforderung. Die jüngsten Entwicklungen auf dem Gebiet der Photobiokatalyse zeigten bereits vielversprechende Ansätze zur Realisierung lichtgetriebener, enzymkatalysierter Reaktionen. Insbesondere die Implementierung von lichtgetriebenen Systemen für Oxidoreduktasen ist aufgrund ihrer breiten Reaktionsspektren von großem Interesse. Rieske-Nicht-Häm-Eisenoxxygenasen (ROs) haben in den letzten Jahren aufgrund ihrer Fähigkeit zur regio- und stereoselektiven Oxidation von Olefinen zunehmend an Bedeutung gewonnen und besitzen daher ein großes Potenzial für organische Synthesen. Ihre Anwendbarkeit wird jedoch durch ihre Abhängigkeit von NAD(P)H sowie ihre Mehrkomponentennatur und der damit verbundenen Instabilität in *in vitro* Systemen beeinträchtigt. Studien haben jedoch gezeigt, dass mittels künstlicher Photosynthese in nicht autotrophen organismen elektronen von von einem geeigneten Elektronendonator über verschiedene Photosensitizer zum aktiven Zentrum der ROs transportieren können welche die inkooperation von Sauerstoff in gewünschte Substrate ermöglichen. Das Ziel dieser Arbeit ist eine tiefere Charakterisierung des vorgeschlagenen lichtgetriebenen Ganzzellansatzes durch das Testen verschiedener Substrate, Elektronendonoren und Photosensibilisatoren. Außerdem, wird die Optimierung des Systems durch Variation der Zelldichte und Reaktionsbedingungen sowie durch Anwendung verschiedener RO-Varianten angestrebt. In der vorliegenden Studie konnte eine verbesserte Funktionalität des beschriebenen lichtgetriebenen Ganzzellansatzes durch die Verwendung von Rose Bengal (RB) als Photosensibilisator und MOPS-Puffer als Elektronendonator gezeigt werden, was zu einem maximalen Substratumsatz von 89% führte.

# Table of contents

Eidesstattliche Erklärung .....	II
Acknowledgments.....	III
Abstract.....	IV
Zusammenfassung .....	V
Table of contents .....	VI
List of abbreviations.....	VIII
1 Introduction .....	1
1.1 Oxidoreductases in biocatalysis.....	1
1.2 Rieske non-heme iron-dependent oxygenases (ROs).....	3
1.3 Natural NAD(P) <sup>+</sup> recycling systems .....	8
1.4 Nicotinamide cofactor regeneration for biocatalytic applications.....	9
1.5 Photo-biocatalysis.....	11
1.6 Thesis aims.....	17
2 Material and Methods .....	19
2.1 Devices & Chemicals .....	19
2.1.1 Incubation devices .....	19
2.1.2 Centrifuge for cell harvesting .....	19
2.1.3 Freeze-drying equipment.....	19
2.1.4 Reactor for light-driven whole-cell biotransformations.....	19
2.1.5 Device for DNA amplification.....	21
2.1.6 Analytic instruments (quantitative).....	21
2.1.7 Analytic instruments (qualitative) .....	22
2.1.8 Chemicals for cultivation and expression .....	22
2.1.9 Agents for long-time storage of cell cultures .....	25
2.1.10 Chemicals for whole-cell biotransformations.....	25
2.1.11 Chemicals used for agarose gel electrophoresis .....	28
2.1.12 Agents used for SDS-PAGE .....	29
2.1.13 Organic solvents used for GC sample preparation .....	30
2.2 Microbiological Methods .....	30
2.2.1 Host strains .....	30
2.2.2 Overnight cultures .....	31
2.2.3 Preparation of glycerol stocks .....	31
2.3 Molecular Biological Methods .....	32
2.3.1 DNA sequencing.....	32
2.3.2 Plasmid constructs .....	32
2.3.3 Preparation of chemo-competent <i>E. coli</i> cells.....	34
2.3.4 Chemical transformation (heat shock method).....	35
2.3.5 Plasmid isolation .....	35
2.3.6 Agarose gel electrophoresis.....	36
2.3.7 Gel extraction.....	36
2.4 Biochemical Methods .....	36
2.4.1 Heterologous protein expression .....	36

2.4.2	Protein extraction .....	37
2.4.3	Protein separation via SDS-PAGE.....	37
2.4.4	Harvesting of <i>E. coli</i> cells.....	38
2.4.5	Light-driven biotransformations.....	38
2.4.6	Growth experiments .....	39
2.4.7	Qualitative enzyme activity assay.....	39
2.5	Biophysical Methods.....	40
2.5.1	Lyophilization of resting cell cultures .....	40
2.6	Analytics.....	40
2.6.1	GC sample preparation .....	40
2.6.2	Quantification of compounds of ( <i>R</i> )-(+)-limonene conversion via GC-FID.....	41
2.6.3	Quantification of compounds of indene conversion via GC-MS .....	44
2.6.4	Quantification of compounds of indene conversion via GC-FID and GC-MS .....	45
2.6.5	Quantification of products of toluene via GC-FID .....	49
3	Results.....	51
3.1	Expression studies with CDO M232A and NDO H295A .....	51
3.2	Light-driven whole-cell biotransformation experiments.....	54
3.2.1	Absorbance spectra of photosensitizers .....	54
3.2.2	Influence of electron donor on product formation .....	55
3.2.3	The effect of cell lyophilization on product formation.....	56
3.2.4	Products obtained in light-driven hydroxylation of ( <i>R</i> )-(+)-limonene.....	58
3.2.5	Choice of substrate for biotransformation with CDO M232A and NDO H295A .....	59
3.2.6	Effect of biocatalyst concentration on product formations .....	60
3.2.7	Byproduct formation observed in light-driven hydroxylation of indene .....	62
3.2.8	Effect of light intensity on biotransformations of indene .....	66
3.2.9	Photochemical background reactions .....	67
3.2.10	Time courses of product formation in light-driven whole-cell biotransformations of indene .....	68
3.2.11	Selectivities of ROs in light-driven biotransformations of indene.....	71
3.2.12	Effect of photosensitizer concentration on product formation during light-driven whole-cell biotransformations.....	73
3.2.13	Growth behavior of <i>E. coli</i> in the presence of substrates used for light-driven whole-cell biotransformations.....	74
3.2.14	Effect of light and PS on the light-driven biotransformations.....	77
4	Discussion .....	80
4.1	Experimental setup for <i>in vivo</i> biotransformations.....	82
4.2	Heterologous expression of CDO M232A and NDO H295A in <i>E. coli</i> .....	88
5	Conclusion.....	89
6	References .....	92
7	Appendices.....	99
	Appendix A.....	99
	Appendix B.....	100
	Appendix C.....	101
	Appendix D.....	103
	Appendix E .....	105

## List of abbreviations

ADH	alcohol dehydrogenase
Amp	ampicillin
AmpR	ampicillin resistance gene
ATP	adenosine triphosphate
CDO	cumene dioxygenase
CE	5(6)-carboxyeosin
<i>de</i>	diastereomeric excess
DNA	deoxyribonucleic acid
ECN	effective carbon number
EDTA	ethylenediaminetetraacetic acid
<i>ee</i>	enantiomeric excess
EtBr	ethidium bromide
EY	eosin Y
Fd	ferredoxin
FdR	ferredoxin reductase
FMN	flavin mononucleotide
G6P	glucose-6-phosphate
GC-FID	gas chromatography with flame ionization detector
GC-MS	gas chromatography–mass spectrometry
LED	light-emitting diode
LPS	lipopolysaccharide
MES	2-( <i>N</i> -morpholino)ethanesulfonic acid
MOPS	3-( <i>N</i> -morpholino)propanesulfonic acid
MV	methyl viologen
NAD(P)H	nicotinamide adenine dinucleotide (phosphate)
NDO	naphthalene dioxygenase
O <sub>2</sub>	molecular oxygen
OM	outer membrane
PS	photosystem
PSs	photosensitizers
RB	rose bengal
RB	rose bengal
ROs	Rieske oxygenases
ROS	reactive oxygen species
SO	safranin O
TEOA	triethanolamine
TfB	transformation buffer
TiO <sub>2</sub>	titanium dioxide
TTN	total turnover number



# 1 Introduction

## 1.1 Oxidoreductases in biocatalysis

The demand for economic and sustainable processes in organic synthesis by the use of biocatalysts has received much attention over the past few decades.[1, 2] Especially the possibility of protein engineering by directed evolution or rational design contributes to an enhanced versatility of recombinant enzymes or microorganisms in biocatalytic applications.[3] Besides their potential of facilitating highly regio-, chemo- and enantioselective reactions under relatively mild conditions, the unnecessary of additional protection and deprotection steps, often required in abiotic organic synthesis, is of peculiar interest.[4] Nowadays, enzyme applications are utilized in the production of fine or bulk chemicals in the textile or food industry as well in the production of pharmaceutical drugs.[2] The enzymatic hydration of acrylonitrile into acrylamide is a well-known example of supplanting a conventional process by the use of nitrile hydratase (EC 4.2.1.84). Due to that, environmental pollution issues caused by the application of high temperatures and the use of copper (Cu) catalysts in the presence of sulfuric acid required in the traditional process can be significantly reduced. This “greener” industrial process contributes to the production of more than 650,000 tons of polyacrylamide monomers per year.[2, 5] The commercial production of sitagliptin (*Januvia*, Merck Sharp & Dohme Ltd. UK), a marketed drug used for the treatment of type 2 diabetes, is another example of the successful practical application of biocatalysts in the pharmaceutical industry. Thereby, the use of an engineered (*R*)-selective transaminase (*Arthrobacter* sp.) yields in an improved conversion (10 %) of pro-sitagliptin ketone into the aminated sitagliptin product compared to the corresponding rhodium-catalyzed organic synthesis.[2] While earlier approaches were mainly restricted to cofactor-free enzyme classes like hydrolases (EC 3.), recent developments favor the implementation of more complex reactions by extending the scope of biocatalysts in industrial processes.[6, 7] Particularly, the efficient and economical use of oxidoreductases (EC 1.) is of high value for the ongoing advancement of industrial biotechnology.[8] This considerable class, comprising about 25 % of all enzymes,[9] catalyzing a range of selective redox reactions by facilitating the

transfer of hydrogen, oxygen, or electrons between oxidants and reductants.[10] By that, a wide array of industrial relevant transformations are feasible, like the oxidation of alcohols, amines, carbonyl compounds, and alkenes.[11] Moreover, the possibility of enzyme-catalyzed functionalization of inactivated C-H bonds is of particular importance in the field of organic synthesis.[11, 12] Corresponding to their catalytic reaction mechanism, oxidoreductases can be divided into reductases and oxidases. A well-known example for the successful industrial application of reductases is the synthesis of montelukast (*Singulair*, Merck Sharp & Dohme Ltd. UK), a drug used in asthma therapy.[2] By the use of an engineered keto-reductase (KRED) from *Lactobacillus kefir* facilitating an asymmetric reduction of a ketone intermediate, the need for the toxic chemical catalyst chlorodiisopinocampheylborane (DIP-Cl) is avoided. Furthermore, no expensive downstream product recovery compared to the former process is needed since the applied reaction conditions favor product crystallization. Today this “green” biocatalytic process is performed at large-scale (> 200kg) and has substituted the former abiotic strategy for the production of montelukast.[2] Oxygenases represent an exciting class of enzymes, which exhibit the capability of selective oxidation by incorporation of activated oxygen yielding in the formation of new hydroxy or carbonyl functionalized groups.[11] Due to the described ability of oxyfunctionalization of organic compounds, these enzymes are considered as promising biocatalysts for a variety of industrially relevant conversions. Dependent on the number of oxygen atoms assimilated by this mechanism, corresponding proteins are further classified either as monooxygenases (EC 1.14) or dioxygenases (EC 1.13).[11] The enzyme family of cytochrome P450 monooxygenases (CYPs) comprises a substantial number of heme-containing proteins that are involved in diverse anabolic and catabolic biochemical pathway reactions within all three domains of life. The membrane-bound CYPs show a preference for molecular oxygen (O<sub>2</sub>) as a terminal oxidant, which determines their catalytic functionality as monooxygenases. Thus, one oxygen atom of the reduced and thereby activated acceptor molecule is then selectively incorporated into a specific substrate while the other oxygen is getting reduced to H<sub>2</sub>O. The well-studied electron transfer is facilitated by a multi-component system which consists of a reductase that shuttles electrons from NAD(P)H either via an iron-sulfur protein or directly towards the Fe<sup>3+</sup> containing heme prosthetic group of the catalytic oxygenase component where the oxygen

activation and substrate oxidation takes place.[13, 14] By this mechanism, CYPs can facilitate various complex biotransformations. Especially, the challenging functionalization of unactivated C-H bonds is beneficial regarding the organic synthesis of valuable products.[11] However, the industrial usage of CYPs is still hampered by their multicomponent nature and relatively low total turnover numbers (TTNs) as a result of unspecific side reactions due to undirected electron transfers (uncoupling reactions).[11] Furthermore, the majority of oxidoreductases shows the need for expensive and relatively unstable nicotinamides (NAD(P)H/ NAD(P)<sup>+</sup>) or flavins (FADH<sub>2</sub>/FAD) as redox cofactors which is considered as unfavorable regarding their use in economic large-scale applications.[7] To avoid an unremunerative increase of overall process costs by providing these molecules in stoichiometric amounts, concepts of whole-cell biotransformation, or the use of purified enzymes in combination with artificial *in situ* regeneration strategies are proposed.[6, 9] Thus, an improved applicability of various oxidoreductases can be achieved, enhancing the scope of industrial relevant reactions.

### 1.2 Rieske non-heme iron-dependent oxygenases (ROs)

ROs are involved in the first step of the microbial degradation of aromatic compounds by catalyzing the oxidation of arenes resulting in non-aromatic *cis*-diol compounds.[15] Furthermore, ROs represent highly potential enzymes for industrial applications since they can catalyze the highly selective formation of vicinal *cis*-diols in one step, which is still a major challenge in organic synthesis.[16] Like in CYPs, electrons derived from a NAD(P)H cofactor are shuttled via the multicomponent system toward an oxygenase where O<sub>2</sub> functions as a terminal acceptor molecule. The activated O<sub>2</sub> is then incorporated into the desired substrate, yielding the hydroxylated product.[17] ROs can be divided into two- or three-component systems, based on the number of proteins interacting in the electron transfer chain. While the electrons in the two-component systems are transferred from a NAD(P)H donor via a flavin reductase and an RO ([2Fe-2S], Fe) to an O<sub>2</sub> molecule, the latter systems involve an additional ferredoxin (Fd) component [2Fe-2S] which facilitates the transfer between the reductase and the terminal oxygenase ([2Fe-2S], Fe).[18] As depicted in **Table 1**, further classification is based on the composition of the reductase. While cumene dioxygenase (CDO)

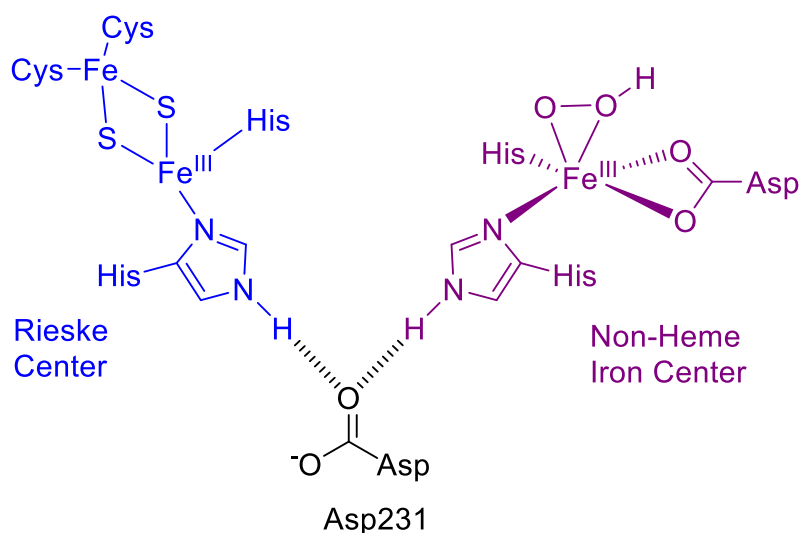
is denoted as a class IIB RO due to the presence of a FAD-dependent reductase and an Fd component, naphthalene dioxygenase (NDO) is assigned to class three due to an additional [2Fe-2S] cluster within the reductase component.

**Table 1: Characterization of several ROs based on the composition of the electron transport chain.[18]**

System	Class	Reductase	Ferredoxin	Oxygenase	Model Enzyme
2-component	IA	FMN, [2Fe-2S]	none	[2Fe-2S], Fe	Phtalate dioxygenase
	IB	FAD, [2Fe-2S]	none	[2Fe-2S], Fe	Benzoate dioxygenase
3-component	IIA	FAD	[2Fe-2S]	[2Fe-2S], Fe	Pyrazon dioxygenase
	IIB	FAD	[2Fe-2S]	[2Fe-2S], Fe	Cumene dioxygenase
	III	FAD, [2Fe-2S]	[2Fe-2S]	[2Fe-2S], Fe	Naphtalene dioxygenase

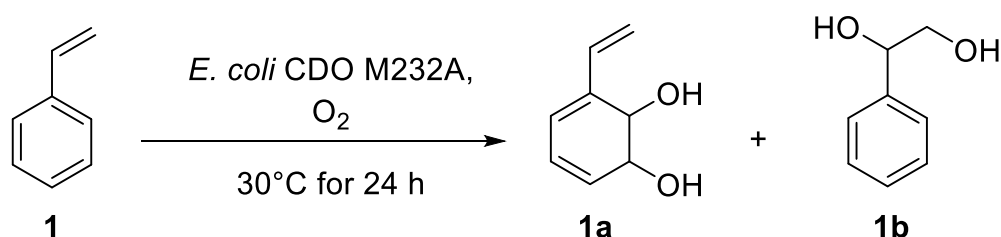
The CDO and NDO from *Pseudomonas fluorescens* IP01 or *Pseudomonas sp.* NCIB 9816-4, respectively, represents well-characterized ROs and are therefore commonly used as model enzymes for studying structure-function relationships of ROs.[18, 19] Structural analysis of the ferredoxin reductase (FdR) component in the CDO reveals the presence of an FAD moiety, which can be reduced in two steps to FADH<sub>2</sub> by the reductive cofactor NAD(P)H.[20] Since the reductase component of NDO harbors an additional iron-sulfur cluster [2Fe-2S], two other electron transfer steps are necessary. Consequently, two electrons enter the electron transport chain of the oxygenase system, which is defined as the initial step. Fd contains a Rieske-type iron-sulfur [2Fe-2S] cluster, which differs from other plant-type clusters in the arrangement of sulfur-containing amino acid residues in the iron-sulfur center. While the plant-type [2Fe-2S] clusters are coordinated by four cysteines, the Rieske-type iron-sulfur [2Fe-2S] clusters are coordinated by two cysteines and two histidines. Although two irons are present in one Rieske-center, only the histidine-coordinated iron shows the possibility for oxidation. Therefore, the ferric Fe(III) is reduced to ferrous Fe(II), while the other iron remains at the more stable Fe(III) form. Because of this, one Fd can store one electron provided by the FdR.[18] The terminal oxygenases of CDO and NDO shows a hetero-hexameric three-fold symmetric structure ( $\alpha_3\beta_3$ ) composed of either three large  $\alpha$ -subunits (CumA1) and three  $\beta$ -subunits (CumA2).[21, 22] While the  $\beta$ -moiety is supposed to affect the substrate specificity and stability of the entire multi-subunit complex, the  $\alpha$ -components are responsible for the catalytic activity of the enzyme.[18] The catalytic domain contains in total three Rieske-type iron-sulfur [2Fe-2S] clusters for electron storage and three mononuclear non-heme irons, which can activate O<sub>2</sub> due to reduction. The 3D-structural analysis revealed that the catalytic

site is located between two adjacent catalytic  $\alpha$ -subunits (**Scheme 1**). The electron provided by the Fd is shuttled to a Rieske cluster within one  $\alpha$ -subunit. Via a conserved aspartic acid residue termed as aspartate-bridge, the electron is transferred to the mononuclear iron of an adjacent  $\alpha$ -subunit where  $O_2$  activation and thus hydroxylation takes place.[17, 18]



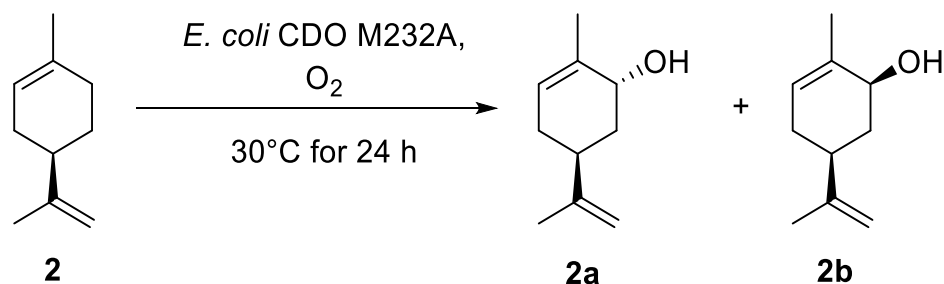
**Scheme 1: The Rieske and non-heme iron center within  $\alpha$ -subunits of CDO.** Electron transfer between the Rieske center (blue) and a non-heme iron center (purple) of two adjacent  $\alpha$ -subunits within the  $\alpha_3\beta_3$  oxygenase complex is mediated by an aspartate residual (Asp231). This aspartate bridge is coordinated by two histidines via hydrogen bonds. Oxygen activation takes place at the reduced non-heme iron center via electron transfer.[17]

A recent study by Gally *et al.* showed that an amino acid exchange at position 232 located in the active site of the catalytic  $\alpha$ -subunit (CumA1) resulted in an alteration of the chemo- and regioselectivity toward several olefin substrates. While the CDO wildtype (CDO WT) favors the dihydroxylation of the aromatic ring (**1a**) of styrene (**1**), the CDO variant M232A preferred hydroxylation at the vinyl group (**1b**) in whole-cell biotransformations (**Scheme 2**).[23]



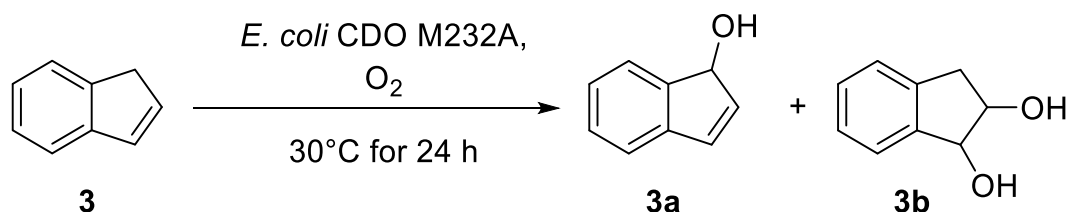
**Scheme 2: Styrene dihydroxylation catalyzed by CDO M232A.** Reaction conditions: 30 °C for 24 h, glucose 20 mM; catalyst: resting *E. coli* cells harboring overexpressed CDO M232A,  $\beta(\text{cells}) = 0.2 \text{ g}_{\text{WCW}} \text{ mL}^{-1}$ . 1: styrene, 1a: 3-vinyl-3,5-cyclohexadiene-1,2-diol, 1b: 1-phenyl-1,2-ethanediol; product formation: CDO-WT:  $71 \pm 6 \%$  (ratio: 0.3:99.7 1a:1b), CDO M232A:  $97 \pm 10 \%$  (ratio: 92:8 1a:1b).[23]

However, simultaneous experiments with (*R*)-limonene showed no alteration of the selectivity but an increase of enzyme activity. In contrast to the biotransformations with styrene (**1**), the variant CDO M232 catalyzed a monohydroxylation on the respective ring structure yielded in the formation of (1*R*,5*S*)-carveol (*ee* >98%) and (1*S*,5*S*)-carveol (**Scheme 3**).[23]



**Scheme 3: (*R*)-Limonene monohydroxylation catalyzed by CDO variant M232A.** Reaction conditions: 30 °C for 24 h, 20 mM glucose added for cofactor regeneration; catalyst: resting *E. coli* cells,  $\beta(\text{cells}) = 0.2 \text{ g}_{\text{WCW}} \text{ mL}^{-1}$ . **2**: *R*-limonene, **2a**: (1*R*,5*S*)-carveol, **2b**: (1*S*,5*S*)-carveol; Product formation: CDO-WT:  $46 \pm 10 \%$ , *ee* % = 98 % (**2a**); CDO M232A: > 99 %, *ee* % = 98 % (**2a**).[23]

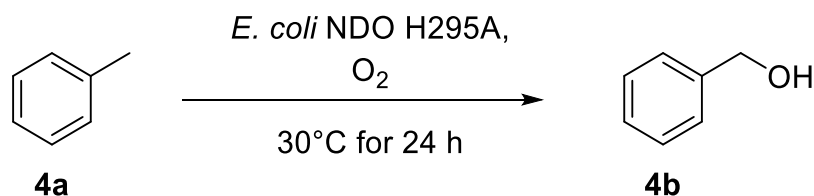
Whole-cell biotransformations with indene (**3**) as substrate yielded in hydroxylation at the cyclopentene ring structure.[23] Both, the formation of 1-indenol (**3a**) as well as the 2,3-indanediol (**3b**) could be observed with either the CDO WT or the M232A variant (**Scheme 4**). However, these two enzymes showed enantio-complementary catalytic properties. While the CDO WT favored the (*R*)-**3a** (*ee* 10 %) and (1*S*,2*R*)-**3b** (*ee* 38 %) products, the CDO variant M232A showed improved enantiomeric excess for (*S*)-**3a** (*ee* 87 %) and (1*R*,2*S*)-**3b** (*ee* 54 %).[23]



**Scheme 4: Indene monohydroxylation and dihydroxylation catalyzed by CDO variant M232A.** Reaction condition: 30 °C for 24 h, 20 mM glucose added for cofactor regeneration; catalyst: resting *E. coli* cells,  $\beta(\text{cells}) = 0.2 \text{ g}_{\text{WCW}} \text{ mL}^{-1}$ . **3**: indene, **3a**: 1-indenol, **3b**: 1,2-indanediol; Product formation: CDO-WT:  $80 \pm 7 \%$  (64:36 **3a**:**3b**), *ee* % = 10 % ((*R*)-**3a**), 38 % ((1*S*,2*R*)-**3b**); CDO M232A:  $80 \pm 11 \%$  (56:44 **3a**:**3b**), *ee* % = 87 % ((*S*)-**3a**), 54 % ((1*R*,2*S*)-**3b**).[23]

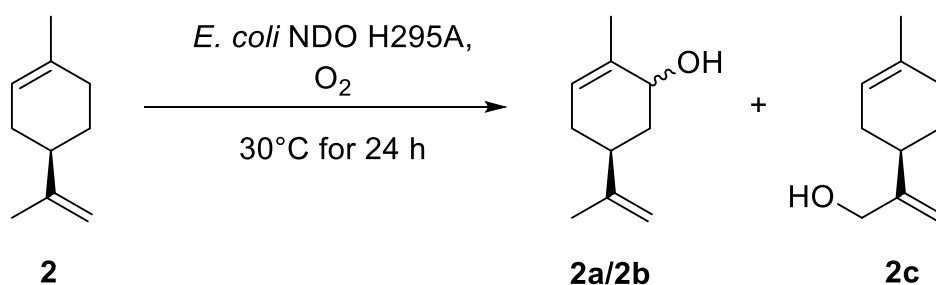
Previous studies revealed that certain single point mutations within the active site of the NDO show an impact on the stereoselectivity and the regioselectivity toward several arene

substrates in whole-cell biotransformations. Accordingly, it is proposed that a single substitution of histidine to alanine at position 295 within the active site of the oxygenase shows enhanced activity (26 %) toward toluene (**4a**) relative to the NDO WT (**Scheme 5**).[19]



**Scheme 5: Toluene monohydroxylation catalyzed by NDO variants.** Reaction condition: 30 °C for 20 h, 20 mM glucose added for cofactor regeneration; catalyst: resting *E. coli* cells,  $\beta(\text{cells}) = 0.2 \text{ g}_{\text{WCW}} \text{ mL}^{-1}$ . 4a: toluene, 4b: benzyl alcohol; Product formation: NDO-WT:  $61 \pm 3 \%$  (> 99 4b); NDO H295A:  $77 \pm 4 \%$  (> 99 4b).[19]

Furthermore, it was observed that the NDO H295A variant is capable of catalyzing the hydroxylation of (*R*)-limonene (**2**) into its hydroxylated products carveol (**2a/2b**) and mentha-1,8-dien-10-ol (**2c**) (**Scheme 6**). Unlike the NDO WT that favored the formation of **2c**, the H295A variant facilitated the monohydroxylation, which yielded in an excess of **2a/2b** (92%).[8]



**Scheme 6: Conversion of mentha-1,8-dien-10-ol and carveol from (*R*)-(+)-limonene during whole-cell biotransformation with *E. coli* harboring NDO.** Reaction condition: 30 °C for 20 h, 20 mM glucose added for cofactor regeneration; catalyst: resting *E. coli* cells,  $\beta(\text{cells}) = 0.2 \text{ g}_{\text{WCW}} \text{ mL}^{-1}$ . 4a: toluene, 4b: benzyl alcohol; Product formation: NDO-WT:  $61 \pm 3 \%$  (> 99 4b); NDO H295A:  $77 \pm 4 \%$  (> 99 4b) 2: (*R*)-limonene, 2a/2b: carveol ; 2c: Metha-1,8-dien-10-ol.[8]

Because of the described cofactor dependency of ROs, their activity is conditioned by the sufficient supply of NAD(P)H. While the interaction of several metabolic pathways contributes to the regeneration of corresponding redox equivalents in living cells, several *in vitro* strategies are currently available.

### 1.3 Natural NAD(P)<sup>+</sup> recycling systems

Every microorganism is harboring a defined amount of either NAD<sup>+</sup> and NADP<sup>+</sup> cofactors at a specific redox state.[24] Therefore, several recycling systems are involved in keeping their supply stable and sufficient. Dependent on the strategy of energy uptake and conversion, an organism can be classified in either heterotrophic or autotrophic. Both systems differ primarily in the preference for specific carbon sources from the environment to maintain the energy household. While heterotrophs utilize organic compounds like sugars, autotrophs use CO<sub>2</sub> as the primary source of carbon.[25] A heterotroph or chemoorganotroph is defined as an organism that shows the need for organic compounds as the natural carbon source to form ATP in the presence (aerobic) or absence (anaerobic) of molecular oxygen. In heterotrophic cells, NAD<sup>+</sup> is mainly consumed during glycolysis (two NAD<sup>+</sup> consumed per mol glucose) and following the citric acid cycle (four NAD<sup>+</sup> consumed per mol of pyruvate) which yield in its reduced form NADH.[26] Aerobes recover their oxidant pool with the help of the respiratory chain producing ATP as a cellular energy equivalent in the presence of molecular oxygen, which functions as the terminal electron acceptor.[27] However, heterotrophic organisms not relying on molecular oxygen use an alternative biochemical pathway since they are incapable of performing oxidative phosphorylation as a consequence of oxygen absence. To re-oxidize the NADH gained in the course of glycolysis, pyruvate is mainly reduced to either lactate or ethanol and CO<sub>2</sub>. [28] In prokaryotes and eukaryotes, NAD<sup>+</sup> functions as a precursor for the *de novo* biosynthesis of NADP<sup>+</sup> facilitated by an NAD<sup>+</sup> kinase. Furthermore, NADP<sup>+</sup>, which is commonly reduced during the lipid and nucleic acid biosynthesis, can be again recycled to recondition the redox state of a biological system. In the pentose phosphate pathway (PPP), the oxidative NADP<sup>+</sup> cofactor is involved in the formation of C5-monosaccharides. The PPP can be divided into an oxidative and a non-oxidative phase. The oxidative part yields in the reduction of NADP<sup>+</sup>, while the last step focuses on the generation of pentoses. In the oxidative part, two moles of NADPH are formed per mole of glucose.[26] Analogous to the first step of the glycolysis pathway, a glucokinase catalyzes the initial phosphorylation of monosaccharide glucose, which yields in the synthesis of glucose-6-phosphate (G6P). Unlike in the glycolysis pathway where the G6P is subsequently converted to its homologous ketose fructose-6-



phosphate by a cofactor-independent isomerase, a competing NADP<sup>+</sup>-dependent glucose-6-phosphate dehydrogenase catalyzes the formation of 6-phosphoglucono- $\delta$ -lactone and NADPH. Since the activity of this dehydrogenase is inhibited by an excess of NADPH, the PPP is strongly regulated based on the actual redox state within the cell.[26, 29] Unlike heterotrophs, autotrophic organisms are capable of utilizing CO<sub>2</sub> as their primary carbon source required for several metabolic pathways generating either energy equivalents (ATP) or essential metabolites for the cell.[25]. The overall carbon fixation mechanism is divided into a light-dependent and a light-independent pathway. Both reaction steps take place within the plastids of autotrophic eukaryotes (e.g., algae, higher plants) or the thylakoid membranes within cyanobacteria.[26, 30] In the light reaction, the reduction of NADP<sup>+</sup> to NADPH and the formation of ATP via an ATP-synthase complex occurs. Furthermore, O<sub>2</sub> is emitted into the atmosphere as a result of the oxidation of H<sub>2</sub>O. In contrast, NADPH and ATP are utilized during the light-independent pathway to reduce CO<sub>2</sub> to form precursor molecules for the synthesis of several hydrocarbons.[26] The conversion of light into electrochemical energy is facilitated by a group of natural photopigments, including chlorophyll and carotenoids.[31, 32] These classes of molecules are essential components in the multiprotein complexes photosystem I (PSI) and photosystem II (PSII) located in the thylakoid membranes of phototrophic organisms.[33, 34] The oxidation of H<sub>2</sub>O (water-splitting reaction) catalyzed by the homodimer PSII is considered as the initial step within the electron transfer chain of the light-dependent photosynthesis system yielding in the formation of O<sub>2</sub> and generates reducing equivalents for the regeneration of NAD(P)H.[32, 35, 36] In the ongoing photosynthesis, NAD(P)H is re-oxidized during the CO<sub>2</sub> assimilation pathway termed as Calvin cycle.[37, 38]

### 1.4 Nicotinamide cofactor regeneration for biocatalytic applications

While initial biotechnological applications at large-scale were mainly restricted to cofactor-free enzyme classes, recent developments in biocatalysis contribute to enhanced accessibility of more complex biotransformation.[6] Especially, the economical use of industrial relevant NAD(P)H-dependent oxidoreductases gained considerable attention over the past decades

due to their broad reaction spectra. To overcome the need for stoichiometric amounts of costly and relatively unstable NAD(P)H, the use of reliable and efficient *in situ* cofactor regeneration systems is crucial for the design of cost-efficient processes.[9] For the evaluation of the efficiency of a proposed regeneration system, the TTN is considered as a suitable reference value, which indicates the amount (mol) of product formed per quantity (mol) of cofactor during the time course of a specific reaction. Dependent on the product value, the TTN of an *in vitro* cofactor regeneration system should be in a range of  $10^3$  -  $10^5$  to be considered as a promising and economically feasible approach for industrial applications.[39] Enzymatic approaches for *in vitro* regeneration propose the extension of the desired biotransformation system by an additional enzyme catalyzing an auxiliary reaction that yields in the formation of specific cofactors. Therefore, both reactions can be catalyzed either by the same enzyme concurrently (coupled-substrate cofactor regeneration) or by the use of an additional biocatalyst (coupled-enzyme cofactor regeneration). As an example, alcohol dehydrogenases (ADHs) catalyzes both the reduction of carbonyl groups to the corresponding alcohols and the oxidative formation of aldehydes or ketones from hydroxylated substrates. Therefore, NADH or NAD<sup>+</sup> is required as either reductive or oxidative cofactors. Since this class of enzymes catalyzes both the forward as well as the reverse reaction, they are used as biocatalysts for coupled-substrate cofactor regeneration approaches.[9] In contrast, the field of whole-cell biocatalysis takes advantage of the natural cofactor supply-system of microorganisms to perform the desired conversions. Since the reactions occur within living systems, whole-cell biocatalysis is, in some cases, superior to the corresponding *in vitro* strategies. In particular, the possible use of unstable or complex multi-component enzyme systems or enzyme cascades not feasible in heterologous environments increases the potential of whole cells as biocatalysts.[40] Although no upstream protein purification processes are needed by that, downstream product isolation is required, which has to be considered in the overall process design.[41] The respective research mainly focuses on the use of bacteria (*Escherichia coli*), fungi (*Pichia pastoris*, *Saccharomyces cerevisiae*, *Aspergillus niger*), and more recently, microalgae (cyanobacteria).[40, 42-45] However, substrate or product toxicity, mass transport limitations due to the cell membrane, and the additional need for cultivation techniques prone to the risk of contamination are the major drawbacks

for a reasonable application in industrial processes. Furthermore, the energy supply for the desired substrate conversion is limited in the whole-cell approach due to competing metabolic pathways necessary for cellular maintenance.[40, 46] To overcome this energy efficiency issue, metabolic engineering, or the use of alternative cofactors are considered as possible strategies for the application in industrial processes. Unlike the described enzymatic cofactor regeneration, recently proposed electrochemical approaches are considered as promising techniques since there is no need for a second auxiliary biocatalyst or cosubstrate. Hence, no interfering byproduct formation takes place.[9, 47] In principle, high overpotentials are applied for the *in situ* regeneration of redox cofactors. Thereby, oxidative or reductive regeneration of nicotinamide cofactors is performed by the use of an anode or cathode, respectively. Previous studies showed the feasibility of a direct oxidative regeneration of NAD(P)<sup>+</sup> performed in a plug-flow reactor by the use of a graphite felt electrode.[48] However, immediate electrochemical reduction of NAD(P)<sup>+</sup> for NAD(P)H cofactor regeneration is considered as a two-step reaction pathway. In the first step, a single electron transfer from a cathode to the oxidized cofactor yielding in the formation of a free NAD(P) radical. In the following step, generated NAD(P)<sup>+</sup> products can undergo either a dimerization reaction yielding in inactive NAD(P)<sub>2</sub> dimers or can be further reduced and protonated to the desired enzymatically relevant NAD(P)H cofactor. Wienkamp et al. reported an indirect regeneration system by the use of a bipyridine rhodium complex [Rh(bpy)<sub>3</sub>]<sup>2+</sup> in the course of cyclohexanone conversion catalyzed by a horse liver alcohol dehydrogenase (HLADH). Thereby, two electrons received from the electrode and one H<sup>+</sup>-proton yield in the formation of a hybrid rhodium complex ion, which facilitated the reduction of NAD(P)<sup>+</sup> cofactor. By that, a total conversion of 26 % and a TTN of 2.9 could be observed.[49] However, yet low efficiencies, the need for high overpotential, and the use of toxic mediator complexes are significant drawbacks in the implementation of industrial economic applications. [9]

### 1.5 Photo-biocatalysis

The concept of photo-biocatalysis defines a sustainable strategy to convert abundant light energy into chemical energy, which can be used for the synthesis of valuable organic products.[41] Thereby, photoreactive properties of organic or inorganic molecules exploited

in conventional photocatalysis are combined with the advantages of biocatalysts to perform enzyme-catalyzed redox reactions under mild conditions and high selectivity induced by light illumination. Besides the omnipresent solar energy in the form of radiant light, the rising supply of renewable electricity enables an environmentally benign use of artificial light sources such as fluorescence lamps or light-emitting diodes (LED) for controlled light-driven bioconversions. Because of this, the demand for sustainable and meaningful photo-biocatalytic applications increased over the last few years. Numerous prior research studies have focused on the light-mediated supply of electrons for purified oxidoreductases by the use of inorganic semiconductors (e.g., cadmium selenide, titanium dioxide (TiO<sub>2</sub>)) or organic photoactive molecules (e.g., fluorescence dyes, flavins), so-called photosensitizers (PSs). These redox mediators are capable of facilitating an electron transfer from an electron donor to a terminal acceptor molecule at a light-excited state.[50] By exploiting these photo-excitability properties, either regeneration or circumvention of reductive cofactors by the use of alternative electron donors in the course of enzymatic conversions could be achieved.[9] Previous studies have especially focused on the development of photocatalytic systems by the use of more stable sacrificial electron donors compared to the natural NAD(P)H counterparts.[50] The old-yellow enzyme (OYEs) family represents well-studied flavin-dependent ene-reductases, which are used as model enzymes in photocatalytic studies since they accept a variety of alternative redox partners.[50, 51] A recent study shows the successful photoenzymatic reduction of the flavin moiety of YqjM from *Bacillus subtilis* by using ethylenediaminetetraacetic acid (EDTA) as sacrificial electron donor and by exploiting the photoexcitability of unbound flavin mononucleotide (FMN) which functions as PS. By this photocatalytic approach, 65 % of the nominal activity of YqjM for the conversion of ketoisophorone could be achieved.[52] Furthermore, the authors suggest that, although EDTA harbors four oxidizable amino moieties in its molecular structure, just two show the potential of reducing the unbound FMN. Due to this low atom efficiency and the formation of amines and formaldehyde side products, the use of EDTA is questionable.[52] Lee *et al.* reported the feasibility of light-driven regeneration systems by the use of triethanolamine (TEOA) as an electron donor in the presence of several xanthene dyes as organic PSs.[20] These photoactive molecules are commonly used in microscopy for fluorescence imaging of

biological events within cells and hence represent potential PSs in whole-cell applications.[53] By the use of TEOA and rose bengal (RB), the feasibility of NAD(P)H-independent selective photoconversion of 2-methylcyclohexenone into its oxidative form (*R*)-2-methylcyclohexanone catalyzed by an OYE variant could be shown. Thereby, a total conversion of 76 % (*ee* > 99 %) could be achieved after 2.5 h under white-light exposure.[20] Furthermore, a correlation between substrate conversion and choice of PS could be drawn. While 73 % conversion of 2-methylcyclohexenone to (*R*)-2-methylcyclohexanone (*ee* > 99 %) was achieved in the presence of erythrosine B, the use of FMN as PS yields in only 4.1 % (*ee* > 99 %).[20] Hollmann and co-workers demonstrated the light-driven regeneration of Baeyer–Villiger monooxygenases to overcome the need for NAD(P)H cofactors by the use of EDTA and FAD as photomediator.[54] By the use of a flavin-dependent phenylacetone monooxygenase variant (PAMO-P3), the light-driven transformation of racemic 2-phenylcyclohexanone into (*R*)-5-phenyloxepan-2-one yielded in 48 % conversion (*ee* > 97 %), which is almost the maximum theoretical value (50 %) regarding the kinetic resolution.[54] Inspired by the PSII of autotrophs, Mifsud et al. proposed the use of H<sub>2</sub>O as a sacrificial electron donor for the enzymatic hydrogenation of conjugated C=C- double bonds catalyzed by an isolated OYE variant of *Thermus scotoductus* SA-01.[55] In the corresponding proof-of-concept study, the potential of TiO<sub>2</sub>-based nanoparticles as suitable semiconductors for the initial water-splitting reaction (H<sub>2</sub>O-oxidation) was revealed as sufficient regarding the supply of reducing equivalents for the enzymatic stereoselective reduction of ketoisophorone yielding (*R*)-levodione. In the presence of FMN, which functions as both redox mediator and prosthetic group of the terminal oxidoreductase, up to 66 % conversion (*ee* 86 %) after 6 h under UV-light irradiation could be achieved.[55] However, non-enzymatic conversion yielding in the racemic substrate could be determined which is assumed to be facilitated by an electron transfer from H<sub>2</sub>O directly to the substrate. Although the feasibility of *in vitro* light-driven biotransformation could be demonstrated in previous literature, the industrial application is still hampered by relatively low TTNs and the undesired formation of reactive free radicals causing unspecific side reactions.[56, 57] Furthermore, the need for protein purification procedures and the common issue of low enzyme stability are major obstacles for the meaningful implementation of the described systems.[40, 58] To extend the

practicability of photo-biocatalytic applications in respect to unstable or multicomponent enzyme systems, the feasibility of light-driven *in vivo* approaches were recently examined. By exploiting the improved atom efficiency of the electron supplying photosynthesis in autotrophs by accepting water as an electron donor, it is assumed to establish highly efficient whole-cell systems catalyzing light-driven biotransformations.[34] Thus, undesired side product formation and the need for stoichiometric amounts of sacrificial cosubstrates can be circumvented, which benefits the implementation at an industrial scale.[59, 60] In regard to biotransformations catalyzed by oxygenases, oxygen generated by the photo-induced oxidation of water can be directly used for incorporation into the substrate.[61] Particularly, recombinant cyanobacteria are considered as auspicious biocatalysts for corresponding applications due to their similarity to the well-studied Gram-negative model organisms such as *E. coli* for which comprehensive knowledge is available today.[62-64] Köninger et al. show the first successful linkage of the natural photosystem of cyanobacteria with a heterogeneous oxidoreductase YqjM. Thereby, light-driven biotransformations of 2-methylmaleimide (100 mg) with *Synechocystis* sp. PCC6803 cells containing YqjM from *Bacillus subtilis* yielded in the formation of 81 mg optically pure (*R*)-2-methylsuccinimide (*ee* > 99 %) after 3 h under semipreparative reaction conditions.[59] In 2019, Hoschek and coworkers reported the first light-driven aeration-independent hydroxylation of volatile cyclohexane catalyzed by *Synechocystis* sp. PCC6803 harboring a CYP from *Acidovorax* sp.[60] Thereby, the supply of electrons and oxygen derived from the water-splitting reaction in PSII could be shown as sufficient to drive the enzymatic conversion yielding in 4.9 g g<sub>CDW</sub><sup>-1</sup> of cyclohexanol at the specific activity of 39.2 ± 0.7 U g<sub>CDW</sub><sup>-1</sup>. [60] Although the feasibility of light-driven redox reactions by the use of recombinant cyanobacteria as biocatalysts could be shown in several proof-of-concept studies[41, 59-61, 65], the lack of efficient genetic engineering tools, significantly lower growth rates compared to *E. coli* and the issue of unfavorable self-shading effects at higher cell densities are currently major challenges in the implementation of cyanobacteria as whole-cell catalyst in biotechnological processes.[62, 65-67] Furthermore, the conversion of solar energy into chemical energy catalyzed by photoautotrophs is considered as relatively inefficient.[68, 69] While approximately 9 % of the solar energy can be used by cyanobacteria for biomass production, higher plants just use 0.5–3%.[42] Because

of this, recent studies have focused on the development of efficient inorganic whole-cell biohybrid photocatalysts by combining the advantages of whole-cell biotransformation techniques with the findings obtained from *in vitro* photo-biocatalytic systems. In this way, an artificial photoinduced electron transfer providing reducing equivalents for enzymatic redox reactions can be introduced in heterotrophic organisms. Particularly, the use of *E. coli* as a model organism for light-driven reaction systems is favorable due to the possibility of simple and cost-efficient high-cell density cultivation and the availability of a mature gene engineering toolbox.[40] Referring to the equivalent conversion of light energy into chemical energy performed by photoautotrophs, the described light-driven systems established in heterotrophs are simply termed as artificial photosynthesis.[57, 58, 70] In 2016, Honda and coworkers proposed the first light-driven whole-cell approach to generate H<sub>2</sub> by the use of recombinant *E. coli* cells harboring [FeFe]-hydrogenase and maturases from *Clostridium acetobutylicum* as biocatalysts.[58] In combination with TiO<sub>2</sub> as photocatalyst and methyl viologen (MV) as an electron mediator, a light-driven electron transfer could be established. Thus, the intracellular concentration of reduced NADH, which provides electrons for the enzymatic water-splitting reaction increases and consequently drives the formation of H<sub>2</sub>. [58] Rowe and coworkers demonstrated the successful implementation of an artificial light-mediated electron transfer in *Shewanella oneidensis* to drive the evolution of H<sub>2</sub> and the hydrogenation of either C=O or C=C-bonds catalyzed by a set of intrinsic oxidoreductases.[68] It was observed that photogenerated electrons derived from TEOA were transferred via water-soluble PSs to MV which shows the ability to permeate cell membranes and thus provide reducing equivalents for the desired reduction of fumarate into succinate by a fumarate reductase, pyruvate into lactate via a lactate dehydrogenase, CO<sub>2</sub> to formate via a formate dehydrogenase and the generation of H<sub>2</sub> via either [FeFe]- or [NiFe]-hydrogenases.[68] However, the need for toxic and relatively costly MV hampers the biotechnological application in large-scale processes.[68, 71] Park et al. reported a cofactor-free whole-cell photoconversion approach by the use of engineered CYP BM3 variants in combination with TEOA as electron donor and eosin Y (EY) as PS.[70] The CYP BM3 from *Bacillus megaterium* belongs to the class II of microsomal P450s. Unlike oxygenases of type I, the transfer of electrons from the reduced nicotinamide cofactor to the catalytic heme

domain of BM3 is catalyzed solely by an NADPH-P450 reductase without the need for an Fd moiety.[70, 72] The author suggested that the need for NAD(P)H could be circumvented as a result of an artificial light-mediated electron transfer chain within resting *E. coli* cells. It was supposed that TEOA and EY simultaneously enter the cytoplasm of *E. coli* in which the electron transfer from the photoexcited PS toward the heme prosthetic group of the CYP takes place.[70] The light-induced activities of various CYP BM3 variants towards marked drugs such as simvastatin, lovastatin and omeprazole were determined via whole-cell biotransformation experiments to evaluate the efficiency of the proposed cofactor-free light-driven system. Furthermore, human variants of CYPs and a steroid substrate (17 $\beta$ -estradiol) were additionally investigated. The light-driven conversion could be observed in all attempts with a maximum product yield of 75  $\mu$ M of 5'-hydroxylated omeprazole after 20 h catalyzed by the CYP variant BM3m10.[70] To determine the electron transfer from TEOA towards the oxygenase, various CYP BM3m2 constructs were designed. Experiments conducted by the use of incomplete CYP BM3m2 variant without the reductase domain exhibit conversions of 7-ethoxycoumarin into dealkylated 7-hydroxycoumarin almost as efficient as the control reaction catalyzed by the complete CYP BM3m2.[70] These results indicate a direct electron transfer from TEOA to the heme-prosthetic group of the terminal catalytic subunit of BM3 via EY and visible light. The authors concluded that the proposed light-driven system has the potential to drive a variety of CYP catalyzed reactions at an industrial scale without the need for expensive and relative unstable redox cofactors and time-consuming protein purification procedures. Furthermore, it was emphasized that the applicability of the reported light-driven whole-cell approach for human CYP variants is of high relevance for the pharmaceutical industry regarding the sustainable and economical production of valuable drugs.[70]

Inspired by these findings, Wied et al. reported the first cofactor-independent whole-cell approach for ROs.[73] It was proposed to establish a suitable and universal applicable light-driven reaction system for multicomponent ROs by the use of alternative, more stable electron donors compared to the preferential NAD(P)H. In a proof-of-concept study, resting *E. coli* cells containing the engineered CDO M232A variant derived from *Pseudomonas fluorescens* IP01 were used as biocatalysts.[23, 73] While TEOA and EDTA were investigated as sacrificial electron donors, EY and RB were suggested as potential PSs. Whole-cell

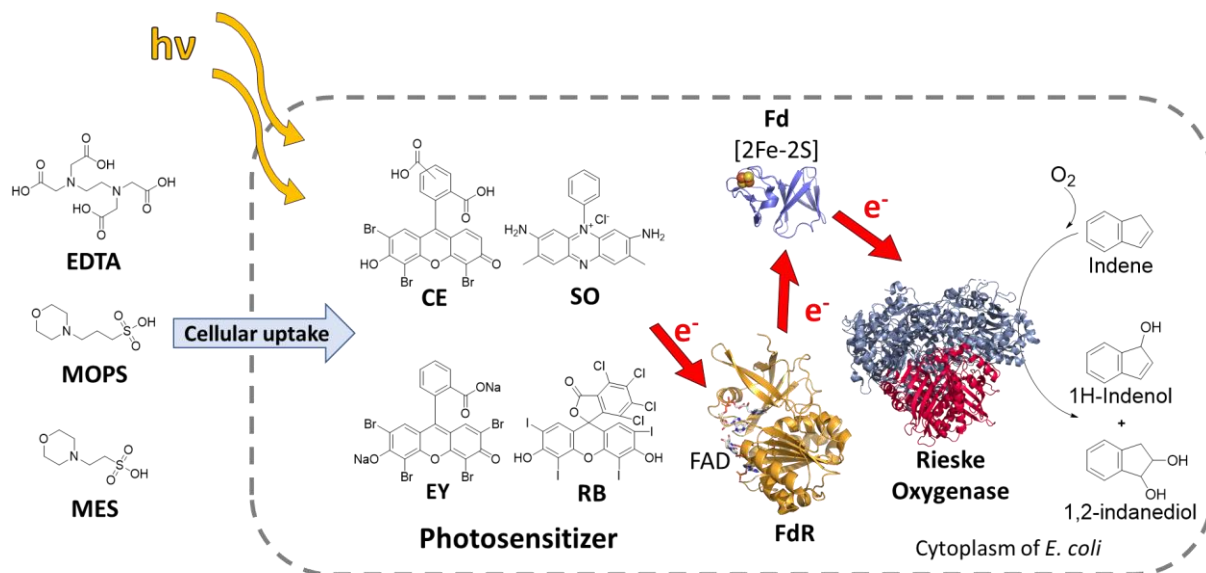


biotransformations of (*R*)-(+)-limonene were performed in either light or dark conditions in the presence or absence of electron donors and the respective PSs. As a control, *in vivo* reactions with glucose supplementation were conducted to determine the enzymatic conversion driven by the cellular cofactor regeneration machinery. While no light-driven conversion of (*R*)-(+)-limonene into desired (1*R*, 5*S*)-carveol could be detected in the presence of TEOA, the use of EDTA in combination of either EY or RB yields in up to 86  $\mu$ M of product after 24 h which correlates to a total conversion of 0.86 %.[73] Since no catalytic activity was observable in corresponding reactions under dark conditions, the author assumed the successful implementation of a cofactor independent light-mediated whole-cell system for CDO M232A. However, compared to the relatively high product yields (2.6 mM) obtained by whole-cell biotransformations of (*R*)-(+)-limonene with glucose supplementation,[73] further characterization and optimization has to be made to establish a reasonable and industrial relevant process for future applications.

### 1.6 Thesis aims

In literature, the term artificial photosynthesis describes a versatile strategy to enable the transformation of radiant energy from light into accessible chemical energy by the use of heterotrophic organisms. Proof-of-concept studies recently revealed the feasibility of whole-cell approaches, which aims to facilitate enzyme-catalyzed redox reactions by the implementation of an artificial light-driven electron transfer, providing reducing equivalents for the terminal oxygenases.[70, 73] Thereby, the photo excitability of PSs was exploited to shuttle electrons from suitable sacrificial electron donors towards the active site of the corresponding oxidoreductase, where oxygen activation and its final incorporation into the desired substrate takes place.[70] The aim of the current study is to characterize a new light-driven cofactor-independent *in vivo* approach for CDO M232A and NDO H295A by the use of various sacrificial electron donors (EDTA, MES and MOPS) and PSs (EY, RB, CE, SO). Furthermore, the stereoselectivity of the proposed reaction system is evaluated by investigating (*R*)-(+)-limonene, indene and toluene as substrates for the corresponding light-driven whole-cell biotransformations. It is suggested that by varying the reaction conditions and adjusting the experimental setup, process optimization towards enhanced productivity is

achievable. Thus, the overall goal is to establish an efficient and universal applicable cofactor-independent tool for multicomponent ROs by the implementation of an artificial light-mediated electron transfer in *E. coli*.



### Electron donor

**Figure 1: Light-driven cofactor-independent whole-cell approach using ROS.** It is supposed that by the use of alternative and stable electron donors like EDTA, MOPS, or MES, the need for NAD(P)H could be circumvented. Via photoexcited photosensitizers (CE: 5(6)-carboxyeosin; SO: safranin O, EY: eosin Y, RB: rose bengal) electrons are transferred to the multicomponent system of an RO composed of a ferredoxin reductase (FdR), ferredoxin (Fd) and the terminal Rieseke oxygenase. The model conversion of indene to 1H-indenol and 1,2-indanediol is depicted. EDTA: ethylenediaminetetraacetic acid; MOPS: 3-(*N*-morpholino)propanesulfonic acid; MES: 2-(*N*-morpholino)ethanesulfonic acid.  $h\nu$ : visible light.

## 2 Material and Methods

### 2.1 Devices & Chemicals

In the following section, all relevant devices and chemicals used throughout the project are summarized. Standard laboratory equipment or reagents not significant for the experimental setup are neglected.

#### 2.1.1 Incubation devices

**Incubation shaker:** Certomat® BS-1, Sartorius (Göttingen, Germany), temperature adjustable within a range of -10 °C to +70 °C. Used for cultivation at 37 °C and either expression or biotransformation experiments at 30 °C.

**Incubation room:** Temperature preset to either 37 °C or 28 °C, respectively. Incubation rooms used for cultivation at 37 °C and either expression or biotransformation experiments at 28 °C.

#### 2.1.2 Centrifuge for cell harvesting

**Refrigerated high-speed centrifuge:** Avanti™ J-20 XP centrifuge provided by Beckman Coulter (Brea, California). Rotor: JA-10

#### 2.1.3 Freeze-drying equipment

**Freeze dryer:** AdVantage Pro freeze dryer with Intellitronics™ controller provided by SP Scientific (Warminster, Pennsylvania).

#### 2.1.4 Reactor for light-driven whole-cell biotransformations

**Self-made 3D-printed LED light reactor, *Peter*:**

At the beginning of the project, light-driven whole-cell biotransformation experiments were performed within a 3D-printed LED-light reactor that has been constructed by Peter Wied (**Figure 2**).<sup>[73]</sup> The reactor was designed via Fusion 360 (Autodesk Inc.) software and printed

by Ultimaker2 (Ultimaker B.V.). This prototype is equipped with conventional LED strips (RGB, 12 V) arranged at the inner surface. Thereby, 12 reactions can be illuminated simultaneously from the side. To ensure sufficient mixing at a specific temperature over time, the reactor was placed into an incubation shaker during biotransformation experiments.

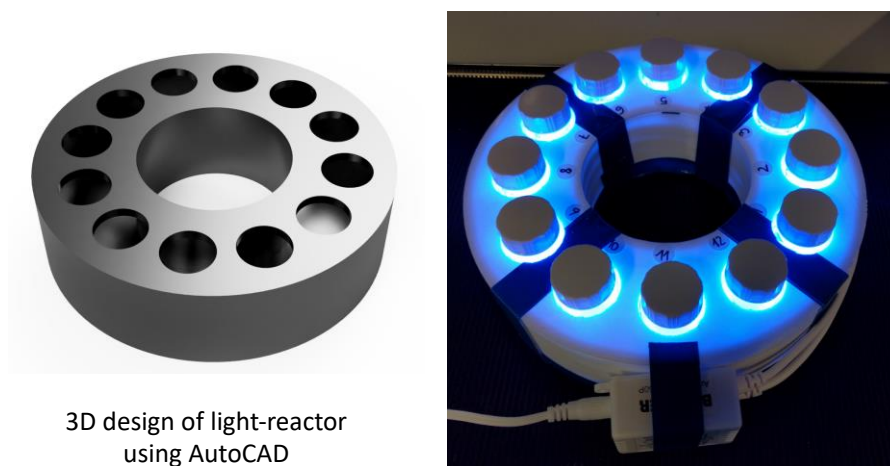


**Figure 2: Self-made 3D-printed LED-light reactor *Peter*.** 3D-printed prototype LED-light reactor for 12 reaction vials used for light-driven whole-cell biotransformation experiments. Left: a computational model designed via Fusion 360 (Autodesk Inc.); right: *Peter* in action.[73]

### Self-made fluorescence lamp light reactor *Lucifer*:

To overcome the increasing number of potential experiments over time, a fluorescent lamp light reactor with 33 vial inlets was constructed (**Figure 3**).

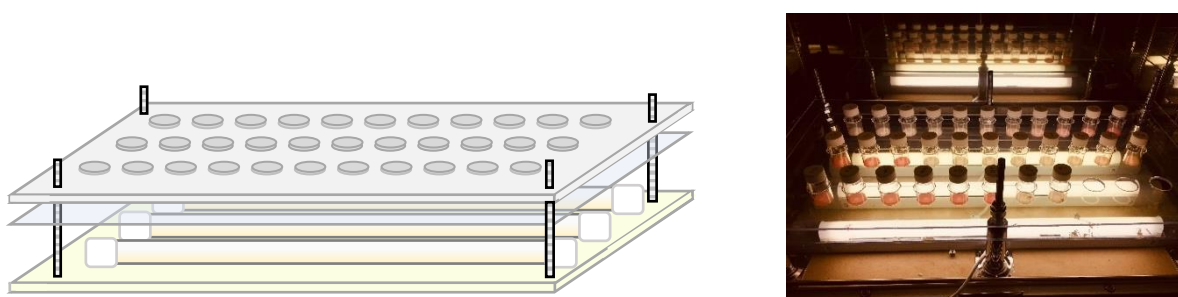


**Figure 3: Self-made fluorescence-light reactor *Lucifer*.** Light reactor with bottom-arranged fluorescent lamps and space for 33 reaction vials. Left: schematic representation of fluorescence-light reactor; right: active light-reactor *Lucifer* during light-driven whole-cell biotransformation experiment.

While the former 3D printed light reactor (LED reactor) shows an increase of temperature (approximately 5 °C) during the biotransformation, triggered by the design, the latter reactor

shows almost no increase in temperature. Furthermore, the bottom arrangement of the fluorescent lamps enables exposure of a larger surface area of each reaction mixture compared to the illumination sidewise in the LED reactor. To ensure sufficient mixing at a specific temperature during the experiments, the reactor was placed into an incubation shaker.

### 2.1.5 Device for DNA amplification

**Thermocycler:** GeneExplorer ADVANCED GE4852T (Bio-Gener Technology Co., Ltd., Hangzhou, China)

### 2.1.6 Analytic instruments (quantitative)

#### **Device for determining light intensities:**

Field Scout Quantum Meter (Spectrum® Technologies, Inc., Bridgend, UK)

#### **Gas chromatograph with flame ionization detector (GC-FID):**

Nexis GC-2030 device (Shimadzu Europa GmbH, Duisburg, Germany) equipped with an AOC-20i plus auto-injector module and a Hydrodex- $\beta$ -6TBDM capillary column (Macherey-Nagel™, Düren, Germany) for enantiomer separation.

Column specification: length: 25 m, inner diameter: 0.25 mm, film thickness: 0.25  $\mu$ M

#### **Gas chromatograph-mass spectrometry (GC-MS):**

GCMS type QP2010 device (Shimadzu Europa GmbH, Duisburg, Germany) equipped with an AOC-20i plus auto-injector module and inert capillary column type ZB-5MSi (Phenomenex®, Torrance, California) as the stationary phase.

Column specification: length: 30 m, inner diameter: 0.25 mm, film thickness: 0.25  $\mu$ M

**OD<sub>600</sub>-spectrophotometer:** BioPhotometer (Eppendorf AG, Hamburg, Germany).

**UV-Vis spectrophotometer:** Cary 100 UV-Vis spectrophotometer (Agilent Technologies, Inc., Santa Clara, California)

### 2.1.7 Analytic instruments (qualitative)

**Gel-imaging device:** G:BOX (Syngene, Cambridge, UK)

### 2.1.8 Chemicals for cultivation and expression

#### **Antibiotics:**

---

#### **Ampicillin-stock solution, $\beta(\text{amp-stock}) = 100 \text{ g L}^{-1}$**

In order to prepare an ampicillin-stock solution, 4.252 g of solid ampicillin sodium salt (99%, Carl Roth GmbH, Karlsruhe, Germany) were dissolved in 40 mL ddH<sub>2</sub>O After sterile filtration through a syringe sterile filter (Filtropur S 0.2, SARSTEDT AG & Co. KG, Nümbrecht, Germany) with a pore size of 0.2  $\mu\text{m}$ , 1 mL aliquots were prepared and stored in the freezer at  $-20 \text{ }^{\circ}\text{C}$  for further use.

#### **Inducing agents:**

---

#### **IPTG-stock solution, $c(\text{IPTG-stock}) = 1 \text{ M}$**

For the preparation of an IPTG-stock solution with a concentration of 1 M, 2.383 g of IPTG ( $\geq 99 \%$ , Carl Roth GmbH, Karlsruhe, Germany) were dissolved in 10 mL ddH<sub>2</sub>O After filtration through a syringe sterile filter (Filtropur S 0.2, SARSTEDT AG & Co. KG, Nümbrecht, Germany) with a pore size of 0.2  $\mu\text{m}$ , 1 mL aliquots were prepared and stored in the freezer at  $-20 \text{ }^{\circ}\text{C}$  for further use.

## Growth media

---

### ***Lysogeny* broth medium (LB-medium)**

16 g of LB Broth-Lennox (Carl Roth GmbH, Karlsruhe, Germany) powder were dissolved in ddH<sub>2</sub>O to a final volume of 800 mL within a 1 L glass flask and autoclaved.

---

Final concentrations:  $\beta(\text{tryptone}) = 10 \text{ g L}^{-1}$ ;  $\beta(\text{yeast extract}) = 5 \text{ g L}^{-1}$ ;  $\beta(\text{NaCl}) = 5 \text{ g L}^{-1}$

### **Terrific broth medium (TB-medium)**

24 g yeast extract (Carl Roth GmbH, Karlsruhe, Germany), 12 g tryptone/peptone (from casein; Carl Roth GmbH, Karlsruhe, Germany) and 5 g of glycerol (purity  $\geq 98 \%$ , anhydrous; Carl Roth GmbH, Karlsruhe, Germany) were dissolved in ddH<sub>2</sub>O to a final volume of 900 mL within a 1 L glass flask and autoclaved.

#### *10x TB-salts solution:*

125.5 g of dipotassium phosphate (K<sub>2</sub>HPO<sub>4</sub>) and 23.2 g of monopotassium phosphate (KH<sub>2</sub>PO<sub>4</sub>; Purity  $\geq 99.5 \%$ ; AppliChem GmbH, Darmstadt, Germany) were dissolved in ddH<sub>2</sub>O to a final volume of 1 L within a 1 L glass flask and autoclaved.

TB-medium and TB-salts have to be autoclaved separately.

Before usage, 100 mL of the 10xTB-salts solution has to be added to the cooled down 900 mL TB-medium.

---

Final concentrations:  $\beta(\text{yeast extract}) = 24 \text{ g L}^{-1}$ ;  $\beta(\text{tryptone/peptone}) = 12 \text{ g L}^{-1}$ ;  $\beta(\text{glycerol}) = 5 \text{ g L}^{-1}$ ;  $\beta(\text{K}_2\text{HPO}_4) = 12.55 \text{ g L}^{-1}$ ;  $\beta(\text{KH}_2\text{PO}_4) = 2.32 \text{ g L}^{-1}$

**ZYP-5052-autoinduction-medium**

20x ZYP-salts solution

54 g of monopotassium phosphate ( $\text{KH}_2\text{PO}_4$ ), 71.196 g of disodium phosphate dihydrate ( $\text{Na}_2\text{HPO}_4 \cdot 2 \text{H}_2\text{O}$ ), and 26.4 g of ammonium sulphate [ $(\text{NH}_4)_2\text{SO}_4$ ] were dissolved in ddH<sub>2</sub>O to a final volume of 400 mL in a 500 mL glass flask and autoclaved.

20x ZYP-sugars solution

40 g of glycerol, 4.4 g of glucose-monohydrate, and 16 g of lactose were dissolved in ddH<sub>2</sub>O to a final volume of 400 mL in a 500 mL glass flask and autoclaved.

100x magnesium sulphate solution

2.46 g of magnesium sulphate ( $\text{MgSO}_4$ ) were dissolved in ddH<sub>2</sub>O to a final volume of 50 mL and subsequently filtrated through a sterile filter (Filtropur S 0.2, Sarstedt AG & CO. KG, Nümbrecht, Germany).

For 1 L of ZYP-5052-medium 10 g of tryptone, 5 g of yeast extract were dissolved in ddH<sub>2</sub>O to a final volume of 890 mL and autoclaved. After the solution cooled down to room temperature, 50 mL of 20x ZYP-salts solution, 50 mL of 20x ZYP-sugars solution, and 16 mL of 100x Magnesium sulphate solution were added and thoroughly mixed by using a magnetic stirrer.

---

Final concentrations:  $\beta(\text{KH}_2\text{PO}_4) = 6.75 \text{ g L}^{-1}$ ;  $\beta(\text{Na}_2\text{HPO}_4 \cdot 2\text{H}_2\text{O}) = 8.9 \text{ g L}^{-1}$ ;  $\beta[(\text{NH}_4)_2\text{SO}_4] = 3.3 \text{ g L}^{-1}$ ;  
 $\beta(\text{glycerol}) = 5 \text{ g L}^{-1}$ ;  $\beta(\text{glucose-monohydrate}) = 0.55 \text{ g L}^{-1}$ ;  $\beta(\text{lactose}) = 2 \text{ g L}^{-1}$ ;  $\beta[\text{MgSO}_4] = 0.492 \text{ g L}^{-1}$ ;  
 $\beta(\text{tryptone}) = 10 \text{ g L}^{-1}$ ;  $\beta(\text{yeast extract}) = 5 \text{ g L}^{-1}$



### 2.1.9 Agents for long-time storage of cell cultures

#### **Aqueous glycerol solution for bacterial stocks, w(glycerol) = 60%**

60 g of glycerol (Carl Roth GmbH, Karlsruhe, Germany) were solved in 40 g ddH<sub>2</sub>O and subsequently autoclaved.

### 2.1.10 Chemicals for whole-cell biotransformations

In this section, the respective chemicals for biotransformation experiments are summarized.

#### **Buffer solutions**

---

For either cell washing and resuspension, the following aqueous buffer systems at a physiological pH of 7.2 and a concentration of 50 mM were used throughout the conducted experiments in this work. Besides its pH regulatory function, 2-(N-Morpholino)ethansulfonsäure (MES) and 3-(N-morpholino)propanesulfonic acid (MOPS) also function as electron donors which were exploited in the proposed light-driven whole-cell biotransformations.

#### **Sodium phosphate buffer (SPB, pH = 7.2), c(SPB) = 50 mM**

To prepare a 50 mM sodium phosphate buffer with a pH-value of 7.2, 1 L solutions of both, mono-sodium phosphate (NaH<sub>2</sub>PO<sub>4</sub>) and disodium phosphate (Na<sub>2</sub>HPO<sub>4</sub>) were prepared. Therefore, respective phosphate salts (NaH<sub>2</sub>PO<sub>4</sub> 2H<sub>2</sub>O and Na<sub>2</sub>HPO<sub>4</sub> 2H<sub>2</sub>O) were dissolved in ddH<sub>2</sub>O at a concentration of c(sodium phosphate) = 0.2 mM. 27.5 mL NaH<sub>2</sub>PO<sub>4</sub> – stock solution and 72.5 mL of the Na<sub>2</sub>HPO<sub>4</sub>-stock solution were then mixed and filled up to 200 mL with ddH<sub>2</sub>O. Finally, the pH was adjusted with a pH-meter to a final value of 7.2.

#### **MOPS buffer (pH = 7.2), c(MOPS) = 50 mM<sup>1</sup>**

For the preparation of 50 mM MOPS-buffer, 20.92 g of solid MOPS (PUFFERAN<sup>®</sup> ≥99.5 %, Carl Roth GmbH, Karlsruhe, Germany) were dissolved in 1.8 L ddH<sub>2</sub>O After adjusting the pH-value to 7.2 the buffer was subsequently filled up to a final volume of 2 L with ddH<sub>2</sub>O.

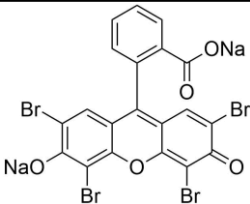
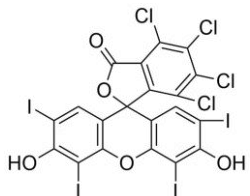
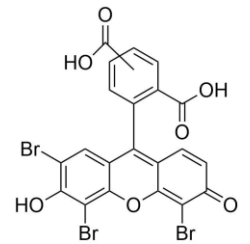
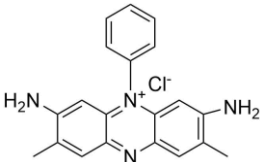
**MES buffer (pH = 7.2), c(MES) = 50 mM**

19.52 g solid MES (PUFFERAN® ≥99 %, Carl Roth GmbH, Karlsruhe, Germany) were dissolved in 2 L ddH<sub>2</sub>O. The pH-value was adjusted to 7.2 by adding acids or bases, respectively.

**Photosensitizer**

For biotransformation experiments, stock solutions of different photosensitizers were prepared at a concentration of c(photosensitizer) = 20 mM. Photosensitizers used in this project are summarized in **Table 2**.

**Table 2: Photosensitizer used for the whole-cell biotransformation experiments.**

Photosensitizer	Structure	MW [g mol <sup>-1</sup> ]	Supplier
<b>Eosin Y (EY)</b> CAS Number: 15086-94-9		647.89	Sigma-Aldrich
<b>Rose Bengal (RB)</b> CAS Number: 632-69-9		973.67	Sigma-Aldrich
<b>5(6)-Carboxyeosin (CE)</b> CAS Number: 132201-84-4		691.90	Marker Gene Technologies, Inc.
<b>Safranin O (SO)</b> CAS Number: 477-73-6		350.85	Sigma-Aldrich

Except for CE, all others showed excellent solubility properties in ddH<sub>2</sub>O at room temperature. To overcome this solubility issue, dimethylformamide as an auxiliary solvent was added

(v/v = 25 %). Each stock solution was prepared in brown 1.5 mL microcentrifuge tubes to minimize exposure to light and was stored at -20 °C for further usage.

### Electron donors

As potential electron donors, 3-morpholinopropane-1-sulfonic acid (MOPS), 2-(N-morpholino)ethanesulfonic acid (MES) and ethylenediaminetetraacetic acid (EDTA) were added to the reaction mixture for whole-cell light-driven biotransformations (**Table 3**). While MOPS and MES are already used as buffer solutions during washing and resuspension of resting whole-cell biocatalysts, EDTA was added during final reaction mixture preparation provided as 500 mM aqueous stock solution (pH = 7.2).

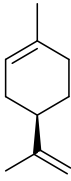
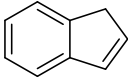
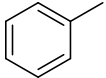
**Table 3: Electron donors used for whole-cell light-driven biotransformation experiments.**

Electron donor	Structure	MW [g mol <sup>-1</sup> ]	Supplier
<b>MOPS</b> CAS Number: 1132-61-2		209.3	Carl Roth GmbH
<b>MES</b> CAS Number: 4432-31-9		195.2	Carl Roth GmbH
<b>EDTA</b> CAS Number: 60-00-4		292.2	Carl Roth GmbH

### Substrates

Substrates provided during whole-cell biotransformation experiments in this project are summarized below. While (*R*)-limonene and indene are considered as suitable compounds for the conversion catalyzed by the respective Rieske oxygenases, glucose was added to enable NAD(P)H cofactor regeneration in the course of control experiments. Unlike (*R*)-limonene and indene, glucose was provided in the form of an aqueous stock solution (c = 200 mM)

Table 4: Substrates used in whole-cell biotransformation experiments.

Substrate	Structure	Purity	Supplier
( <i>R</i> )-Limonene CAS Number: 5989-27-5		97 %	Sigma-Aldrich
Indene CAS Number: 95-13-6		≥ 99 %	Sigma-Aldrich
Toluene CAS Number: 108-88-3		99.8 %	Sigma-Aldrich

### 2.1.11 Chemicals used for agarose gel electrophoresis

#### 50x TAE buffer (50x)

In total, 242 g of solid tris, 57.1 mL of acetic acid and 100 mL of EDTA stock solution (0.5 M, pH = 8) were dissolved in ddH<sub>2</sub>O to prepare 1 L of 50x TAE buffer.

#### Agarose polysaccharide

LabQ Standard Agarose LE (LabConsulting, Vienna, Austria) was used to prepare 1 % agarose gels for DNA-fragment separation via electrophoresis.

#### Fluorescence dyes for DNA detection

By the use of fluorescence dyes, DNA fragments separated via gel electrophoresis could be visualized under UV-light. All fluorescent agents used in this work are summarized in **Table 5**.

Table 5: Fluorescence dyes for DNA detection.

Fluorescence dye	Concentration	Supplier
Ethidium bromide	1 % in water	Carl Roth GmbH, Karlsruhe, Germany
GelGreen™	10 000X	LabQ, LabConsulting, Vienna, Austria
GelRed™	20 000X	LabQ, LabConsulting, Vienna, Austria

### Sample loading dye

In the course of sample preparation for gel electrophoresis, DNA gel loading dye (6X) supplied by Thermo Scientific™ (Massachusetts, USA) was used.

#### 2.1.12 Agents used for SDS-PAGE

### SDS-PAGE gels

Precast SDS-PAGE gels provided by GenScript (ExpressPlus™ 4-12%-PAGE Gels) or Invitrogen™ (NuPAGE Bis-Tris Gels, 4 – 12 %) were used in this project for qualitative protein separation.

### Running buffer

For the electrophoresis with GenScript precast gels, the Tris-MOPS-SDS running buffer (GenScript) was used. NuPAGE™ MES-SDS running buffer was used for related NuPAGE™ Bis-Tris Gels.

### Sample buffer and reducing agents

For sample preparation for SDS-PAGE with GenScript precast gels, a prestained sample buffer was used (Table 6).

**Table 6: Composition of prestained sample buffer used for SDS-PAGE with GenScript precast gels.**

Volume [mL]	Component
1.25	TRIS-HCl-solution (ph = 6.8), c = 0.5 M
2	SDS-solution, w = 10 %
0.5	β-mercaptoethanol
2.5	glycerol
3.75	ddH <sub>2</sub> O

Since the commercially available NuPAGE™ LDS sample buffer does not contain any reducing agent, the NuPAGE™ sample reducing agent (10x) has to be added separately during sample preparation.

### 2.1.13 Organic solvents used for GC sample preparation

In this work, GC-MS and GC-FID techniques were applied to determine residual substrate and products within the reaction mixtures. In **Table 7**, solvents and the corresponding internal standards used for the quantification via GC-MS or GC-FID are summarized.

**Table 7: Organic solvents and internal standards used for GC sample preparation.**

Substrate	Solvent	Internal Standard	GC Technique
(R)-Limonene	Dichloromethane	Acetophenone 2 mM	GC-FID
Indene	Dichloromethane	Acetophenone 2 mM	GC-MS
Toluene	ethyl acetate	Dodecane 2 mM	GC-FID

## 2.2 Microbiological Methods

### 2.2.1 Host strains

#### ***E. coli* Top10F'**

Genotype: *mcrA*,  $\Delta$ (*mrr-hsdRMS-mcrBC*), *Phi80lacZ*(del)M15,  $\Delta$ *lacX74*, *deoR*, *recA1*, *araD139*,  $\Delta$ (*ara-leu*)7697, *galU*, *galK*, *rpsL*(SmR), *endA1*, *nupG*

Due to the high transformation efficiency, chemically competent *E. coli* Top10 F' cells are commonly used for cloning and plasmid preparation. Furthermore, the mutation in *recA1* results in high stability of extrachromosomal DNA molecules, which is required for successful transformation.

#### ***E. coli* JM109**

Genotype: *endA1*, *recA1*, *gyrA96*, *thi*, *hsdR17* (*rk-*, *mk+*), *relA1*, *supE44*,  $\Delta$ (*lac-proAB*), [*F'* *traD36*, *proAB*, *laqlqZ* $\Delta$ M15]

Throughout the entire work, the *E. coli* JM109 strain was mainly used as a host for the expression of the respective recombinant proteins. One major advantage of this strain in

terms of molecular cloning is the enhanced stability of extrachromosomal DNA (plasmids) based on a mutated *recA* gene. Chemically competent cells for transformation were provided by Promega GmbH (Madison, USA).

### ***E. coli* JM109 (DE3)**

Genotype: *endA1, recA1, gyrA96, thi, hsdR17* ( $r_k^-$ ,  $m_k^+$ ), *relA1, supE44, λ-*,  $\Delta(lac-proAB)$ , [ $F'$ , *traD36, proAB, lacI<sup>q</sup>ZΔM15*], IDE3.

Non-competent *E. coli* JM109 (DE3) cells were provided by Promega GmbH (Madison, USA).

#### **2.2.2 Overnight cultures**

To prepare an overnight culture (ONC), 50 mL of LB-amp [ $\beta$ (ampicillin) = 0.1 g L<sup>-1</sup>] medium was inoculated with the respective cell material within a 300 mL baffled Erlenmeyer flask. For inoculation, either 50  $\mu$ L glycerol stock (stored at -20 °C or -80 °C) or a colony picked from an agar plate was used, respectively. To enable gas exchange during cultivation, the lid of the flask was closed with an autoclaved air-permeable cotton cloth. The overnight incubation, at 37 °C and 130 rpm, was carried out either in an incubation shaker or a tempered incubation room.

#### **2.2.3 Preparation of glycerol stocks**

For long-time storage of cells, 2 mL glycerol stocks were prepared. Therefore, a 1 mL aliquot of a high cell density suspension (ONC) was mixed with the equal amount of aqueous glycerol solution [ $w(\text{glycerol}) = 60\%$ ] within a 2 mL cryotube. Storage was performed at -20 °C or -80 °C respectively.

## 2.3 Molecular Biological Methods

### 2.3.1 DNA sequencing

The sequencing of DNA fragments was carried out by Microsynth Austria GmbH. Therefore a plasmid DNA concentration of 40 -100 ng  $\mu\text{L}^{-1}$  is required. Primers were added at a concentration of 2  $\mu\text{M}$ . All primers used for sequencing are summarized in **Table 31** and **Table 32**.

### 2.3.2 Plasmid constructs

#### **pUC19** (2686 bp)

The gene cluster of CDO was encoded within a pUC19 vector backbone (2686 bp), which is commonly used for molecular cloning and expression in *E. coli*. In this work, wild-type pUC19 is used as a control plasmid to evaluate background reactions. The vector map of pUC19 is depicted in **Figure 32A**.

#### **pINC** (7257 bp)

The construct designated as pINC refers to an incomplete (INC) variant of the wild-type CDO multi-protein complex. While the genes for the terminal  $\alpha$ -subunit (CumA1) and  $\beta$ -subunit (CumaA2) subunit of the terminal oxygenase, as well as the iron-sulfur protein Fd (CumA3), are unaltered, the reductase is shortened compared to the gene sequence of the CDO WT. This construct was provided by Hideaki Nojiri (The University of Tokyo, Japan) and was applied to generate the complete CDO by Gibson assembly<sup>®</sup> techniques. However, in this work, pINC was used as a control plasmid to evaluate the necessity of the reductase during conversion. The vector map for pINC is depicted in **Figure 32B**.

#### **pCDO\_M232A** (7690 bp)

The pUC19-based plasmid pCDO\_M232A contains a variant of the wild-type CDO with a mutation on position 232 in the catalytic subunit (CumA1), which results in an exchange of



the amino acid methionine to alanine. This variant was engineered by Gally *et al.* to enhance activity and selectivity toward various substrates.[23]

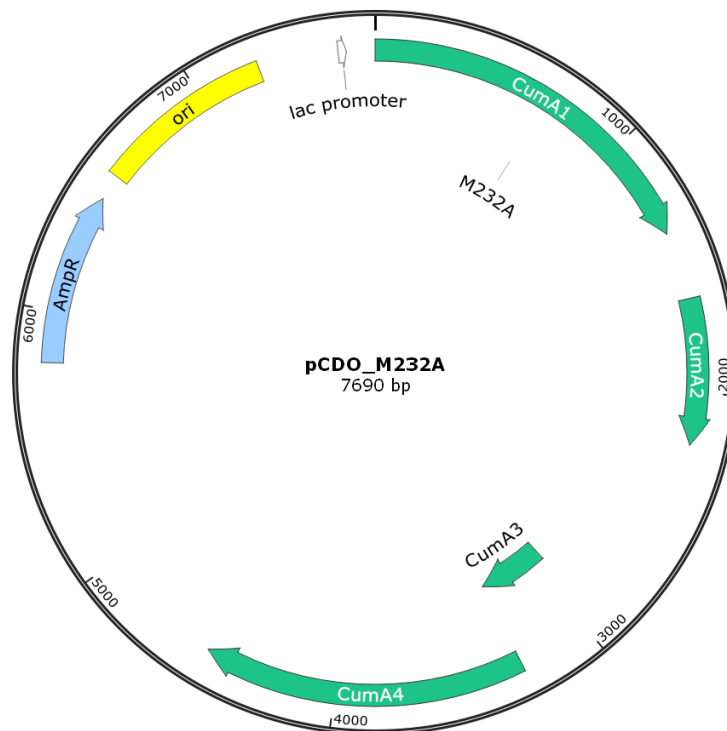


**Figure 4: pCDO\_M232A (7690 bp) vector map.** Green: Rieske oxygenase gene cluster; CumA1 (1380 bp):  $\alpha$ -subunit of CDO M232A; CumA2 (561 bp):  $\beta$ -subunit of CDO M232A; CumA3 (330 bp): ferredoxin; CumA4 (1236 bp): ferredoxin reductase. Yellow: Origin of replication (ColE1). Blue: ampicillin resistance gene (AmpR). M232A: single point mutation.

### NDO H295A (6192 bp)

The NDO was kindly provided by Rebecca Parales (College of Biological Sciences, California) encoded on the pDTG141 plasmid backbone under the control of a T7 promoter. An ampicillin resistance enables growth under selective pressure. The NDO H295A variant has been created previously by Fatma Feyza Özgen (Institute of Molecular Biotechnology, Graz University of Technology, Graz, Austria) via QuikChange™ mutagenesis and exhibits an amino acid exchange at position 295 within the  $\alpha$ -subunit of the oxygenase component (**Figure 5**). Halder *et al.* designed the NDO H295A variant in order to enhance activity and selectivity toward several substrates.[19] DNA-sequencing revealed a lack of a *lacI* gene on the vector backbone, which yields in an increased basal expression compared to a conventional pET-T7 expression system.

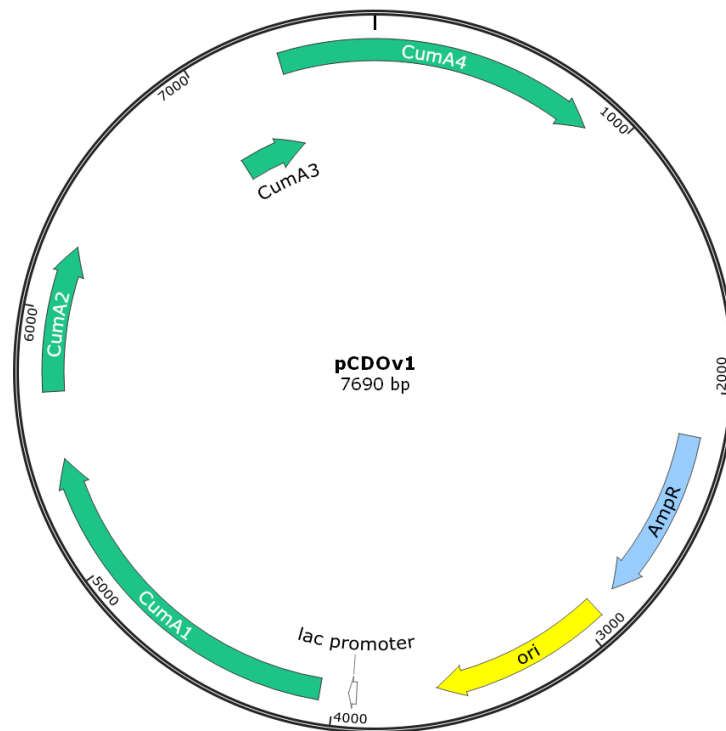


**Figure 5: pCDO\_M232A (6192 bp) vector map.** Green: Rieske oxygenase gene cluster; NDO  $\alpha$ -subunit (1350 bp); NDO  $\beta$ -subunit (585 bp); ferredoxin (315 bp); ferredoxin reductase (979 bp). Blue: Origin of replication (ColE1). Blue: ampicillin resistance gene (AmpR). H295A: single point mutation.

### 2.3.3 Preparation of chemo-competent *E. coli* cells

100 mL of LB-medium are inoculated with an ONC at an initial  $OD_{600}$  of 0.1. After incubation at 37 °C (200 rpm) and a cell density of  $OD_{600}$  0.4 - 0.5, cells were harvested for 15 min at 4 °C and 4000 x *g*. Afterward, the cell pellet was resuspended in 3.2 mL aqueous  $MgCl_2$ -solution and 30 mL Transformation buffer (TfB) 1 and subsequently incubated on ice for 15 min. After another centrifugation step (10 min, 4 °C, and 4000 x *g*), the obtained cell pellet was resuspended in 4 mL of TfB 2. This resuspension was then incubated on ice for 15 min before aliquoting á 50  $\mu$ L samples and stored at – 80 °C. The composition of the respective solutions used in this protocol is summarized in **Table 8**.

Table 8: Composition of buffers and MgCl<sub>2</sub> solution used for the preparation of chemo-competent *E. coli* cells.

500 mL Tfb1		500 mL Tfb2		50 mL MgCl <sub>2</sub> -solution	
Compound	Amount	Compound	Amount	Compound	Amount
Potassium acetate	1.47 g	Potassium chloride	0.37 g	MgCl <sub>2</sub> · 6 H <sub>2</sub> O	5.78g
Potassium chloride	3.73 g	Calcium chloride	5.55 g	ddH <sub>2</sub> O	Up to 500 mL
Calcium chloride	0.55 g	MOPS	1.05 g		
Glycerol	65 mL	Glycerol	65 mL		
ddH <sub>2</sub> O	Up to 500 mL	ddH <sub>2</sub> O	Up to 500 mL		

#### 2.3.4 Chemical transformation (heat shock method)

Each conducted chemical transformation in this work was carried out according to the following protocol:

5 µL of plasmid solution were added to a 50 µL aliquot of electrocompetent cells (stored at -80 °C) and incubated on ice for 20 min. After incubation at 42 °C for 42 seconds, the mixture was incubated on ice for two min. Afterward, 400 µL of LB-SOC medium were added, and cells were subsequently regenerated at 37 °C for 45 min. Finally, 100 µL or 200 µL were plated out onto an LB-amp agar plate and incubated at 37 °C overnight.

#### 2.3.5 Plasmid isolation

For plasmid isolation, a miniprep kit provided by either Promega (Wizard® Plus SV Minipreps DNA Purification System) or Thermo Scientific™ (Massachusetts, USA) GeneJET Plasmid Miniprep Kit was used. The standard protocol given by Promega GmbH (Madison, USA) was carried out with the following modifications:

For the final elution of plasmid DNA, 50 µL (protocol: 100 µL) preheated (60 °C) ddH<sub>2</sub>O was used.

### 2.3.6 Agarose gel electrophoresis

For DNA-fragment separation, the agarose gel electrophoresis is a commonly used technique in molecular biology. For this purpose, an agarose gel was prepared in advanced. Therefore, an appropriate amount of agarose polysaccharide (LabQ Standard Agarose LE, LabConsulting, Vienna, Austria) was dissolved in a corresponding amount of 1xTAE-Buffer to achieve a final concentration of 1 % agarose. Heating by the use of a microwave oven increased solubility. For visualization of DNA-molecules after electrophoresis, 4  $\mu$ L of ethidium bromide (EtBr)-solution ((EtBr) = 1 % in water, Carl Roth GmbH, Karlsruhe, Germany) per 100  $\mu$ L of gel was added. After complete polymerization, the gel was carefully transferred into an electrophoresis chamber filled with 1xTAE buffer and subsequently loaded with defined aliquots of DNA samples.

Running condition: 120V constant for approximately one hour by the use of the nanoPAC-300 power supply device.

### 2.3.7 Gel extraction

For the isolation of DNA fragments from an agarose gel, a clean-up kit (Wizard<sup>®</sup> SV Gel and PCR Clean-Up System) provided by Promega GmbH (Madison, USA) was used. Thereby, the standard protocol given by Promega GmbH (Madison, USA) was followed.

## 2.4 Biochemical Methods

### 2.4.1 Heterologous protein expression

To induce the expression of the respective enzymes, 400 mL or 200 mL of the liquid growth medium (TB-amp medium or ZYP-5052-amp medium, respectively) were inoculated with a proper amount of an ONC to an initial OD<sub>600</sub> of 0.1.

Afterward, the Erlenmeyer flask was sealed with an autoclaved air-permeable cloth and subsequently incubated again at 37 °C and 130 rpm by the use of the incubation shaker or within the incubation room. At a cell density in a range between OD<sub>600</sub> 0.6 and 0.8,

heterologous gene expression was induced. While adding isopropyl  $\beta$ -D-1-thiogalactopyranoside (IPTG) at a final concentration of  $c(\text{IPTG}) = 0.2 \text{ mM}$  is required to induce heterologous expression in TB-amp cultivated cells, induction of cells in ZYP-medium needs no supplementation of an inducing agent. The conditions for expression were adjusted to a temperature of constant  $30 \text{ }^\circ\text{C}$  and a rotation speed of  $130 \text{ rpm}$  for up to  $19 \text{ h}$ .

### 2.4.2 Protein extraction

BugBuster™ protein extraction represents a rapid and straightforward alternative to other mechanical methods like sonification or French press for cell disruption. Therefore, a specific volume of cell culture was pelleted and subsequently resuspended in  $150 \text{ }\mu\text{L}$  of BugBuster™ protein extraction reagent. After  $15 \text{ min}$  incubation at room temperature and a centrifugation step ( $16.000 \text{ rpm}$  for  $20 \text{ min}$ ), the supernatant, which represents the soluble fraction, was transferred into a new  $1.5 \text{ mL}$  microcentrifuge tube. After washing with SPB, the pellet was resuspended in  $150 \text{ }\mu\text{L}$  of the same buffer for further analysis (insoluble fraction). Throughout the entire project, the volume of cell culture for BugBuster™ protein extraction was calculated using **Equation (1)** below.

$$V(\text{cell culture, mL}) = \frac{7 \text{ mL}}{\text{OD}_{600}(\text{cell suspension})} \quad (1)$$

### 2.4.3 Protein separation via SDS-PAGE

For the protein separation via electrophoresis, precast SDS-PAGE gels were provided. During sample preparation,  $15 \text{ }\mu\text{L}$  aliquots of extract (soluble or insoluble fraction, respectively) were mixed with  $5 \text{ }\mu\text{L}$  of prestained SDS-sample buffer (x4) and incubated at  $95 \text{ }^\circ\text{C}$  for  $5 \text{ min}$  using a heat block. To avoid protein loss due to condensation events, the samples were shortly centrifuged. After the samples ( $25 \text{ }\mu\text{L}$ ) were loaded onto the SDS gel, the volt was set to  $200$ , and the amperage at  $60 \text{ mA}$  per SDS gel. Tris-MOPS-SDS or MES-SDS were applied as running buffers. After  $1 \text{ h}$  of electrophoresis, successful protein separation was achieved. The gel was stained by the use of a staining solution containing Coomassie blue. Destaining was conducted

with a destaining solution. The compositions of staining and destaining solutions are summarized in **Table 9** PageRuler™ prestained protein ladder (Thermo Scientific™, Massachusetts, USA) was used as a size marker.

**Table 9: Staining and destaining solution used for visualization of Proteins separated via SDS-PAGE**

Coomassie staining solution		Destaining Solution	
1 g	Coomassie Brilliant R-250	100 mL	glacial acetic acid
100 mL	glacial acetic acid (conc.)	300 mL	ethanol
300 mL	Ethanol	600 mL	ddH <sub>2</sub> O
600 mL	dH <sub>2</sub> O		

#### 2.4.4 Harvesting of *E. coli* cells

For *in vivo* biotransformation experiments, the whole-cell biocatalyst has to be available at a defined concentration. Furthermore, interfering cellular metabolic activities have to be minimized to obtain reproducible reaction outcomes regarding the actual conversion catalyzed by the respective Rieske enzymes. Because of this, *E. coli* cells harboring certain enzymes have to be transferred into a resting state, which is achieved by 15 min centrifugation at 4500 g and 4 °C. The remaining cell pellet was then washed in 50 mL of the respective buffer solution and centrifuged again under the same conditions as applied previously. The choice of the buffer depends on the electron donor investigated during the subsequent biotransformations. To determine the wet cell weight (WCW) of the whole-cell biocatalyst, the supernatant was carefully discarded before weighing; subtraction of the tare results in the WCW. For the sake of simplicity, the WCW was used as a value for the total biocatalyst mass. Related to that, the washed cell pellet was carefully resuspended in a calculated volume of corresponding buffer solution to establish a homogeneous cell suspension with a mass concentration of  $\beta(\text{cell suspension}) = 200 \text{ g(WCW) L}^{-1}$ . To minimize both undesired metabolic activities and cell death due to, e.g., apoptosis, the cells were continuously kept on ice.

#### 2.4.5 Light-driven biotransformations

To investigate and characterize the proposed light-driven hydroxylation catalyzed by the CDO and NDO variants, several whole-cell biotransformations were performed. By varying either

the reaction conditions and the composition of the reactants, it was supposed to obtain valuable knowledge about the considered reaction system. Each biotransformation mixture (total volume of 1 mL) was prepared in a 20 mL air-tight sealed GC glass vial (screw neck 24-400, Macherey-Nagel); to assure proper oxygen supply and to prevent alteration of concentrations by the loss of volatile organic compounds within the reaction mixture during the conducted experiments.

Regarding the proposed light-driven whole-cell approach, a standard reaction mixture contained the artificial electron donor, photosensitizer, substrate, resting cells as biocatalysts, and buffer solution to a final total volume of 1 mL. The biotransformations under light conditions were performed in the self-made light reactors at 30 °C and 120 rpm over a specific time. Alterations of standard reaction conditions are indicated in the result section at relevant positions.

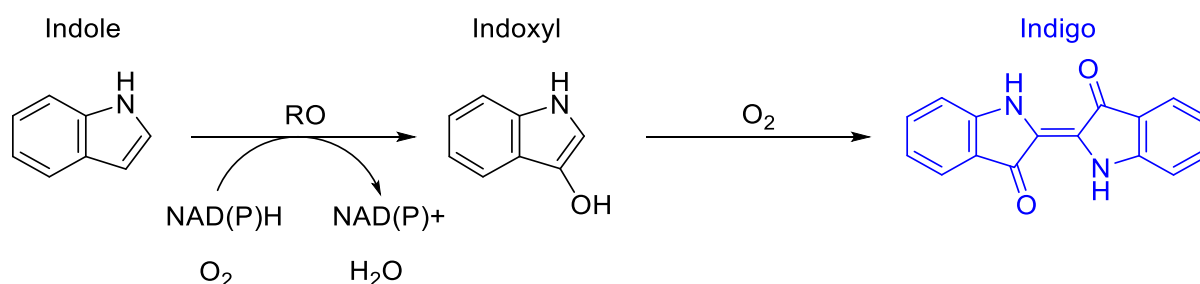
### 2.4.6 Growth experiments

For the purpose of investigating the cell growth behavior of *E. coli* cells in the presence of various organic compounds associated with the light-driven biotransformations, growth experiments were conducted. Therefore, 300 mL of TB-Amp (100 mg mL<sup>-1</sup>) growth medium were inoculated by a defined amount of preculture (*E. coli* JM109 (DE3)) containing NDO H295A) to an initial OD<sub>600</sub> of 0.1. This main culture was then inoculated at 37 °C and 120 rpm in an incubation shaker till a cell density of OD<sub>600</sub> 0.5. After partitioning into 50 mL aliquots, defined amounts of desired chemicals were added directly to the cultures. Cell growth was recorded every 30 min by measuring the OD<sub>600</sub> during incubation at 30 °C at 120 rpm over five hours.

### 2.4.7 Qualitative enzyme activity assay

Proposed by previous literature, an indole assay represents a simple and quick colorimetric method to screen for cells harboring the active Rieske enzymes.[16] This assay is based on the capability of Rieske oxygenases to catalyze the conversion of indole to indoxyl, which itself

undergoes a spontaneous dimerization reaction yielding in the formation of the natural dye indigo (**Scheme 7**).



**Scheme 7: Reaction mechanism of indigo formation during indole assay.** Indole is converted by a Rieske oxygenase (RO) to indoxyl. Spontaneous dimerization of indoxyl results in the formation of indigo, which can be detected as a color change to blue.

Practically, a Whatman filter soaked with a liquid mixture of indole (w = 10 %) in acetone was placed in the lid of a bottom-up culture agar plate showing single colonies of corresponding *E. coli* cells. After several minutes at room temperature, a color change of the respective colonies to dark blue indicates the hydroxylation of indole to indoxyl by an active oxygenase followed by spontaneous dimerization to indigo.

## 2.5 Biophysical Methods

### 2.5.1 Lyophilization of resting cell cultures

Freeze-drying of resting cells was performed in an AdVantage Pro freeze dryer with Intellitronics™ Controller. For that, a certain amount of entirely frozen cell mass (-80 °C) was lyophilized under vacuum until no residual water was observed. Freeze-dried biomass was stored at -80 °C for long time usage.

## 2.6 Analytics

### 2.6.1 GC sample preparation

After completed biotransformation, 500 µL of the reaction mixture were transferred into a 1.5 mL microcentrifuge tube. After adding a constant amount of solid sodium chloride (1



spatula micro spoon) to minimize the miscibility of the aqueous and organic phase during extraction, the mixture was vortexed for 3 seconds. After that, 500  $\mu\text{L}$  of the desired solvent were added to the mixture and vortexed. The mixture was centrifuged for 2 min at a rotation speed of 14.000 g by the use of a tabletop centrifuge. Since both the substrate and the products formed during biotransformation are considered as organic compounds, the organic phase is of higher interest for further analysis. To remove residual water within the organic phase, anhydrous magnesium sulfate ( $\text{MgSO}_4$ ) was used for dehydration. Therefore, the organic phase was carefully transferred into a new 1.5 mL microcentrifuge tube and thoroughly vortexed with anhydrous  $\text{MgSO}_4$ . After further centrifugation (10 min, 14.000 g), 200  $\mu\text{L}$  of extract were pipetted into a GC-vial equipped with a glass inlet.

### 2.6.2 Quantification of compounds of (*R*)-(+)-limonene conversion via GC-FID

Each GC-FID analysis was performed using a Shimadzu Nexis GC-2030 device equipped with an AOC-20i auto-injector module. For enantiomeric separation, a Hydrodex- $\beta$ -6TBDM capillary column was used. Furthermore, nitrogen was used as the carrier gas.

An overview of all applied parameters and the method of use are depicted in **Table 10**.

**Table 10: GC-FID parameters applied for quantitative analyses of organic compounds after biotransformation with (*R*)-limonene as substrate.**

<b>Chiral GC-FID parameters – (<i>R</i>)-limonene detection</b>	
Instrument	Nexis GC-2030 (Shimadzu Europa GmbH.)
Column	Hydrodex- $\beta$ -6TBDM (Macherey-Nagel)
Length	25 m, inner diameter: 0.25 mm, film thickness: 0.25 $\mu$ M
Injection volume	1 $\mu$ L
Injection temp.	230 °C
Injection mode	Split
Flow control mode	velocity
Pressure	83.1 kPa
Total flow	106.0 mL / min
Column flow	1.02 mL / min
Linear velocity	30 cm / s
Purge flow	3 mL / min
Split ratio	100
Oven temp. program	5 min at 100 °C, 15 °C min <sup>-1</sup> to 230 °C, 5 min at 230 °C
FID temperature	250 °C

For the determination of total quantities via the GC-FID method, the calibration curves of the respective organic compounds must be prepared initially. Expected products obtained from monooxygenation of pure (*R*)-limonene are (1*R*,5*S*)-carveol (**2a**), and (1*S*,5*S*)-carveol (**2b**) (**Scheme 3**). Additionally, the generation of carvone could be detected during biotransformation experiments, which was considered as an undesired byproduct. However, due to the impurity of the provided (*R*)-limonene substrate stock by small amounts of its counterpart (*S*)-limonene, the undesired formation of (1*S*,5*R*)-carveol and (1*R*,5*R*)-carveol could be additionally expected. Unfortunately, suitable stocks of (+)-carveols were not commercially available at that time. Under the assumption that (1*S*,5*R*)-carveol and (1*R*,5*R*)-carveol show similar chemical properties to their homologous configurational isomers (1*R*,5*S*)-carveol and (1*S*,5*S*)-carveol, calibration curves with a mixture of (-)-carveol isomers (Sigma-Aldrich) were established. Although not precisely described by the supplier, a racemic ratio of enantiomers was assumed. By plotting integrated peak areas (IPAs) against the respective concentrations, calibration curves could be generated.

In **Figure 6A**, the determined IPAs versus respective (*R*)-limonene (Retention time (RT) = 6.9 min) concentrations [mM] are plotted in a scatter diagram. The calibration curve for the

quantification of (1*S*,5*R*)-carveol (RT = 10.9 min) is depicted in **Figure 6B**. Settings applied for the quantitative GC-FID analysis are summarized in **Table 10**.

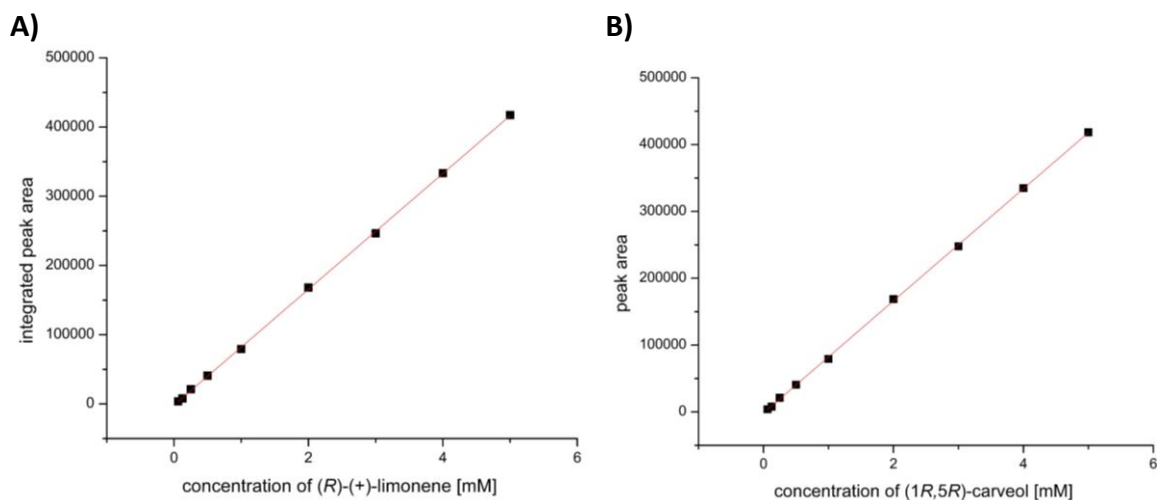


**Figure 6: Determined calibration curves for (*R*)-limonene and *trans*-carveol quantified via GC-FID.** A: Calibration curve for (*R*)-limonene (RT = 6.9 min):  $y = 83172x$ ;  $R^2 = 0.9998$ . B: Calibration for (1*S*,5*R*)-carveol (RT = 10.9 min):  $y = 83464x$ ;  $R^2 = 0.9998$ . Linear regression is depicted as a red line. Applied GC-FID parameters are summarized in **Table 10**.

Determined linear equations for (*R*)-limonene and (1*S*,5*R*)-carveol are summarized in **Table 11**.

In **Figure 7A**, the determined IPAs versus respective (1*R*,5*R*)-carveol (RT = 11.355 min) concentrations [mM] are plotted in a scatter diagram. The calibration curve for the quantification of carvone (RT = 10.886 min) is depicted in **Figure 7B**. Settings applied for the quantitative GC-FID analysis are summarized in **Table 10**.

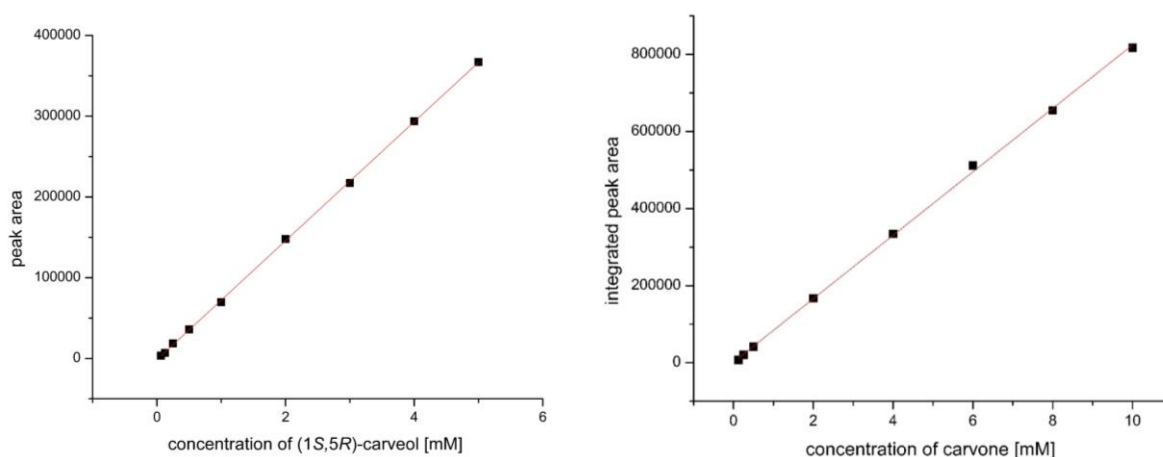


**Figure 7: Determined calibration curves for *cis*-carveol and carveone quantified via GC-FID.** A: Calibration curve for (1*R*,5*R*)-carveol (RT = 11.355 min):  $y = 73225x$ ;  $R^2 = 0.9998$ . B: Calibration for carveone (RT = 10.886 min):  $y = 82501x$ ;  $R^2 = 0.9994$ . Linear regression is depicted as a red line. Applied GC-FID parameters are summarized in **Table 10**.

Determined linear equations for (1*R*,5*R*)-carveol and carveone are summarized in **Table 11**.

**Table 11: Linear equation determined of compounds involved in the conversion of (*R*)-limonene.**

Compound	Linear equation	R <sup>2</sup>
( <i>R</i> )-Limonene	$Y = 83172X$	0.9998
(1 <i>S</i> ,5 <i>R</i> )-Carveol	$Y = 83464X$	0.9998
(1 <i>R</i> ,5 <i>R</i> )-Carveol	$Y = 73225X$	0.9998
Carvone	$Y = 82501X$	0.9994

Calibrations of (1*S*,5*R*)-carveol and (1*R*,5*R*)-carveol were also applied for quantification of (1*R*,5*S*)-carveol or (1*S*,5*S*)-carveol, respectively.

### 2.6.3 Quantification of compounds of indene conversion via GC-MS

For the quantitative detection of organic products formed in whole-cell biotransformations with indene as substrate, a Shimadzu GCMS type QP2010 device equipped with an inert capillary column type ZB-5MSi (Phenomenex®, Torrance, California) was used. Furthermore, helium was used as a carrier gas.

Detailed parameter settings are depicted in **Table 12** below.

**Table 12: GC-MS parameters used for quantitative analyses of organic compounds after biotransformation with indene as substrate.**

<b>GC-MS parameters – Indene detection</b>	
Instrument	GCMS-QP2010 SE (Shimadzu Europa GmbH.)
Column	Zebron ZB-5MSi (Phenomenex Inc.)
Length	30 m, inner diameter: 0.25 mm, film thickness: 0.25 $\mu$ M
Injection volume	1 $\mu$ L
Injection temp.	250 $^{\circ}$ C
Injection mode	Split
Flow control mode	linear velocity
Pressure	70.6 kPa
Total flow	14.8 mL / min
Column flow	1.17 mL / min
Linear velocity	39.5 cm / s
Purge flow	3 mL / min
Split ratio	9.1
Oven temp. program	4 min at 60 $^{\circ}$ C, 10 $^{\circ}$ C min <sup>-1</sup> to 340 $^{\circ}$ C, 4 min at 340 $^{\circ}$ C
<b>MS parameters</b>	
Ion source temp.	250 $^{\circ}$ C
Interface temp.	320 $^{\circ}$ C
Mode:	Scan
Scan range	50 – 500 m / z

Quantitative analysis of organic compounds was performed under the assumption that the sum of IPAs of expected products and residual indene substrate corresponds to the initial substrate concentration.

#### 2.6.4 Quantification of compounds of indene conversion via GC-FID and GC-MS

It is known from previous studies that CDO and NDO variants are capable of catalyzing the mono and *cis*-hydroxylation of indene yielding in 1H-indenol and both stereoisomers of 1,2-indanediol (**Scheme 4**). In order to quantify absolute concentrations of desired products or residual substrate within the reaction mixture after biotransformation, calibration curves for *cis*-/*trans*-1,2-indanediol via GC-FID were monitored. Furthermore, nitrogen was used as a carrier gas.

Detailed parameter settings are depicted in **Table 13** below.

**Table 13: GC-FID parameters used for quantitative analyses of organic compounds gained after biotransformation with indene as substrate.**

<b>Chiral GC-FID parameters – indene detection</b>	
Instrument	Nexis GC-2030 (Shimadzu Europa GmbH.)
Column	Hydrodex- $\beta$ -6TBDM (Macherey-Nagel)
Length	25 m, inner diameter: 0.25 mm, film thickness: 0.25 $\mu$ M
Injection volume	1 $\mu$ L
Injection temp.	230 °C
Injection mode	Split
Flow control mode	velocity
Pressure	70.1 kPa
Total flow	85.8 mL / min
Column flow	0.82 mL / min
Linear velocity	25.4 cm / s
Purge flow	3 mL / min
Split ratio	100
Oven temp. program	5 min at 100 °C, 15 °C min <sup>-1</sup> to 180 °C, 5 min at 200 °C, hold 5 min, 15 °C min <sup>-1</sup> to 230 °C, hold 5 min
FID temperature	250 °C

The total product concentrations were determined by comparing the obtained peak areas with the respective calibration curves for *cis*-1,2-indanediol and *trans*-1,2-indanediol. The IPAs applied for the calibration of *cis*-1,2-indanediol were considered as the sum of IPAs detected for (1*R*,2*S*)-indanediol (RT = 18 min) and (1*R*,2*R*)-indanediol (RT = 18.2 min). Regarding the calibration of *trans*-1,2-indanediol, IPAs of (1*R*,2*R*)-indanediol (RT = 19.2 min) and (1*S*,2*S*)-indanediol (RT = 19.4 min) were summarized.

In **Figure 8A**, the determined IPAs versus respective *cis*-1,2-indanediol concentrations [mM] are plotted in a scatter diagram. The calibration curve for the quantification of *trans*-1,2-indanediol is depicted in **Figure 8B**. Settings applied for the quantitative GC-FID analysis are summarized in **Table 13**.

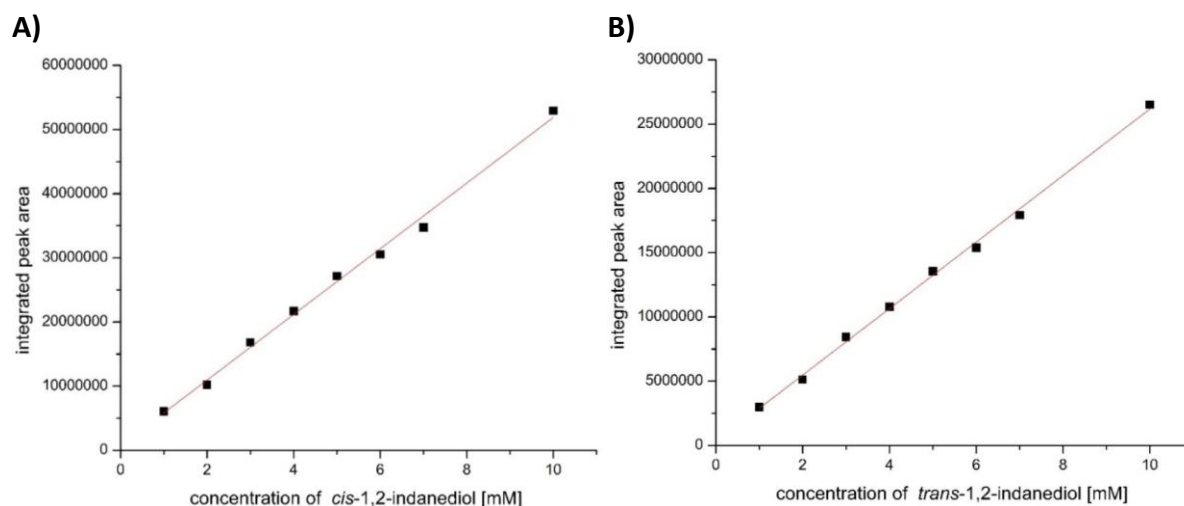


**Figure 8** Determined calibration curves for *cis*-1,2-indanediol and *trans*-1,2-indanediol monitored via GC-FID. A: Calibration curve for *cis*-1,2-indanediol:  $y = 7866783.16x$ ;  $R^2 = 1.0$ . B: Calibration for *trans*-1,2-indanediol:  $y = 7861699.17x$ ;  $R^2 = 1.0$ . Linear regression is depicted as a red line. Applied GC-FID parameters are summarized in **Table 13**.

Determined linear equations for *cis*- and *trans*-1,2-indanediol are summarized in **Table 11**.

**Table 14:** Linear equation determined for diastereomers of 1,2-indanediol.

Compound	Linear equation	$R^2$
<i>cis</i> -1,2-indanediol	$Y = 7866783.16X$	1.0
<i>trans</i> -1,2-indanediol	$Y = 7861699X$	1.0

Since no 1H-indenol was commercially available, the concentration was determined by a mathematical approach using the corresponding response factors ((5)). Therefore, a calibration curve for 1-indanone (**Table 12**) was used as a template for the quantification of 1H-indenol via the effective carbon number (ECN) approach.

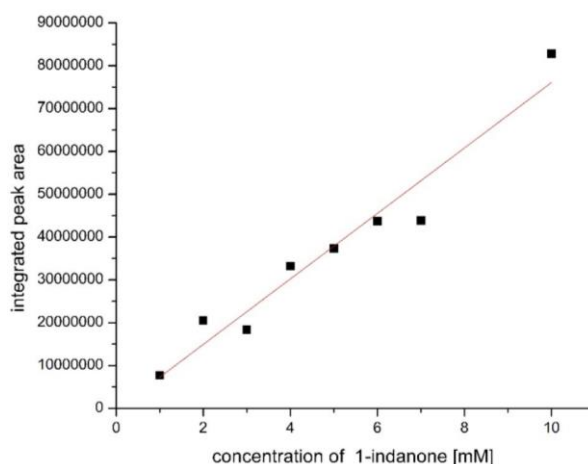


**Figure 9: Determined calibration curve for 1-indanone determined via GC-MS.**  $Y = 7586716.16x$ ;  $R^2 = 0.95$ . Linear regression is depicted as a red line. Applied GC-MS parameters are summarized in **Table 12**

The linear equation of the described calibration curve for 1-indanone is shown in equation (2).

$$y = 7861699.17 \times x \quad (2)$$

In this work, equation (2) was used to estimate the total concentration of 1-indanone and serves as a template for the ECN calculating approach to determine the concentration of 1H-indenol. Based on the calibration curve for the 1-indanone byproduct (**Figure 9**), a calibration for 1H-indenol could be established by using the relative response factor (RRF) and the IPAs of both compounds. The RRF is defined as the ratio of response factors (RF) for the compound of interest (1H-indenol) to the RF of a known internal standard (IS), which is, in this case, stated as the 1-indanone (3).

$$RRF = \frac{RF(1H-indenol)}{RF(1-indanone)} \quad (3)$$

The values for described response factors used in (3) are determined as the ratio of the ECNs of 1H-indenol to 1-indanone (4).

$$RF(1H-indenol) = \frac{ECN(1H-indenol)}{ECN(1-indanone)} \quad (4)$$

The literature values for the respective ECNs and the determined RFs for both compounds are summarized in **Table 15**.



Table 15: Overview of ECNs and RFs for 1H-indenol and 1-indanone.

Compound	ECN	RF
1H-indenol	8.35	0.93
1-indanone	9	1

Finally, the concentration of 1H-indenol can be calculated using equation (5) below.

$$c(1\text{H-indenol, mM}) = \frac{\text{IPA}(1\text{H-indenol})}{\text{IPA}(1\text{-indanone}) \times \text{RRF}} \times c(1\text{-indanone, mM}) \quad (5)$$

### 2.6.5 Quantification of products of toluene via GC-FID

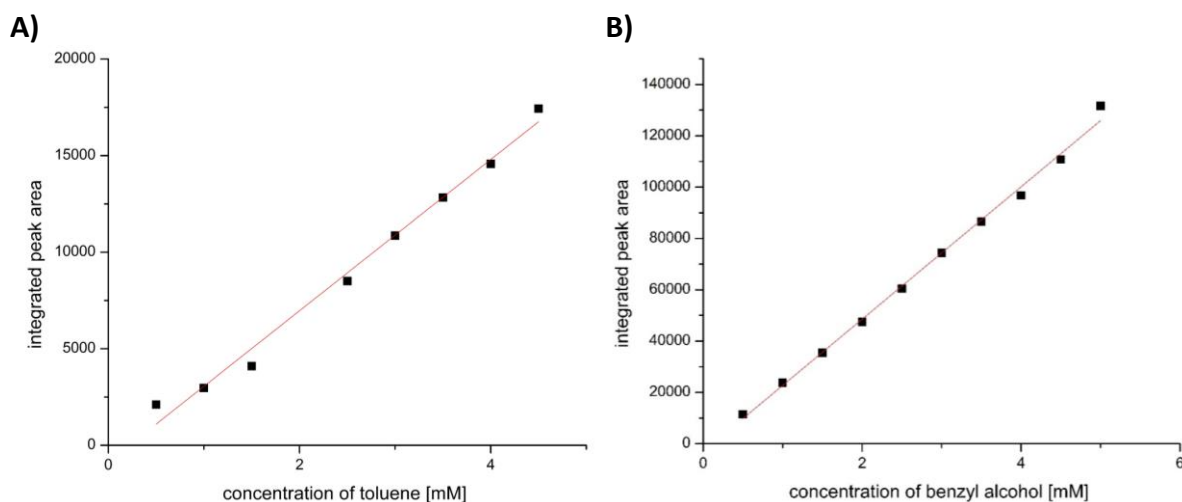
For the quantitative detection of organic products formed during whole-cell biotransformations with toluene as substrate via GC-FID, a Shimadzu GC-FID type Nexis GC-2030 device equipped with a Hydrodex- $\beta$ -6TBDM (Macherey-Nagel) was used. Detailed parameter settings are depicted in **Table 16** below.

Table 16: GC-FID parameters used for quantitative analyses of organic compounds gained after biotransformation with toluene.

<b>Chiral GC-FID parameters – Toluene detection</b>	
Instrument	Nexis GC-2030 (Shimadzu Europa GmbH.)
Column	Hydrodex- $\beta$ -6TBDM (Macherey-Nagel)
Length	25 m, inner diameter: 0.25 mm, film thickness: 0.25 $\mu\text{M}$
Injection volume	1 $\mu\text{L}$
Injection temp.	230 $^{\circ}\text{C}$
Injection mode	Split
Flow control mode	velocity
Pressure	76.1 kPa
Total flow	115.1 mL / min
Column flow	1.11 mL / min
Linear velocity	30.0 cm / s
Purge flow	3 mL / min
Split ratio	100
Oven temp. program	5 min at 60 $^{\circ}\text{C}$ , 10 $^{\circ}\text{C min}^{-1}$ to 230 $^{\circ}\text{C}$ , hold 5 min at 230 $^{\circ}\text{C}$
FID temperature	250 $^{\circ}\text{C}$

As described in the introduction section, the NDO H295A variant shows an enhanced activity for the conversion of toluene to benzyl alcohol compared to NDO wildtype. In order to

quantify the concentration of either the substrate or the desired product after the biotransformation, respective calibration curves for each compound were established via GC-FID. In **Figure 8A**, the determined IPAs versus respective toluene (RT = 5.817 min ) concentrations [mM] are plotted in a scatter diagram. The calibration curve for benzyl alcohol (RT = 10.886 min) is depicted in **Figure 8B**. Settings applied for the quantitative GC-FID analysis are summarized in **Table 13**.



**Figure 10: Determined calibration curves for toluene and benzyl alcohol quantified via GC-FID.** A: Calibration curve for toluene (RT = 5.817 min):  $y = 3974.8x$ ;  $R^2 = 0.9003$ . B: Calibration for benzyl alcohol (RT = 10.886 min):  $y = 24920x$ ;  $R^2 = 0.9945$ . Linear regression is depicted as a red line. Applied GC-FID parameters are summarized in **Table 16**.

Determined linear equations for toluene and benzyl alcohol are summarized in **Table 11**.

**Table 17: Linear equation determined for enantiomers of 1,2-indanediol.**

Compound	Linear equation	$R^2$
Toluene	$Y = 3974.8X$	$R^2 = 0.9003$
Benzyl alcohol	$Y = 24920X$	$R^2 = 0.9945$

## 3 Results

### 3.1 Expression studies with CDO M232A and NDO H295A

In the multicomponent electron transfer systems of both CDO and NDO, four distinct proteins are involved, which are termed as reductase, Fd, and large and small subunits of the oxygenases. However, sufficient expression levels of each described protein are essential for high activities in whole-cell biotransformations. To investigate the formation of soluble and thus active proteins over time, expression studies with CDO M232A and NDO H295A were carried out. Although all ORFs (CumA1, CumA2, CumA3, and CumA4) involved in the multicomponent CDO system are under the control of a single lac promoter (-140 bp of ORF1), the conducted expression studies show a significant difference in the formation of the target proteins in *E. coli* JM109 cells. This circumstance was observed by protein analysis via SDS-PAGE. Both the soluble and insoluble fraction obtained due extraction were separated through SDS-PAGE. **Figure 11** shows a Coomassie-stained SDS-PAGE gel after accomplished protein separation.

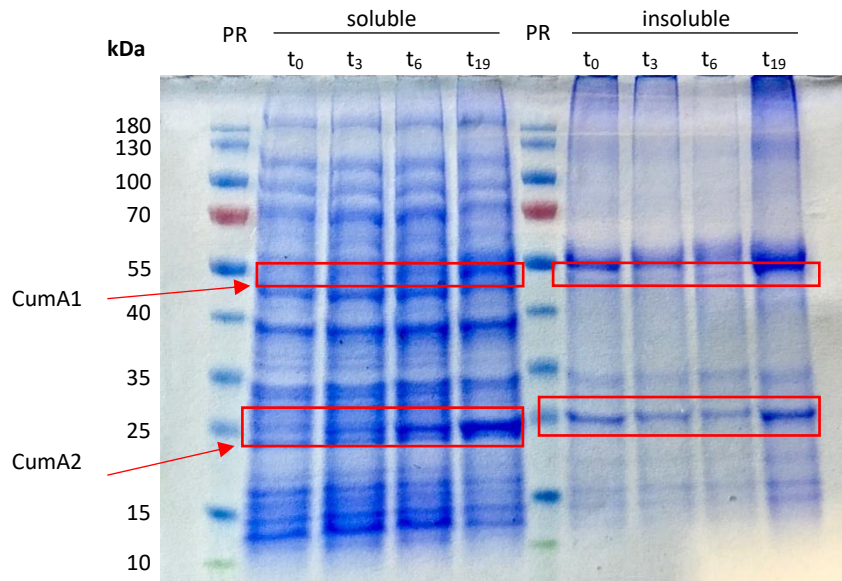


**Figure 11: Coomassie-stained SDS-PAGE gel (4-12 %) showing separated soluble and insoluble proteins obtained after 19 h expression of CDO M232A in *E. coli* JM109.** Lane 1 and 6 contain a prestained protein ladder (PageRuler™, Thermo Scientific™, Massachusetts, USA) as a standard. Lanes 2-5 shows the soluble protein fractions after 0, 3, 6, and 19 h expression of *E. coli* JM109 harboring the pCDO\_M232A construct. Lanes 8-10 show the respective insoluble fractions. Protein size: CumA1 52.3 kDa; CumA2: 23.4 kDa; CumA3: 11.8 kDa; CumA4: 43.3 kDa. Separation conditions: 200V and 60 mA for 1 h.

While a significant increase of the small  $\beta$ -subunit (CumA2) with a molecular weight of 23.4 kDa could be detected in either the soluble or insoluble fractions, the larger  $\alpha$ -subunit (CumA1) with a molecular weight of 52.3 kDa shows only a slight increase in the soluble fraction. Furthermore, a weak band at the height of 43.3 kDa is visible in the soluble fractions, which could be assigned to the FdR (CumA4). No formation of Fd (11.8 kDa) could be observed in both protein fractions. However, it is assumed that the resolution quality of the SDS-PAGE gel is insufficient to detect small amounts of Fd. All relevant proteins and their corresponding molecular masses in kDa are summarized in **Table 18**.

**Table 18: Proteins involved in the multicomponent system of CDO.**

Gene	Protein	Molecular mass [kDa]
CumA1	Large subunit of CDO ( $\alpha$ )	52.3
CumA2	Small subunit of CDO ( $\beta$ )	23.4
CumA3	Fd	11.8
CumA4	FdR	43.3

Unlike the CDO, the gene cluster for NDO variant H295A is encoded on a pDTG141 vector backbone controlled by a T7-promoter. However, the *lacI* gene in the promoter region is missing. Thus, a tightly controlled expression as compared to a conventional pET System could not be expected. To investigate the formation of the corresponding NDO H295A proteins over time, expression studies with *E. coli* JM109 were initially performed. For that, samples were taken at specific time-points before ( $t_{-1}$ ) and during 18 h expression after induction with IPTG. As a control sample after 18 h-expression of *E. coli* harboring the empty vector backbone pUC19 were taken. After protein extraction, the soluble and insoluble protein fractions were separated via SDS-PAGE by the use of bis-tris gels (4 – 12 %) and MES-buffer. The Coomassie-stained gel is depicted in **Figure 13** below.

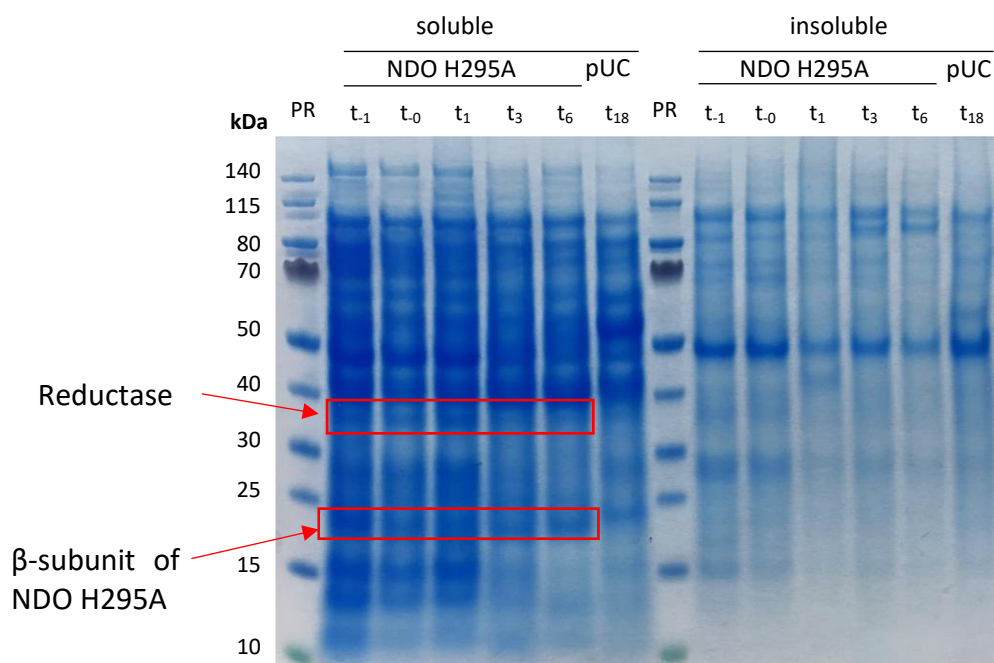


**Figure 13: Coomassie-stained SDS-PAGE gel (bis-tris gels, 4 – 12 %) showing separated soluble and insoluble proteins obtained after 18 h expression of NDO H295A in *E. coli* JM109.** Lane 2-6 shows the soluble fractions of proteins expressed by *E. coli* JM109 (NDO H295A) 1 h before and 0, 1, 3, 6, 18 h after induction. Corresponding insoluble fractions are visualized in lane 9-13. Soluble and insoluble protein fractions obtained after 18 h expression of *E. coli* JM109 (NDO H295A) are separated in lane 7 or 14, respectively. *E. coli* JM109 cells harboring an empty pUC vector were used as controls. PR: Protein ladder (PageRuler™, Thermo Scientific™)

Weak bands corresponding to the FdR (35.5 kDa) and the small  $\beta$ -subunit (22.94 kDa) of the NDO H295A could be detected in the soluble protein fractions. However, both bands are also visible in the sample taken one hour before induction, which indicates a basal expression due

to a leaky promoter. Strong bands visible in both the soluble and insoluble fractions in all samples indicates the presence of an unspecific protein with similar size of the  $\alpha$ -subunit (49.61 kDa) of NDO H295A. Because of that, a proper evaluation of expression levels of the larger subunit is not possible. However, heterologous expression of the small Fd component could not be observed. Relevant proteins of the multicomponent system of the NDO H295A and their corresponding molecular masses are summarized in **Table 19**.

**Table 19: Proteins involved in the multicomponent system of NDO.**

Protein	Molecular mass [kDa]
Large subunit of NDO ( $\alpha$ )	49.61
Small subunit of NDO ( $\beta$ )	22.94
Fd	11.45
FdR	35.51

Expression studies with *E. coli* JM109 (DE3) harboring pDTG141\_NDOH 295A revealed no further improvements in the expression levels of each component of the NDO system.

## 3.2 Light-driven whole-cell biotransformation experiments

### 3.2.1 Absorbance spectra of photosensitizers

In order to investigate the absorption behavior of PSs used in this project, the absorbances at different wavelengths were recorded. Therefore, aqueous dilutions of each prepared PS stock solution (20 mM) were measured within a range of 400 nm and 650 nm at a scan rate of 600 nm min<sup>-1</sup> and an interval of 1 nm.

The spectrum of each used PS was determined and are depicted as an overlapping line graph in **Figure 14**.

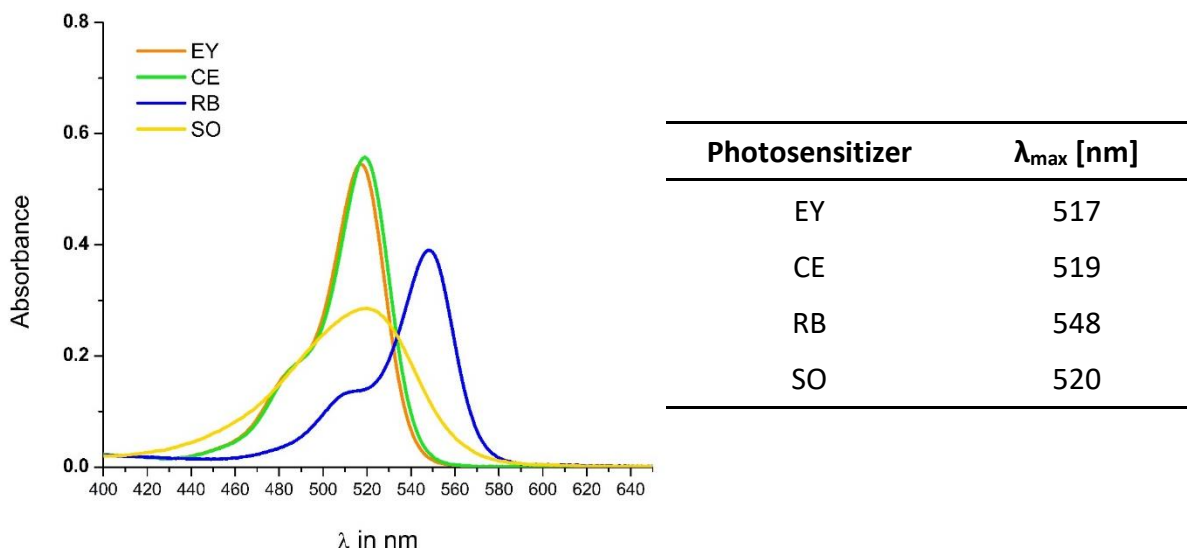


**Figure 14: UV-Vis spectra of PSs used for corresponding light-driven whole-cell biotransformation experiments.** Left: Spectra recorded within a wavelength ( $\lambda$ ) of 400 nm to 650 nm and a scan rate of 600 nm min<sup>-1</sup>. Right: wavelengths at detected absorbance maxima.  $\lambda$  = wavelength.

The UV-Vis spectra determined for EY, CE, and SO reveal absorbance maxima at a wavelength of approximately 520 nm. Although RB shows an absorbance maximum at 548 nm, all investigated PSs exhibit optimal photoexciting at wavelengths covering the green light.

### 3.2.2 Influence of electron donor on product formation

Previous work revealed that EDTA as a sacrificial electron donor in light-driven whole-cell biotransformations of (*R*)-limonene with CDO yields in low conversions.[73] However, EDTA is also known as a chelating agent which has the potential to form stable complexes by binding metal cations like Fe<sup>3+</sup>. Since the hydrophobic active site of the terminal oxygenase  $\alpha$ -subunit (CumA1) contains a mononuclear iron in its native form, it can be concluded that the provided EDTA can sequester the metal iron(III) in its ferrous oxidized state. Thus, no O<sub>2</sub> activation would occur, which results in a loss of enzyme activity. To avoid this, biotransformations with either MOPS or MES as an alternative were carried out. The product concentrations obtained in the light-driven whole-cell hydroxylation reaction of (*R*)-limonene by using EDTA or MOPS

as electron donors, respectively, are shown in **Figure 15**.

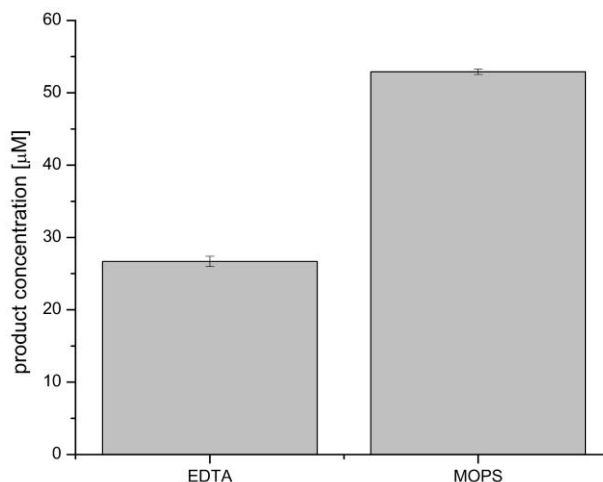


**Figure 15** Observed product formation after 24 h of *in vivo* biotransformation of (*R*)-(+)-limonene with *E. coli* CDO M232A under light conditions. Reaction conditions: 100 μM SO, 10 mM (*R*)-limonene, 25 mM EDTA/ 50 mM MOPS, 100 g<sub>WCW</sub> L<sup>-1</sup> whole cells (19h expression), white light (max. 230 μmol m<sup>-2</sup> s<sup>-1</sup>), 30°C, 120 rpm. Reactions were carried out in duplicates. Standard deviations are indicated as error bars.

The reactions were carried out in duplicates. Results are summarized in **Table 20**

**Table 20:** Determined product concentrations obtained after biotransformations of (*R*)-limonene with different *E. coli* JM109 CDO\_M232A cells using (*R*)-limonene as substrate.

Electron Donor	c(Product), μM	σ
EDTA (25 mM)	26.69	0.72
MOPS-buffer (50 mM)	52.91	0.37

Reaction conditions: 100 μM SO, 10 mM (*R*)-limonene, 25 mM EDTA/ 50 mM MOPS, 100 g<sub>WCW</sub> L<sup>-1</sup> whole cells (19h expression), white light (max. 230 μmol m<sup>-2</sup> s<sup>-1</sup>), 30°C, 120 rpm. Reactions were carried out in duplicates.

### 3.2.3 The effect of cell lyophilization on product formation

To enhance the permeability of the cell membrane in order to facilitate an easier PS and substrate uptake, lyophilization of *E. coli* JM109 cells harboring the CDO, cultivated in ZYP-5052-amp medium, was carried out. To evaluate a correlation between lyophilized cells and product formation during biotransformations, experiments in the dark were performed by adding 20 mM glucose for cofactor regeneration and 10 mM (*R*)-limonene as substrate. The product yields obtained at different amounts of catalysts are displayed in **Figure 16**.



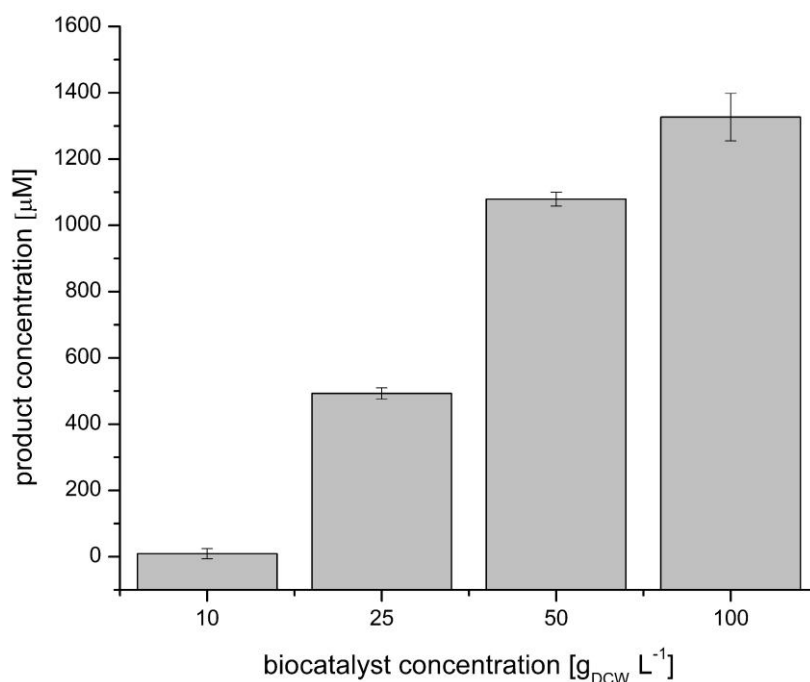


**Figure 16: Correlation between lyophilized cell concentration (*E. coli* JM109 pCDO\_M232A) and product formation ((1*R*,5*S*)-carveol) after 24 h.** Reaction conditions: 10 mM (*R*)-limonene, 50 mM SPB, 10-100 g<sub>DCW</sub> L<sup>-1</sup> whole cells (19h expression), 20 mM glucose, 30°C, 120 rpm. Reactions were carried out in duplicates. Standard deviations are indicated as error bars.

It is apparent that the carveol product formation increases with the amount of cells used as biocatalysts. Thereby a maximum product formation of approximately 1.3 mM could be detected in the presence of 100 g<sub>DCW</sub> L<sup>-1</sup>. The obtained product concentrations are summarized in **Table 21**.

**Table 21: Determined product concentrations obtained after 24 h-biotransformations with different concentrations of lyophilized *E. coli* JM109\_pCDO\_M232A cells and (*R*)-limonene as substrate.**

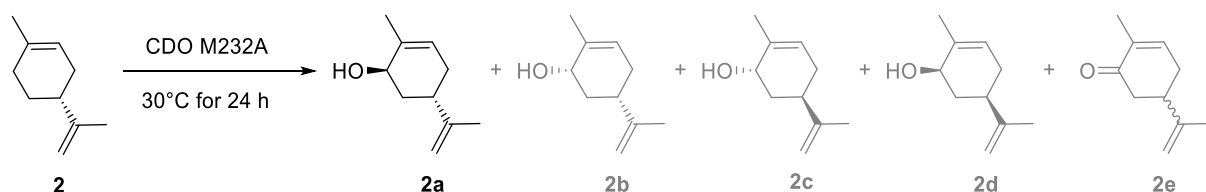
Biocatalyst concentration [g <sub>DCW</sub> L <sup>-1</sup> ]	Product concentration [μM]
10	9.23 ± 15.40
25	492.61 ± 16.99
50	1079.0 ± 21.08
100	1326.47 ± 71.53

Reaction conditions: 10 mM (*R*)-limonene, 50 mM SPB, 10-100 g<sub>DCW</sub> L<sup>-1</sup> whole cells (19h expression), 20 mM glucose, 30°C, 120 rpm. Reactions were carried out in duplicates.

However, analogous experiments with *E. coli* JM109 cells harboring CDO M232A cultivated in TB-amp medium indicate no product formation beyond a background reaction. Based on these findings, it is assumed that the choice of medium has a significant effect related to the stability of the enzyme. This effect can be attributed to a higher concentration of salts within the ZYP-5052 medium, which may function as cryo-protectors.

### 3.2.4 Products obtained in light-driven hydroxylation of (*R*)-(+)-limonene

As described in literature, CDO M232A favors the formation of (1*R*,5*S*)-carveol in the whole-cell conversion of (*R*)-limonene.[23] During the course of the whole-cell biotransformations conducted in the current project, byproduct formation of (1*S*,5*S*)-carveol, (1*S*,5*R*)-carveol, (1*R*,5*R*)-carveol and carvone could be observed (**Scheme 8**).



**Scheme 8: Products observed in whole-cell biotransformations with (*R*)-limonene.** 2: (*R*)-limonene, 2a: (1*R*,5*S*)-carveol, 2b: (1*S*,5*S*)-carveol, 2c: (1*S*,5*R*)-carveol, 2d: (1*R*,5*R*)-carveol, 2e: carvone.

To evaluate the byproduct formation during whole-cell biotransformations with (*R*)-limonene under light illumination, light reactions with carboxyeosin (CE) as a photosensitizer, and MES as electron donor were performed. As a control, biotransformations under dark conditions with glucose supplementation by using *E. coli* cells containing CDO M232A were carried out. The observed product concentrations are summarized in **Table 22**.

**Table 22: Product and byproduct formation in**

Product	Product concentration [ $\mu\text{M}$ ]	
	Dark + Glucose	Light + CE/MES
(1 <i>R</i> ,5 <i>S</i> )-Carveol	1141.3 $\pm$ 34.9	340.5 $\pm$ 30.9
(1 <i>S</i> ,5 <i>S</i> )-Carveol	28.1 $\pm$ 1.4	4.1 $\pm$ 0.1
(1 <i>S</i> ,5 <i>R</i> )-Carveol	5.7 $\pm$ 0.1	13.1 $\pm$ 0.4
(1 <i>R</i> ,5 <i>R</i> )-Carveol	13.4 $\pm$ 0.4	7.5 $\pm$ 0.8
Carvone	0.7 $\pm$ 0.0	4.5 $\pm$ 0.3

Reaction conditions: 10 mM (*R*)-limonene 100 g<sub>WCW</sub> L<sup>-1</sup> whole cells (19h expression), 30°C, 140 rpm; Dark conditions: 50 mM SPB, 20 mM glucose; Light conditions: 100  $\mu\text{M}$  CE, 50 mM MES, white light (max. 230  $\mu\text{mol m}^{-2} \text{s}^{-1}$ ), 30°C, 120 rpm. Reactions were carried out in duplicates.

While reactions under light illumination (CE and MES) result in a product ratio (main product/byproduct) of 92 : 8, the byproduct ratio generated in the corresponding dark reaction with glucose supplementation is 95:5. The control experiments without CDO M232A were performed to evaluate a possible background conversion. Therefore, *E. coli* JM109 cells

harboring the empty pUC19 vector backbone were used in whole-cell biotransformations under light (MES/CE) and dark (with glucose supplementation) (**Table 23**).

**Table 23: Byproduct formation in**

Product	Product concentration [ $\mu\text{M}$ ]	
	Dark + Glucose	Light + CE/MES
(1 <i>R</i> ,5 <i>S</i> )-Carveol	4.9 $\pm$ 0.3	7.1 $\pm$ 0.2
(1 <i>S</i> ,5 <i>S</i> )-Carveol	0.7 $\pm$ 0.2	3.5 $\pm$ 0.5
(1 <i>S</i> ,5 <i>R</i> )-Carveol	5.5 $\pm$ 0.4	15.5 $\pm$ 0.08
(1 <i>R</i> ,5 <i>R</i> )-Carveol	4.1 $\pm$ 0.2	8.1 $\pm$ 0.6
Carvone	0.2 $\pm$ 0.2	3.2 $\pm$ 0.2

Reaction conditions: 10 mM (*R*)-limonene 100 g<sub>wcW</sub> L<sup>-1</sup> whole cells (19h expression), 30°C, 140 rpm; Dark conditions: 50 mM SPB, 20 mM glucose; Light conditions: 100  $\mu\text{M}$  CE, 50 mM MES, white light (max. 230  $\mu\text{mol m}^{-2} \text{s}^{-1}$ ), 30°C, 120 rpm. Reactions were carried out in duplicates.

Based on this, background reactions up to 15.5  $\mu\text{M}$  regarding (1*S*,5*R*)-carveol byproduct formation could be observed. Except for (1*R*,5*S*)-carveol, background formation seems to have a crucial impact on the overall product formation in light-driven conversions of (*R*)-limonene. In total, 98 % formation of (1*R*,5*S*)-carveol can be contributed to the light-driven whole-cell reaction catalyzed by CDO M232A.

### 3.2.5 Choice of substrate for biotransformation with CDO M232A and NDO H295A

Based on previous results, (*R*)-limonene was considered as a suitable substrate for the light-driven whole-cell biotransformations catalyzed by CDO M232A.[73] To extend the scope of promising substrates for the proposed cofactor-free light-driven approach, indene and toluene were additionally investigated. Thereby, light-driven biotransformations with CDO M232A and NDO H295A in the presence of CE (100  $\mu\text{M}$ ) and MES (50 mM) were conducted. Furthermore, control reactions in the dark with glucose (20 mM) were carried out. In all reactions, the relevant substrates were applied at concentrations of 10 mM. The associated product formations obtained after 24 h of biotransformations with whole-cell *E. coli* biocatalysts (100 g<sub>wcW</sub> L<sup>-1</sup>) harboring CDO M232A or NDO H295A are depicted in **Figure 42**. The highest amount of hydroxylated products could be obtained by the light-driven reaction with indene yielding in the formation of 8.5 mM 1-indenol and 1,2-indanediol after 24 h under white light illumination (max 230  $\mu\text{mol m}^{-2} \text{s}^{-1}$ ). However, corresponding biotransformations with (*R*)-limonene or toluene show the result in significant lower conversions. While the light-

driven conversion of (*R*)-limonene yields in the formation of 0.34 mM product, the use of the latter substrate show product formations of up to 0.209 mM. The control reactions in the presence of glucose yielded in slightly higher product formations in the course of conversions of (*R*)-limonene (1.16 mM) and toluene (0.63 mM). However, corresponding biotransformations of indene in the dark revealed a significant lower product formation (2.2 mM) compared to the associated reaction under light conditions in the presence of CE and MES (8.5 mM). Based on these findings, indene was considered as the most suitable substrate for the characterization and optimization of the investigated cofactor-free light-driven whole-cell approach.

### 3.2.6 Effect of biocatalyst concentration on product formations

To evaluate the optimum concentration of biocatalyst in terms of maximum conversion, experiments with various cell densities (*E. coli* JM109) harboring the CDO variant M232A were performed. The whole-cell reactions were carried out under dark conditions and by supplementation of 20 mM glucose. In **Figure 17**, the obtained product concentrations after 24 h catalyzed by different amounts of resting *E. coli* cells are shown. Although the product yield of (1*R*,5*S*)-carveol increases proportionally from 1.27 mM to 2.77 mM by the increase of the cell concentration from 10 to 25 g<sub>wcW</sub> L<sup>-1</sup>, higher biocatalyst concentrations seem to have no further effect on the overall product formation.

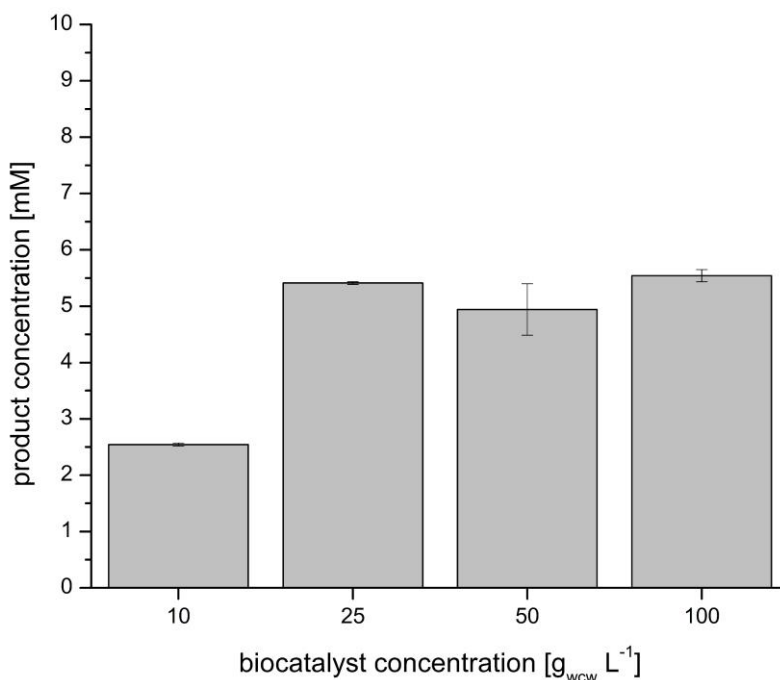


**Figure 17: Correlation between cell concentration (*E. coli* JM109 pCDO\_M232A\_V205G) and product formation ((1*R*,5*S*)-carveol) after 24 h.** Reaction conditions: 10 mM (*R*)-limonene in DMSO, 50 mM SPB, 10-100  $\text{g}_{\text{wCW}} \text{L}^{-1}$  whole cells (19h expression), 20 mM glucose, 30°C, 120 rpm. Reactions were carried out in duplicates. Standard deviations are indicated as error bars.

Hence, 100  $\text{g}_{\text{wCW}} \text{L}^{-1}$  was considered as the optimum concentration of biocatalyst in the biotransformation of (*R*)-limonene under dark conditions and natural cofactor regeneration. To investigate the optimum concentration of resting *E. coli* cells in the light-driven biotransformations with indene as substrate, whole-cell experiments were carried out at ascending cell densities. Furthermore, a possible correlation between electron donor concentration and product formation was examined by using MES buffer at two different concentrations. According to this, reaction mixtures containing 100  $\mu\text{M}$  CE as PS, 25 – 300  $\text{g}_{\text{wCW}} \text{L}^{-1}$  *E. coli* JM109 cells harboring NDO H295A and MES buffer at a concentration of 50 mM or 100 mM were prepared. As a substrate, 10 mM indene was added. After 24 h of incubation at 30 °C and 120 rpm, the obtained product concentrations were determined (**Figure 18**). Although an increase of biocatalyst from 25 to 100  $\text{g}_{\text{wCW}} \text{L}^{-1}$  seems to have a positive effect on the overall product formation in the presence of both, 50 mM and 100 mM MES buffer, a higher amount of resting cells show no further product accumulation. A maximum of 9.1 mM of hydroxylated products could be observed at the concentrations of 150  $\text{g}_{\text{wCW}} \text{L}^{-1}$  *E. coli* cells and 100 mM of MES buffer. This experimental outcome correlates

with the previous results obtained from the conversion of (*R*)-limonene determined under dark conditions in the presence of glucose.

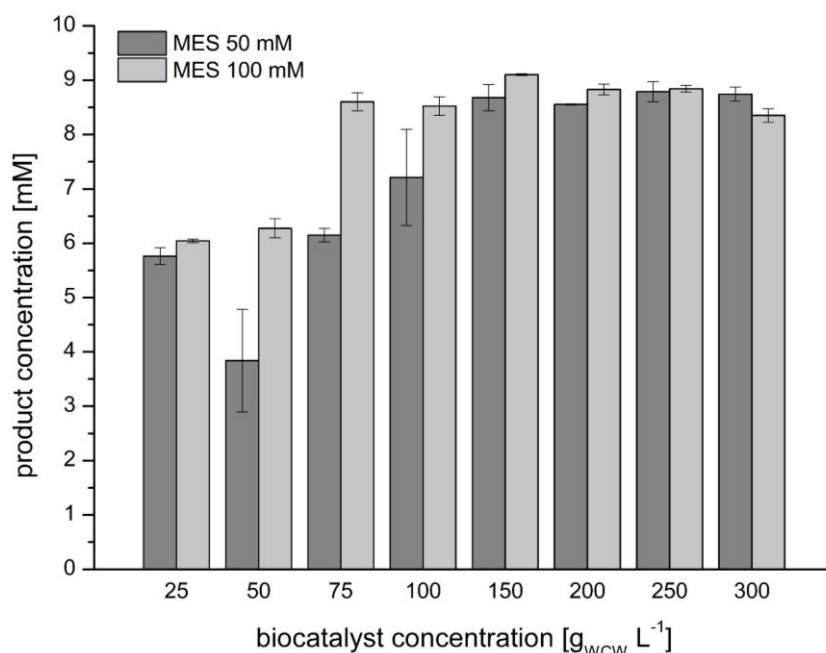
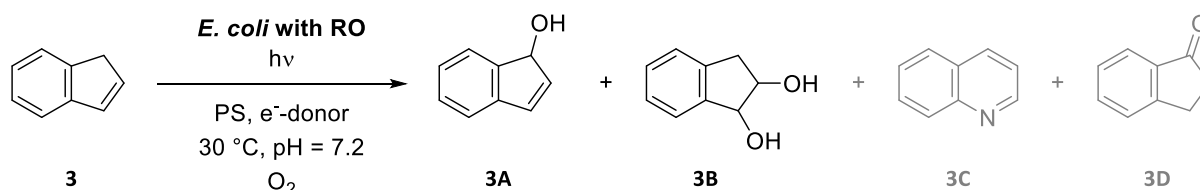


**Figure 18:** Product formations obtained at different biocatalyst (*E. coli* JM109 NDO h295A) and electron donor concentrations in light-driven whole-cell biotransformations of indene after 24 h. Reaction conditions: 100  $\mu$ M CE, 10 mM indene, 50/100 mM MES, 100-300 g<sub>wcw</sub> L<sup>-1</sup> whole cells (19h expression), white light (max. 230  $\mu$ mol m<sup>-2</sup> s<sup>-1</sup>), 30°C, 120 rpm. Reactions were carried out in duplicates. Standard deviations are indicated as error bars.

### 3.2.7 Byproduct formation observed in light-driven hydroxylation of indene

In previous light-driven biotransformations of indene, a fluctuation of product ratios dependent on the combination of PS and electron donor could be observed. Besides the desired product formation of 1H-indenol (**3A**) and 1,2-indanediol (**3B**), the presence of quinoline (**3C**), and 1-indanone (**3D**) could be detected (**Scheme 9**). Thus, the occurrence of unspecific background reactions facilitated by light irradiation or *E. coli* is assumed.



**Scheme 9:** Observed products formed during the light-driven whole-cell biotransformations with indene as substrate. While desired products 3A and 3B are formed by recombinant ROs, non-enzymatic formation of 3C and 3D could be detected, additionally. 3: indene; 3A: 1H-indenol; 3B: 1,2-indanediol; 3C: quinoline; 3D: 1-indanone.

In order to investigate a contingent impact of the interaction between electron donor and PS on the product distribution, light-driven whole-cell experiments with CDO M232A and NDO H295A were conducted. Residual substrate and obtained product formations were quantified, assuming that 10 mM indene is converted exclusively into **3A**, **3B**, **3C**, and **3D**. All evaluated reaction outcomes of light-driven biotransformations catalyzed by CDO M232A and NDO H295A are depicted as stacked bar charts in **Figure 19**. The detailed data obtained for CDO M232A and NDO H295A are summarized in **Table 24** and **Table 25**, respectively.

The occurrence of byproduct formation could be observed in all reactions to a variable extent. A maximum of byproduct could be obtained in the presence of EDTA in combination with EY revealing values of 4.5 mM with CDO M232A and 4.7 mM with NDO H295A. In contrast, only 0.62 mM of byproduct could be detected in the reaction with NDO H295A in the presence of CE and MOPS, representing the overall lowest byproduct formation in the conducted experiments. Additionally, the latter reaction outcome reveals a 13-fold excess of the desired products over byproducts, which represents the highest product ratio observed in all reactions. Full conversion of indene could be achieved with both Rieske variants in combination with EY/MOPS and CE/MES. However, the use of EDTA as an alternative electron donor seems to be unfavorable in combination with CE due to the low conversion with values of approximately 70 % achieved in the biotransformations with indene catalyzed by CDO M232A and NDO H295A. Concerning the maximum product formation, the use of MES with CE was considered as the most promising combination for future light-driven *in vivo* biotransformations with indene as substrate. Thus maximum product concentrations of 8.36 mM with CDO variant M232A and 8.89 mM with NDO H295A could be obtained.

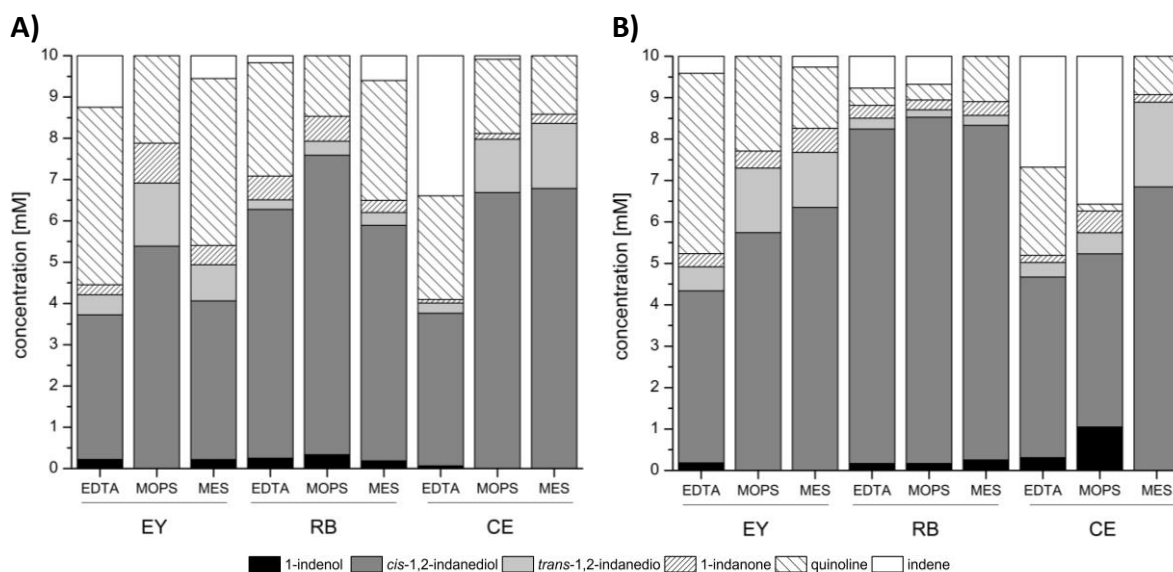


**Figure 19: Concentrations of products and residual substrate obtained by *in vivo* photobiocatalytic hydroxylations.** Summary of product distribution after whole-cell biotransformations of indene catalyzed by CDO M232A (A) or NDO H295A (B). Samples were taken according to the time point at which maximum product concentration in corresponding time-course experiments could be observed (Table 27 and Table 28). Reaction conditions: 100  $\mu\text{M}$  EY/RB/CE, 10 mM indene, 25 mM EDTA, 50 mM MOPS/MES, 100  $\text{g}_{\text{WCW}} \text{L}^{-1}$  whole cells (19h expression), white light (max. 230  $\mu\text{mol m}^{-2} \text{s}^{-1}$ ), 30°C, 120 rpm.

**Table 24: Products obtained during light-driven whole-cell biotransformations of indene catalyzed by CDO M232A.**

Photosensitizer/ Electron Donor	Product Concentration <sup>[a]</sup> [mM]	Concentration Quinoline [mM]	Concentration 1-Indanone [mM]	Conversion <sup>[b]</sup> [%]
EY/EDTA	4.21	4.30	0.24	88
EY / MOPS	6.92	2.12	0.97	100
EY / MES	4.94	4.05	0.47	94
RB / EDTA	6.51	2.75	0.58	98
RB / MOPS	7.93	1.47	0.60	100
RB / MES	6.20	2.90	0.29	94
CE / EDTA	4.0	2.51	0.08	66
CE / MOPS	7.98	1.80	0.14	99
CE / MES	8.36	1.42	0.22	100

Reaction conditions: 100  $\mu\text{M}$  EY/RB/CE, 10 mM indene, 25 mM EDTA, 50 mM MOPS/MES, 100  $\text{g}_{\text{WCW}} \text{L}^{-1}$  whole cells (19h expression), white light (max. 230  $\mu\text{mol m}^{-2} \text{s}^{-1}$ ), 30°C, 120 rpm.

<sup>[a]</sup> Product concentration is defined as the total amount of 1H-indenol and 1,2-indanediol. <sup>[b]</sup> Conversion of indene into main products and byproducts. The overall maximum product concentrations are depicted.



**Table 25: Products obtained during light-driven whole-cell biotransformation of 10 mM indene catalyzed by NDO H295A.**

Photosensitizer/ Electron Donor	Product Concentration <sup>[a]</sup> [mM]	Concentration Quinoline [mM]	Concentration 1-Indanone [mM]	Conversion <sup>[b]</sup> [%]
EY/EDTA	4.92	4.35	0.32	96
EY / MOPS	7.30	2.29	0.41	100
EY / MES	7.68	1.48	0.58	97
RB / EDTA	8.50	0.42	0.31	92
RB / MOPS	8.71	0.38	0.24	93
RB / MES	8.57	1.10	0.33	100
CE / EDTA	5.02	2.13	0.17	73
CE / MOPS	5.74	0.16	0.52	64
CE / MES	8.89	0.93	0.18	100

Reaction conditions: 100  $\mu\text{M}$  EY/RB/CE, 10 mM indene, 25 mM EDTA, 50 mM MOPS/MES, 100  $\text{g}_{\text{WCW}} \text{L}^{-1}$  whole cells (19h expression), white light (max. 230  $\mu\text{mol m}^{-2} \text{s}^{-1}$ ), 30°C, 120 rpm.

<sup>[a]</sup> Product concentration is defined as the total amount of 1H-indenol and 1,2-indanediol. <sup>[b]</sup> Conversion of indene into main products and byproducts. The overall maximum product concentrations are depicted.

In a dark control experiment with NDO H295A and glucose supplementation, the conversion of indene to 1-indanone reveals a value of 1.4 %. A formation of quinoline could not be detected. Additionally, control experiments with an empty vector control were performed to evaluate a possible product formation catalyzed by the *E. coli* host strain itself. Therefore, light-driven biotransformations of indene in the presence of MES and CE were performed by the use of *E. coli* cells containing pUC19 plasmid. The results obtained after 24 h and 48 h are summarized in **Table 26**.

**Table 26: Product distribution observed in light-driven whole-cell biotransformations of 10 mM indene with pUC19 after 24 h and 48 h.**

Photosensitizer/ Electron Donor	Incubation time	Product Concentration <sup>[a]</sup> [mM]	Concentration Quinoline [mM]	Concentration 1-Indanone [mM]
CE/MES	24	4.40 $\pm$ 0.51	3.28 $\pm$ 0.22	0.12 $\pm$ 0.01
CE/MES	48	4.65 $\pm$ 0.88	3.4 $\pm$ 0.36	0.17 $\pm$ 0.01

Reaction conditions: 100  $\mu\text{M}$  CE, 10 mM indene, 50 mM MES, 100  $\text{g}_{\text{WCW}} \text{L}^{-1}$  whole cells (19h expression), white light (max. 230  $\mu\text{mol m}^{-2} \text{s}^{-1}$ ), 30°C, 120 rpm.

<sup>[a]</sup> Product concentration is defined as the total amount of 1H-indenol and 1,2-indanediol.

Based on these results, no significant increase in product formation could be observed between 24 h and 48 h of biotransformation with pUC19. Thereby, a product formation of approximately 45 % could be determined. However, no product formation could be observed in the empty vector control with glucose supplementation under dark conditions.

### 3.2.8 Effect of light intensity on biotransformations of indene

Due to the experimental setup used in light-driven whole-cell biotransformations, variations in reaction conditions could be observed. Especially the variation of light intensities attributable to the light reactor design was supposed to have a significant impact on product formation. The fluorescence light-reactors used in this work were designed to have almost constant reaction conditions in terms of either temperature and bottom-up light exposure. Unexpectedly, light exposures at relevant positions within the reactors show noticeable differences that were determined by a quantum meter at full light (**Figure 20A**) and also dimmed-light conditions (**Figure 20B**).

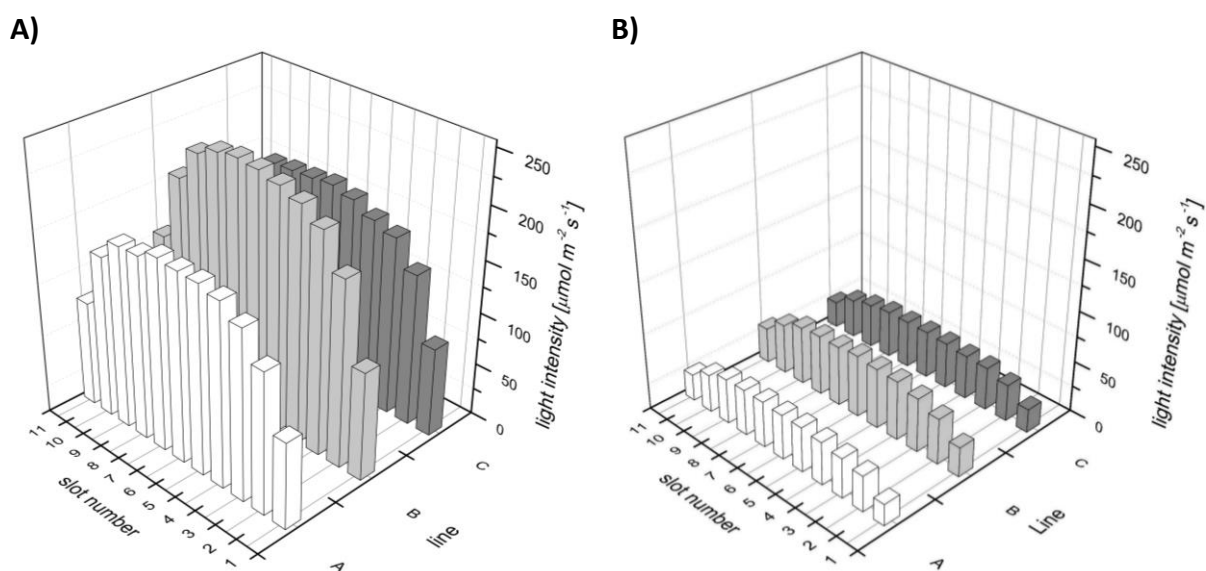


**Figure 20: Determined light intensities of fluorescence light reactor *Stella*.** Light intensities determined at relevant positions within the light reactor under full-light (A) and dimmed-light (B) conditions. Line and slot numbers refer to the actual local position within the light reactor. Values for light intensities were determined with a light measure device and depicted as the number of photons count per square meter per second [ $\mu\text{mol m}^2 \text{s}^{-1}$ ].

To evaluate a possible correlation between light exposure and product formation in the course of light-driven whole-cell biotransformations, the formal conversion of 10 mM indene catalyzed by *E. coli* JM109 harboring NDO H295A was proposed. Therefore, 1 mL reaction mixtures were prepared with final concentrations of 100 g<sub>wcW</sub> L<sup>-1</sup> resting *E. coli* cells resuspended in 50 mM MES buffer. As a PS, CE at a final concentration of 100  $\mu\text{M}$  was added. After 24 h of incubation at 28 °C, the product concentrations gained at individual light

intensities were determined. To extend the data range, analogous experiments with paper-dimmed light sources (dimmed by approximately 75 %) were additionally conducted.



**Figure 21: Product concentrations obtained at different light intensities in whole-cell biotransformations after 24 h.** A) Scatter plot displays detected product concentrations against applied light intensities in whole-cell biotransformations of indene catalyzed by *E. coli* cells harboring NDO H295A. B) Product formation observed after 24 h. Reaction conditions: 100 μM CE, 10 mM indene, 50 MES, 100-300 g<sub>WCW</sub> L<sup>-1</sup> whole cells (19h expression), white light (max. 230 μmol m<sup>-2</sup> s<sup>-1</sup>), 28°C, 120 rpm.

**Figure 21** shows the detected product concentrations in both full- and dimmed-light conditions plotted against respective light intensities. While a significant increase of product formations could be observed between light intensities of 0 to 100 μmol m<sup>-2</sup> s<sup>-1</sup>, higher photon concentrations up to 250 μmol m<sup>-2</sup> s<sup>-1</sup> seem to have no further effect on the reaction outcome. The product concentrations range between 1.2 mM under the dark condition to a maximum value of 9.0 mM obtained at a light intensity of 103 μmol m<sup>-2</sup> s<sup>-1</sup>. Due to these results, proper positions in the light-reactor were defined to maximize the product formation and to avoid significant variations in product formations for further light-driven experiments.

### 3.2.9 Photochemical background reactions

An undesired non-enzymatic background formation of the product could be observed for indene under light exposure. To investigate the extent of this photochemical conversion, reaction mixtures containing 10 mM indene, 50 mM MES buffer, and 100 μM CE were

incubated for 24 h at 30 °C under full-light condition. The obtained product concentrations are depicted in **Figure 22**. Approximately 4.8 mM of 1,2-indanediol at a *cis:trans* ratio of 72:28 is formed by the photochemical background conversion. No byproduct formation of quinoline or 1-indanone could be observed.

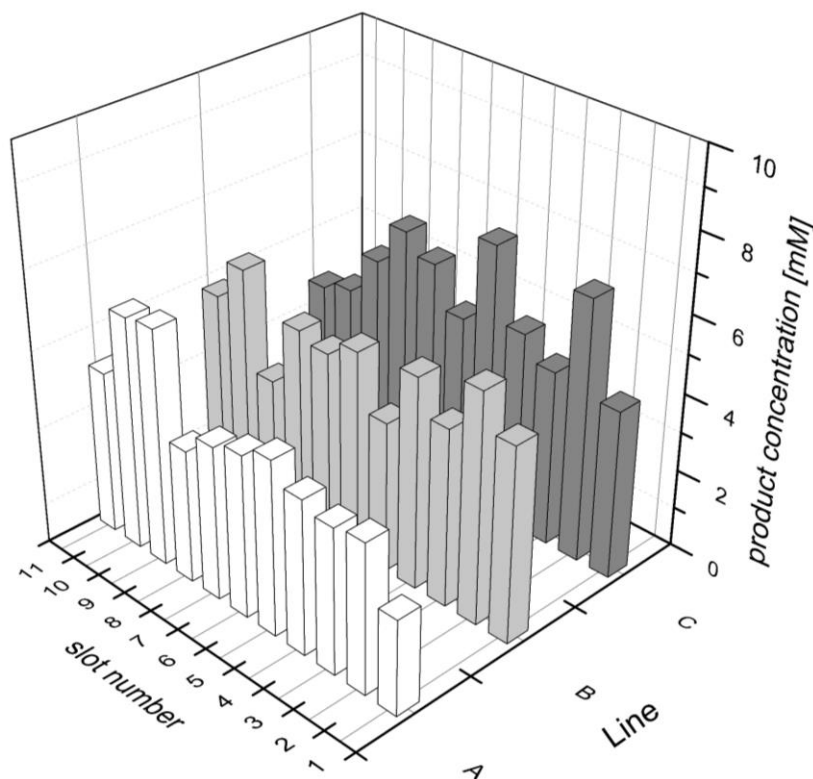


**Figure 22: Non-enzymatic photochemical background reaction in the different positions within the fluorescence lamp light reactor.** Reaction conditions: 100  $\mu\text{M}$  CE, 10 mM indene, 50 mM MES, 100  $\text{g}_{\text{WCW}} \text{L}^{-1}$  whole cells (19h expression), white light (max. 230  $\mu\text{mol m}^{-2} \text{s}^{-1}$ ), 30 °C, 120 rpm. Product concentration is defined as the sum of concentrations of 1H-indenol, *cis*-1,2-indanediol, and *trans*-1,2-indanediol.

### 3.2.10 Time courses of product formation in light-driven whole-cell biotransformations of indene

For the characterization of the light-driven whole-cell approach in terms of reaction kinetics, the product formation over time was recorded. Because of this, 1 mL samples were taken at specific time points during the biotransformation of 10 mM indene within a period of 24 or 48 hours. The total amount of product in each time probe was then quantified. Several experiments were carried out in order to investigate each combination of electron donor

(MES, MOPS, and EDTA) with PS (CE, SO, EY, and RB) using resting *E. coli* JM109 cells ( $\beta = 100 \text{ g}_{\text{WCW}} \text{ L}^{-1}$ ) harboring either NDO H295A or CDO M232A, respectively. Some of the recorded time courses are summarized in **Figure 23**. While reactions in the presence of CE show the highest maximum product concentrations or initial rates, SO seems to have no significant effect on the overall light-driven hydroxylation of indene.

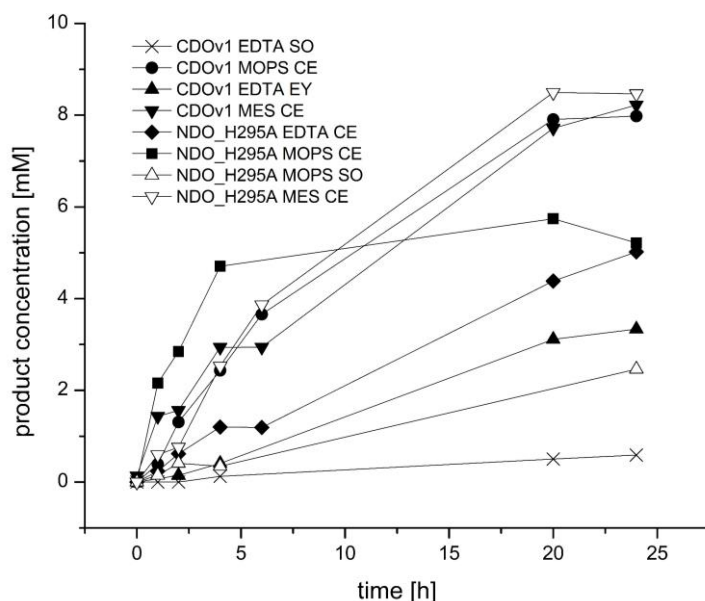


**Figure 23: Overview of product formation time courses in light-driven whole-cell biotransformations over 24 h.** Summary of product formations after 0, 1, 2, 4, 6, 20, and 24 h biotransformation of indene catalyzed by resting *E. coli* JM109 cells harboring NDO H295A or CDO M232A. Reaction conditions:  $100 \mu\text{M}$  CE/EY/SO,  $10 \text{ mM}$  indene,  $25 \text{ mM}$  EDTA or  $50 \text{ mM}$  MES/MOPS,  $100 \text{ g}_{\text{WCW}} \text{ L}^{-1}$  whole cells (19h expression), white light (max.  $230 \mu\text{mol m}^{-2} \text{ s}^{-1}$ ),  $30^\circ\text{C}$ ,  $120 \text{ rpm}$ . Product concentration is defined as the sum of concentrations of 1H-indenol, *cis*-1,2-indanediol, and *trans*-1,2-indanediol.

Based on the initial rates, the specific activities [ $\text{U g}_{\text{WCW}}^{-1}$ ] were calculated (6).

$$\text{Specific activity } [\text{U g}_{\text{WCW}}^{-1}] = \frac{\text{Initial rate } [\text{mM h}^{-1}] \times 1000 \frac{\mu\text{M}}{\text{mM}}}{\text{concentration of cells } [\text{g}_{\text{WCW}} \text{ L}^{-1}] \times 60 \frac{\text{min}}{\text{h}}} \quad (6)$$

As indicated below, all combinations of described PS and electron donors contribute to the desired product formations in light-driven biotransformations catalyzed by CDO M232A (**Table 27**) or NDO H295A (**Table 28**). In general, as well the overall maximum as the lowest product concentrations could be detected during the reaction in the presence of CE. While approximately  $8.6 \text{ mM}$  product could be obtained when using MOPS buffer as electron donor, the overall lowest value of  $4.0 \text{ mM}$  product was achieved when using EDTA as the electron donor in the biotransformation of indene catalyzed by the CDO M232A.

**Table 27: Summary of obtained results of the light-driven whole-cell biotransformation experiments using the CDO M232A variant.**

Photosensitizer/ Electron Donor	Maximum Concentration [mM] <sup>[a]</sup>	Initial rate [mM h <sup>-1</sup> ]	Specific activity [U g <sub>wcW</sub> <sup>-1</sup> ]
EY / EDTA	3.7 ± 0.4	0.18	0.029
EY / MOPS	6.8 ± 0.03	0.13	0.021
EY / MES	4.7 ± 0.2	0.25	0.041
RB / EDTA	6.8 ± 0.3	1.59	0.265
RB / MOPS	7.3 ± 0.6	0.94	0.156
RB / MES	5.8 ± 0.4	1.65	0.275
CE / EDTA	4.0 ± 0.01	0.26	0.043
CE / MOPS	8.6 ± 0.6	0.61	0.102
CE / MES	8.3 ± 0.08	0.75	0.124

Reaction conditions: 100 μM EY/RB/CE, 10 mM indene, 25 mM EDTA or 50 mM MES/MOPS, 100 g<sub>wcW</sub> L<sup>-1</sup> whole cells (19h expression), white light (max. 230 μmol m<sup>-2</sup> s<sup>-1</sup>), 30°C, 120 rpm. <sup>[a]</sup> Product concentration is defined as the sum of concentrations of 1H-indenol, *cis*-1,2-indanediol and *trans*-1,2-indanediol. Reactions were carried out in duplicates.

Correspondingly, a maximum product formation of 8.5 mM could be detected in the light-driven hydroxylation catalyzed by NDO H295A with CE and MES. In terms of specific activity, the combinations with rose bengal show the most promising results comprising the overall maximum value of 275.3 mU g<sub>wcW</sub><sup>-1</sup> with MES and CDO M232A.

**Table 28:** Summary of obtained results of the light-driven whole-cell biotransformation experiments using the NDO H295A variant.

Photosensitizer/ Electron Donor	Maximum Concentration [mM] <sup>[a]</sup>	Initial rate [mM h <sup>-1</sup> ]	Specific activity [U g <sub>WCW</sub> <sup>-1</sup> ]
EY/EDTA	4.7 ± 0.2	0.23	0.047
EY / MOPS	7.7 ± 0.4	0.37	0.061
EY / MES	7.4 ± 0.3	0.52	0.087
RB / EDTA	7.5 ± 1.0	0.32	0.053
RB / MOPS	7.5 ± 1.2	0.89	0.148
RB / MES	7.9 ± 0.6	0.45	0.079
CE / EDTA	5.5 ± 0.5	0.30	0.050
CE / MOPS	7.3 ± 0.4	0.86	0.143
CE / MES	8.5 ± 0.4	0.64	0.107

Reaction conditions: 100 μM EY/RB/CE, 10 mM indene, 25 mM EDTA or 50 mM MES/MOPS, 100 g<sub>WCW</sub> L<sup>-1</sup> whole cells (19h expression), white light (max. 230 μmol m<sup>-2</sup> s<sup>-1</sup>), 30°C, 120 rpm. <sup>[a]</sup> Product concentration is defined as the sum of concentrations of 1H-indenol, *cis*-1,2-indanediol and *trans*-1,2-indanediol. Reactions were carried out in duplicates.

### 3.2.11 Selectivities of ROs in light-driven biotransformations of indene

In order to evaluate the product selectivity of CDO M232A and NDO H295A, the distribution of products formed during light-driven whole-cell hydroxylations with indene as substrate were determined via chiral GC-FID. In **Table 29** and **Table 30** below, observed product ratios and byproduct formations determined after light-driven biotransformations of 10 mM indene in combination with various electron donors and PSs were summarized. The determined product concentrations obtained in light-driven whole-cell biotransformations with 10 mM indene catalyzed by CDO variant M232A are summarized in **Table 29**.

Table 29: Product contribution in the photobiocatalytic hydroxylation of 10 mM indene catalyzed by CDO M232A.

Photosensitizer/ Electron Donor	Maximum Concentration [mM] <sup>[a]</sup>	Diastereomeric ratio <i>cis:trans-3b</i> [%]	Distribution 3a:3b [%]
EY/EDTA	3.7 ± 0.4	80 : 20	3 : 97
EY / MOPS	6.8 ± 0.03	47 : 53	0 : 100
EY / MES	4.7 ± 0.2	81 : 19	4 : 96
RB / EDTA	6.8 ± 0.3	88 : 12	4 : 96
RB / MOPS	7.3 ± 0.6	60 : 40	4 : 96
RB / MES	5.8 ± 0.4	95 : 5	3 : 97
CE / EDTA	4.0 ± 0.01	76 : 24	2 : 98
CE / MOPS	8.6 ± 0.6	49 : 51	0 : 100
CE / MES	8.3 ± 0.08	47 : 53	0 : 100

Reaction conditions: 100 μM EY/RB/CE, 10 mM indene, 25 mM EDTA or 50 mM MES/MOPS, 100 g<sub>WCW</sub> L<sup>-1</sup> whole cells (19h expression), white light (max. 230 μmol m<sup>-2</sup> s<sup>-1</sup>), 30°C, 120 rpm<sup>[a]</sup> Product concentration is defined as the sum of concentrations of 1H-indenol, *cis*-1,2-indanediol and *trans*-1,2-indanediol. Reactions were carried out in duplicates.

The product concentrations obtained in the corresponding light-driven whole-cell biotransformations of 10 mM indene catalyzed by NDO H295A are summarized in **Table 30**.

Table 30: Product contribution in the photobiocatalytic hydroxylation of 10 mM indene catalyzed by NDO H295A.

Photosensitizer/ Electron Donor	Maximum Concentration [mM] <sup>[a]</sup>	Diastereomeric ratio <i>cis : trans-3b</i> [%]	Distribution 3a:3b [%]
EY/EDTA	4.7 ± 0.2	88 : 12	4 : 96
EY / MOPS	7.7 ± 0.4	79 : 21	2 : 98
EY / MES	7.4 ± 0.3	83 : 17	4 : 96
RB / EDTA	7.5 ± 1.0	86 : 14	0 : 100
RB / MOPS	7.5 ± 1.2	80 : 20	2 : 98
RB / MES	7.9 ± 0.6	77 : 23	3 : 97
CE / EDTA	5.5 ± 0.5	93 : 7	6 : 94
CE / MOPS	7.3 ± 0.4	66 : 34	18 : 82
CE / MES	8.5 ± 0.4	77 : 23	0 : 100

Reaction conditions: 100 μM EY/RB/CE, 10 mM indene, 25 mM EDTA or 50 mM MES/MOPS, 100 g<sub>WCW</sub> L<sup>-1</sup> whole cells (19h expression), white light (max. 230 μmol m<sup>-2</sup> s<sup>-1</sup>), 30°C, 120 rpm<sup>[a]</sup> Product concentration is defined as the sum of concentrations of 1H-indenol, *cis*-1,2-indanediol and *trans*-1,2-indanediol. Reactions were carried out in duplicates.

It is assumed that both CDO M232A and NDO H295A favor the dihydroxylation of indene to 1,2-indanediol independent from the combination of the PS with the electron donor. Thereby, ratios of 1H-indenol and 1,2-indanediol of up to 0:100 could be observed. However, evaluated diastereomeric ratios between *cis*-1,2-indanediol and its *trans*-stereoisomer shows no general trend due to the photochemical background reaction. While light-driven biotransformations with *E. coli* cells harboring NDO H295A generate an excess of *cis*-1,2-



indanediol of up to 93:7 in combination with CE and EDTA, equivalent experiments with CDO M232A in the presence of EY or CE and either MOPS or MES reveal a slight preference for the formation of *trans*-1,2-indanediol.

### 3.2.12 Effect of photosensitizer concentration on product formation during light-driven whole-cell biotransformations

Since CE exhibits suitable properties regarding activity and maximum product formation in the course of whole-cell biotransformations (see **3.2.10**), it is considered as promising PS for future light-driven experiments. In order to determine an optimum amount of CE concerning maximum product formation, whole-cell experiments under full-light conditions were performed. Besides MES buffer (50 mM) as electron donor and indene (10 mM) as substrate, resting *E. coli* cells harboring the NDO H295A at a concentration of  $100\text{g}_{\text{WCW}}\text{L}^{-1}$  were used as biocatalysts. Various amounts of CE per reaction mixture were added to set a concentration gradient from 0 to  $320\ \mu\text{M}$  of PS. After 24 h incubation at  $30\ ^\circ\text{C}$  and 120 rpm, the amount of product defined as the sum of concentrations of 1H-indenol, *cis*-1,2-indanediol and *trans*-1,2-indanediol were quantified. In **Figure 24**, determined product concentrations gained at different CE concentrations are depicted. While small amounts of PS ( $2\ \mu\text{M}$  –  $6\ \mu\text{M}$ ) seem not to affect the reaction outcome, a significant increase of product formation of up to 9.2 mM product within a range of  $10\ \mu\text{M}$  to  $100\ \mu\text{M}$  CE indicates a positive correlation. Since additional CE up to  $320\ \mu\text{M}$  has no further effect, it is assumed that an excess of PS absorbs the majority of photons required for the light-driven electron transfer. Due to these results,  $100\ \mu\text{M}$  CE was considered as a proper concentration in order to maximize the product formation and to avoid an excess of PS, which may have a negative effect on the experiments.

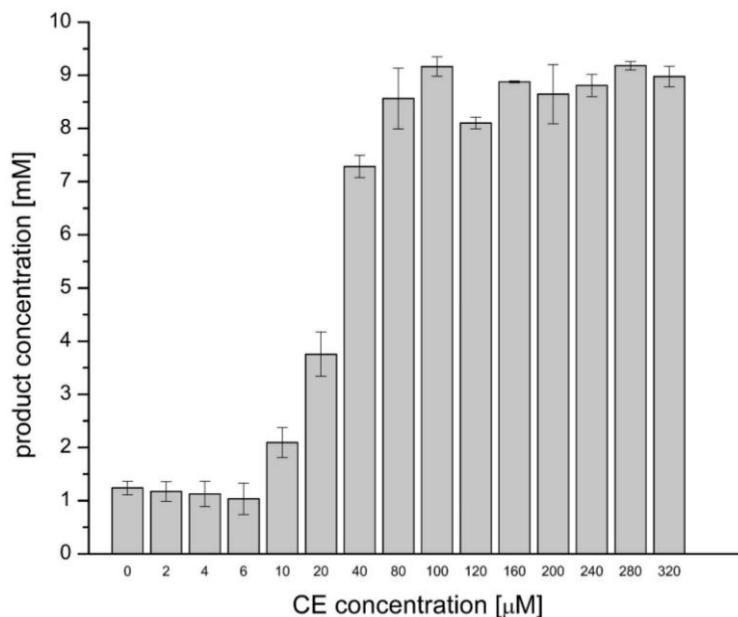


**Figure 24: Product formation at different CE concentrations in light-driven whole-cell biotransformations of indene with *E. coli* JM109 NDO h295A after 24 hours.** Reaction conditions: 100  $\mu\text{M}$  CE, 10 mM indene, 50 mM MES, 100  $\text{g}_{\text{wCW}} \text{L}^{-1}$  whole cells (19h expression), white light (max. 230  $\mu\text{mol m}^{-2} \text{s}^{-1}$ ), 30°C, 120 rpm Product concentration is defined as the sum of concentrations of 1H-indenol, *cis*-1,2-indanediol, and *trans*-1,2-indanediol. Reactions were carried out in duplicates. Product concentration is defined as the sum of concentrations of 1H-indenol, *cis*-1,2-indanediol, and *trans*-1,2-indanediol. Reactions were carried out in duplicates. Standard deviations are indicated as error bars.

### 3.2.13 Growth behavior of *E. coli* in the presence of substrates used for light-driven whole-cell biotransformations

It is supposed that substrates, although considered as suitable for hydroxylations catalyzed by Rieske enzymes, may have a negative effect on cell viability due to their toxicity. For the proposed light-driven approach, an intact cell structure is obligatory to preserve the functionality of the multicomponent electron transfer system of the NDO and CDO. The cell growth of *E. coli* JM109 (DE3) in the exponential phase in the presence of the respective substrates at different concentrations has been investigated. By this, it is assumed to get sufficient knowledge about the highest possible amount of the respective compounds in terms of their toxicity on the cells. In corresponding cell growth experiments, indene (0-10 mM), (*R*)-limonene (0-10 mM), and styrene (0-5 mM) were investigated. Additionally, the toxicity of indole (0-5 mM) used for the activity assay and the organic solvent DMSO (0-5 mM) were examined. The cell densities at specific time-points during incubation at 30 °C were determined via spectrophotometric measurements. In **Figure 25** to **Figure 29**, several cell growth curves obtained during the described experiment were summarized. Based on these

data, the amount of indene exceeding 2 mM completely inhibits cell growth within 3.5 hours (**Figure 25**). However, enhanced accumulation of biomass could be observed at higher amounts of indene after 6 h. Microbial contamination or indene evaporation over time are considered as most likely causing the delayed exponential growth. An absence of cell-growth could also be detected. Similar to that, the absence of cell growth could be observed for *E. coli* cultures in the presence of indole (**Figure 28**). While indole concentrations of up to 2 mM have no significant effect on the maximum growth rate, higher amounts prevent the transition into the exponential growth phase. In contrast, an increase of styrene yields in a decrease of the maximum growth rate. However, complete growth inhibition could not be detected up to a concentration of 5 mM of styrene. Cell growth is not significantly affected by the presence of (*R*)-limonene and DMSO when concentrations of up to 5 mM were used (**Figure 26** and **Figure 29**).

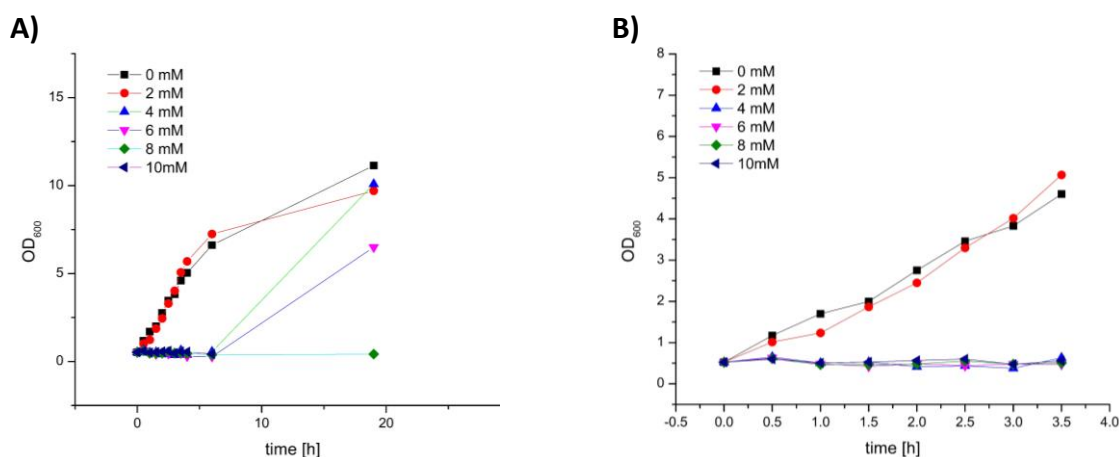


**Figure 25: Growth curves of *E. coli* JM109 (DE3) at the presence of 0-10 mM indene.** A) Summary of biomass formation of *E. coli* JM109 in the presence of 0-10 mM indene over 19 h. B) Enlarged extract of the cell growth curves within 0-3.5 h. Cell growth conditions: *E. coli* JM109 (DE3) containing NDO H295A, 30 °C at 120 rpm in 50 mL TB-Amp (100). X-axis: time [h]; Y-axis: cell density in OD<sub>600</sub>.

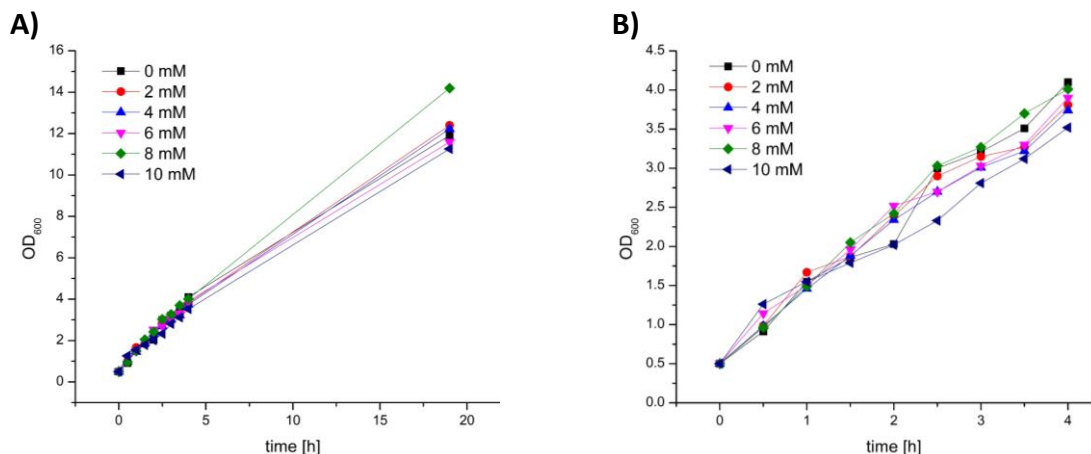


**Figure 26: Growth curves of *E. coli* JM109 (DE3) at the presence of 0-10 mM (R)-limonene.** A) Summary of biomass formation of *E. coli* JM109 in the presence of 0-10 mM (R)-(+)-limonene over 19 h. B) Enlarged extract of the cell growth curves within 0-4 h. Cell growth conditions: *E. coli* JM109 (DE3) containing NDO H295A, 30 °C at 120 rpm in 50 mL TB-Amp (100). X-axis: time [h]; Y-axis: cell density in OD<sub>600</sub>.

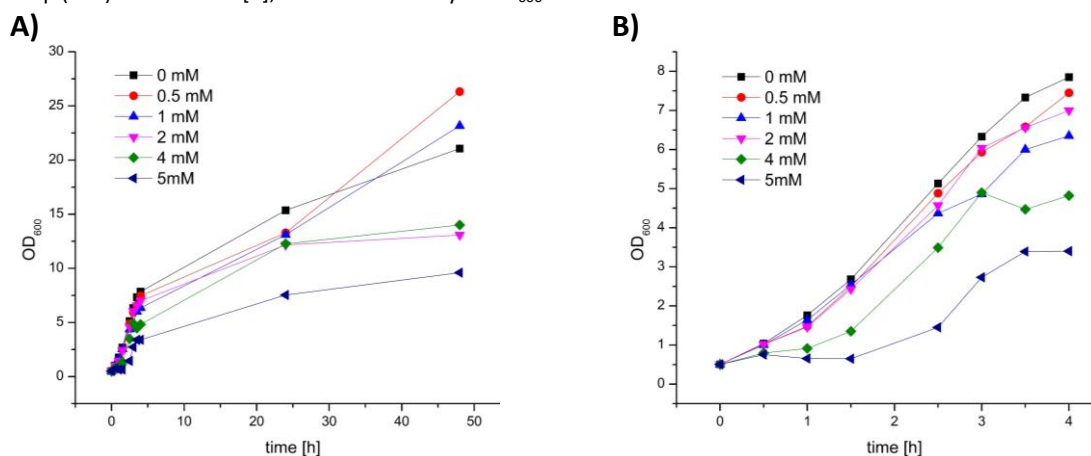


**Figure 27: Growth curves of *E. coli* JM109 (DE3) at the presence of 0-5 mM styrene.** A) Summary of biomass formation of *E. coli* JM109 (DE3) in LB-Amp in the presence of 0-5 mM styrene over 48 h. B) Enlarged extract of the cell growth curves within 0-4 h. Cell growth conditions: *E. coli* JM109 (DE3) containing NDO H295A, 30 °C at 120 rpm in 50 mL TB-Amp (100). X-axis: time [h]; Y-axis: cell density in OD<sub>600</sub>.

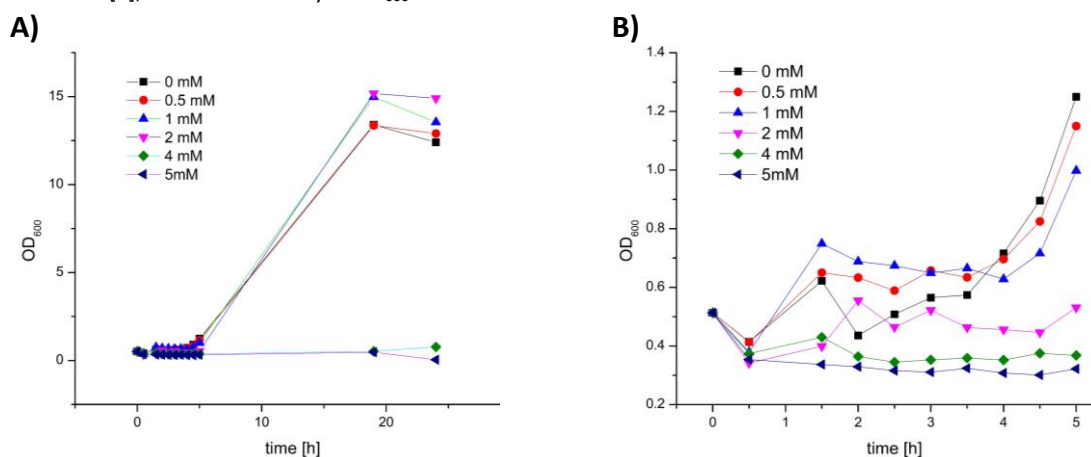


**Figure 28: Growth curves of *E. coli* JM109 (DE3) at the presence of 0-5 mM indole.** A) Summary of biomass formation of *E. coli* JM109 (DE3) in the presence of 0-5 mM indole over 24 h. B) Enlarged extract of the cell growth curves within 0-5 h. Cell growth conditions: *E. coli* JM109 (DE3) containing NDO H295A, 30 °C at 120 rpm in 50 mL TB-Amp (100). X-axis: time [h]; Y-axis: cell density in OD<sub>600</sub>.

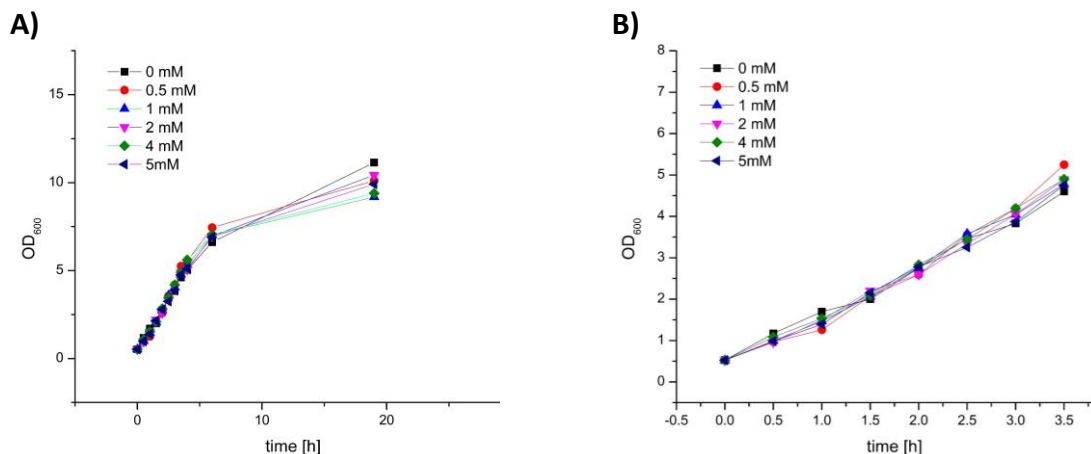


**Figure 29: Growth curves of *E. coli* JM109 (DE3) at the presence of 0-5 mM DMSO.** A) Summary of biomass formation of *E. coli* JM109 (DE3) in the presence of 0-5 mM DMSO over 19 h. B) Enlarged extract of the cell growth curves within 0-3.5 h. Cell growth conditions: *E. coli* JM109 (DE3) containing NDO H295A, 30 °C at 120 rpm in 50 mL TB-Amp (100). X-axis: time [h]; Y-axis: cell density in OD<sub>600</sub>.

### 3.2.14 Effect of light and PS on the light-driven biotransformations

It is proposed that a light excited PS is capable of mediating the electron transfer from a sacrificial electron donor to the multicomponent Rieske system. Via an electron transfer chain, electrons are then shuttled to the active site of the terminal oxygenase, where the hydroxylation of a substrate into the desired product takes place. To investigate the effect of the interaction between photo-excited PS and electron donor on the whole-cell biotransformations, experiments with CDO M232A under light and dark conditions, respectively, were conducted. Therefore, various combinations of PSs and electron donors were investigated in the course of the biotransformation of 10 mM indene. In addition, control reactions without PS were performed under light and dark conditions. The obtained product formations were determined and are depicted in the bar charts below (**Figure 30**). It can be seen that all *in vivo* biotransformations in the presence of PS (red bars) show higher conversions of indene into the desired products under light exposure than under dark conditions. For instance, in light-driven reactions with 100  $\mu$ M RB and 25 mM EDTA as an electron donor, a product formation of approximately 7 mM was detected (**Figure 30A**). However, the corresponding repetition under dark conditions revealed a 90 % lower conversion with a product formation of 0.84 mM. An overall maximum of product formation could be determined in biotransformations with CE and MOPS (**Figure 30B**). Thereby, product concentrations of approximately 8.5 mM could be obtained under full-light conditions.

Furthermore, the corresponding dark controls yielded 1.5 mM of product, which corresponds to the previous findings with EDTA as an electron donor. All experiments without PSs exhibited product formations of approximately 1.25 mM under light and 0.59 mM under dark conditions

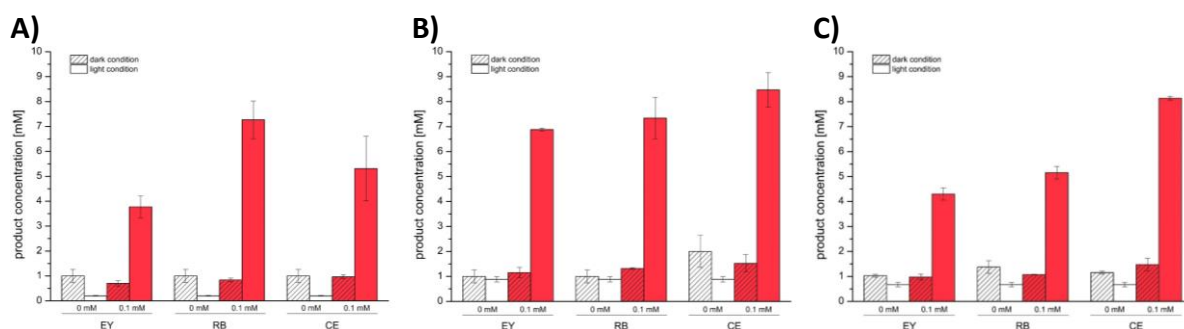


**Figure 30: Whole-cell biotransformations of indene catalyzed by *E. coli* CDO M232A performed under light or dark conditions and in the presence of various PS and electron donors.** Summary of product formations determined after whole-cell biotransformations of indene with *E. coli* JM109 cells ( $100 \text{ g}_{\text{WCW}} \text{ L}^{-1}$ ) harboring CDO M232A as biocatalysts. While red bars represent reactions in the presence of indicated PS, white bars show experiments carried out without PS. For comparison, all reactions were carried out under either dark (hatched bars) or light conditions. As sacrificial electron donors, either 25 mM of EDTA (A), 50 mM MOPS (B), or 50 mM MES (C) were added, respectively. Reaction conditions: Reaction conditions: 0 or  $100 \mu\text{M}$  EY/RB/CE, 10 mM indene,  $100 \text{ g}_{\text{WCW}} \text{ L}^{-1}$  whole cells (19h expression), white light (max.  $230 \mu\text{mol m}^{-2} \text{ s}^{-1}$ ),  $30^\circ\text{C}$ , 120 rpm. Product concentration is defined as the sum of concentrations of 1H-indenol, *cis*-1,2-indanediol, and *trans*-1,2-indanediol. The reaction was carried out in duplicates.

Based on these findings, a relation between PSs and light exposure affecting the overall product formation in whole-cell biotransformations of indene could be revealed. Accordingly, the proposed light-mediated electron transfer from an alternative electron donor to the Rieske system facilitated by a PS could be confirmed. However, empty vector controls performed with *E. coli* pUC19 revealed a background product formation up to 3.5 mM after light-driven biotransformation of 10 mM indene in the presence of RB and EDTA (**Figure 31**). Since no significant product formation could be observed without PSs, a non-enzymatic conversion is assumed. These observations correlate with previous findings, indicating the occurrence of an undesired photochemical background reaction dependent on the choice of PS and electron donor.

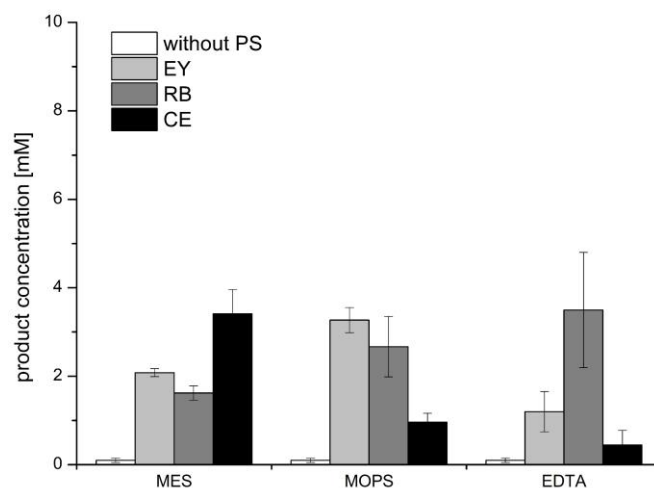


**Figure 31: Whole-cell biotransformations of indene catalyzed by *E. coli* pUC19 performed under light conditions and in the presence of various PS and electron donors.** Summary of product formations determined after whole-cell biotransformations of indene with *E. coli* JM109 cells ( $100 \text{ g}_{\text{WCW}} \text{ L}^{-1}$ ) harboring pUC19. White bars show experiments carried out without PS. As sacrificial electron donors, either 25 mM of EDTA (A), 50 mM MOPS (B), or 50 mM MES (C) were added, respectively. Reaction conditions: Reaction conditions: 0 or 100  $\mu\text{M}$  EY/RB/CE, 10 mM indene,  $100 \text{ g}_{\text{WCW}} \text{ L}^{-1}$  whole cells (19h expression), white light (max.  $230 \mu\text{mol m}^{-2} \text{ s}^{-1}$ ),  $30^\circ\text{C}$ , 120 rpm, 24 h. Product concentration is defined as the sum of concentrations of 1H-indenol, *cis*-1,2-indanediol, and *trans*-1,2-indanediol. The reaction was carried out in duplicates.

## 4 Discussion

Today, the prevention of environmental pollution and its dangerous effects caused by the excessive use of fossil fuels and the production of ecologically harmful waste is probably the biggest challenges for a sustainable society. Thus, the need for alternative strategies that aim to halt these alarming progress has increased inevitably over the past decades. As part of these considerations, the concept of green chemistry emerged, which addresses the sustainable and environmentally benign synthesis, manufacturing, and application of chemical products.[74] Thereby, the approach of biocatalysis focuses on the application of biocatalysts as sustainable substitutes for conventional and often toxic chemical catalysts applied in organic synthesis. Especially, their high selectivity and activity at ambient temperatures are considered highly beneficial regarding a sustainable and cost-efficient production of useful and valuable products.[4] While earlier approaches were limited to cofactor-independent enzymes (e.g., Hydrolases), recent developments focus on the use of oxidoreductases due to their potential to catalyze a variety of industrial relevant conversions. Among these biocatalysts, ROs can catalyze a range of exciting redox reactions yielding in mono- or dihydroxylated products.[16] Notably, the asymmetric single-step formation of vicinal *cis*-diols is superior to conventional organic synthesis in which additional protection and deprotection steps are required.[4] Furthermore, by the use of ROs, the need for toxic metal catalysts can be avoided, which thus contributes to the overall process sustainability.[16] Due to that, this class of enzymes attracts much attention in recent years as promising biocatalysts for industrial applications. However, the need for relatively unstable and expensive NAD(P)H cofactors and the instability of ROs are currently the main throwbacks in the implementation of economic *in vitro* large-scale processes [11, 16, 75]. To overcome the cofactor-dependency issue of oxidoreductases in terms of industrial applications, several cofactor regeneration concepts have been successfully established.[9] Besides, *in vivo* approaches exploiting the cofactor supply maintained by the intrinsic cell metabolism, several *in vitro* strategies based on enzymatic, electrochemical, or photochemical approaches are currently available. While the feasibility of *in vitro* NAD(P)H regeneration could be reported for single-domain oxidoreductases like OYEs,[52, 76, 77] the application of multi-component



ROs is mainly restricted to whole-cell systems. While the use of *E. coli* as the host organism for corresponding biotransformations is favorable due to the possibility of cost-efficient and straightforward high-cell density cultivation and the availability of a mature gene engineering toolbox,[40] autotrophs like cyanobacteria have the potential to drive redox reactions by utilizing renewable and abundant light energy. However, low growth rates, undesired self-shading effects at higher cell densities, and the lack of reliable genetic engineering techniques are currently significant obstacles for a broad application of recombinant cyanobacteria. [62, 65-67] The concept of artificial photosynthesis aims to combine the advantage of heterotrophic model organisms with the capability of transforming light into chemical energy. Therefore, the photoexcitability of photoactive molecules (PSs) is exploited to establish an artificial electron transfer from a sacrificial electron donor towards a terminal oxidoreductase, catalyzing the desired conversion. Thus, the need for NAD(P)H can be circumvented and whole cells as chassis for such multi-component enzymes can be applied, which is favorable regarding the industrial usage of oxidoreductases. Park and coworker recently proposed a light-driven whole-cell approach for CYP variants by creating artificial photosynthesis in resting *E. coli* cells to enable a cofactor-free hydroxylation of different substrates.[70] Thereby, a maximum conversion of 7.5 % could be achieved after 20 photocatalytic biotransformation of 1 mM omeprazole into 5'-omeprazole enabled by an artificial light-driven electron transfer based on the interaction of TEOA as electron donor and EY functioned as suitable PS.[70] Besides the favorable independency on NAD(P)H redox cofactors, the authors further suggested the possibility to overcome the need for the CYP reductase component, since photoexcited electrons from the PS are directly mediated to the heme prosthetic group of the terminal oxygenase component.[70] Inspired by the study of Park *et al.*, a proof-of-concept study by Wied *et al.* revealed a new light-mediated whole-cell approach to drive the hydroxylation of (*R*)-(+)-limonene to carveol by an engineered CDO from *Pseudomonas fluorescens* IP01.[73] The authors suggested that by the implementation of artificial photosynthesis realized by a light-mediated electron transfer, the need for NAD(P)H could be circumvented. Unlike the suggested use of TEOA as a sacrificial electron donor for the light-driven system with CYPs [70], no photocatalytic activity could be observed in corresponding light-driven biotransformations with CDO.[73] However, the combination of

EDTA and EY as PS yielded in the formation of up to 89  $\mu\text{M}$  of (1*R*,5*S*)-carveol (*ee* > 99 %), which corresponds to a maximum conversion of 0.89 % after 24 h.[73] Inspired by these findings, the current thesis focuses on the in-depth characterization of the proposed light-driven approach by extending the enzyme, PS, electron donor, and substrate scope. For optimization reasons, reaction conditions and reaction composition were adjusted in order to enhance the corresponding product conversion.

#### 4.1 Experimental setup for *in vivo* biotransformations

At the beginning of *in vivo* biotransformation studies, a complete experimental setup was designed to ensure uniform and appropriate reaction conditions throughout the entire project. Thus, it was suggested to generate reliable and reproducible data, contributing to a more profound knowledge about the light-driven whole-cell system. Wied et al. suggested a 3D-printed LED light reactor for light-driven biotransformations.[73] This prototype has a capacity for 10 20 mL glass vials and enables horizontal light exposure of the corresponding reaction mixtures. Unfortunately, an interfering increase of temperature of up to +5 °C due to the introversive arrangement of the LED stripes and insufficient air circulation within the reactor could be observed over time. To overcome this drawback, a fluorescent lamp light reactor capable of performing 33 reactions in parallel was designed. By the bottom arranged light sources, exposure of a relatively large surface area of each reaction mixture compared to the illumination sidewise set up in the former LED reactor could be ensured. Moreover, no undesired heat development was observed, which is considered beneficial for the experimental reproducibility. Despite the advantage of having an increased sample capacity and constant incubation conditions, a correlation between light intensity and location within the light reactor could be determined by measuring the photon flux [ $\mu\text{mol s}^{-1}\text{m}^2$ ] at each relevant position (**Figure 20**). A formal conversion of 10 mM indene with NDO H295A in the presence of CE and MES buffer reveals an asymptotic behavior in which the product yield approaches a maximum value of approximately 9 mM by increasing the light intensity (**Figure 21**). On account of the described findings, proper positions within the fluorescent lamp light reactor were chosen concerning high product yields and reproducibility. However, despite avoiding inappropriate position located mainly in the middle of the light reactor, a standard

deviation of  $\pm 0.5$  mM could not be impeded. Reported whole-cell biotransformation studies revealed the successful realization of artificial photosynthesis in non-autotrophic *E. coli* cells, which provides a sustainable strategy to convert light energy into accessible chemical energy accompanied by the avoidance of NAD(P)H as redox cofactor for ROs. Therefore, the efficiency of several PSs in combination with potential sacrificial electron donors was evaluated regarding the maximum product formation determined after whole-cell biotransformations performed under light conditions. Besides CDO,[73] NDO from *Pseudomonas* sp. NCIB 9816-4 was additionally investigated. Conditioned by the catalytic properties of engineered CDO M232 and NDO H295A variants,[19, 23] (*R*)-(+)-limonene, indene, and toluene were considered as suitable substrates. To evaluate the applicability of essential photoinduced electron transfer, providing reducing equivalents for desired enzymatic hydroxylations, interactions of EDTA, MES, or MOPS with EY, CE, RB, or SO function as PSs were evaluated. Remarkably, initial light-driven whole-cell biotransformations confirmed the feasibility of all relevant combinations of biocatalysts, ROs, sacrificial electron donors, PSs, and substrates. To get further knowledge about the overall system, the influence of corresponding reaction components were evaluated by varying concentrations and reaction conditions. According to previous studies,[73] resting *E. coli* cells harboring the respective RO were considered as suitable biocatalysts for experiments in the current work. For the sake of system optimization, an appropriate concentration of catalyst was initially evaluated. However, findings in the current thesis correspond to the results reported by Wied et al., emphasizing an optimum biocatalyst concentration of  $100 \text{ g}_{\text{WCW}} \text{ L}^{-1}$  (**Figure 17** and **Figure 18**). While high cell-density cultures of photosynthetic organisms are prone to unfavorable self-shading effect,[78] the current study revealed that an increase of cell-density of up to  $300 \text{ g}_{\text{WCW}} \text{ L}^{-1}$  seems to have no significant effect on the overall efficiency of the proposed light-driven approach (**Figure 18**). These findings favor the upscaling of the proposed light-driven systems to industrial large-scale for commercial purposes.[79] The choice of PSs for the described light-driven whole-cell approach was initially based on the compatibility with the associated prokaryotic host. In this work, EY, CE, SO, and RB, which are commonly used as fluorescence dyes for staining bacterial cells in microscopical applications, are considered as most suitable in terms of tolerability, toxicity, and cellular uptake.[80-82]

The recorded absorption spectra revealed the optimum wavelengths for photoexcitation of the respective PSs at a range corresponding to green-light (**Figure 14**). Since visible white light illumination was applied for all light-driven biotransformations throughout this project, it cannot be ruled out that the use of pure green light enhances the overall efficiency of the proposed light-driven biotransformations. For CE, an optimum concentration of 100  $\mu\text{M}$  in terms of maximum substrate conversion was determined (**Figure 24**), which correlates to the PS concentration applied in previous studies.[73] Since a further increase of CE up to 320  $\mu\text{M}$  shows no further effect on the overall product formation, it is supposed that either the PS uptake by the cells is hampered at a specific concentration or the supply of CE is saturated, respectively (**Figure 24**). Furthermore, the inhibitory effects of CE on the proposed light-driven whole-cell approach could be precluded. Besides EDTA as an electron donor suggested in previous studies,[73] MES and MOPS buffers were additionally investigated in this work. In the light-driven biotransformation with *E. coli* JM109 cells harboring CDO M232A, a 100 % improved conversion of (*R*)-limonene in the presence of MOPS and EY compared to the reaction with EDTA could be observed (**Figure 15**). Due to these findings, a correlation between the choice of sacrificial electron donor and reaction efficiency was assumed. While the buffer capacity of MES and MOPS enables constant pH-conditions within the reactions, EDTA has the potential to sequester metal ions by forming chelate complexes. Thus it was assumed that the essential non-heme iron of the Rieske oxygenase component might get translocated by that.[83] However, EDTA has the property of destabilizing the outer membrane (OM) of gram-negative bacteria.[84, 85] By chelating divalent cations (e.g.,  $\text{Mg}^{2+}$ ,  $\text{Ca}^{2+}$ ) within the lipopolysaccharide (LPS) structure, the permeability of the OM is increased, which was assumed to benefit an enhanced mass transfer through the bacterial cell membrane.[84, 85]. However, findings obtained in the current study show that either the assumed lack of enzyme functionality caused by a loss of the non-heme iron in the presence of EDTA or the supposed increase of cell permeability does not implicitly affect the overall reaction outcome (**Table 26**). Regarding the mass transfer limitation, these findings correlate with the results of whole-cell biotransformations with (*R*)-limonene by using lyophilized *E. coli* cells. While a maximum product yield of approximately 1.3 mM was obtained by the use of freeze-dried cells ( $100 \text{ g}_{\text{DCW}} \text{ L}^{-1}$ ) precultivated in ZYP-5052 autoinduction-medium, attempts

with cells cultured in TB-medium shows no significant product formation (**Table 21**) in the presence of glucose. It is supposed that salts within the autoinduction medium may function as cryoprotectants contributing to the stability of the cellular structure and proteins during freeze-drying, which would be one explanation for the lack of conversion in TB-medium cultivated cells. However, due to a moisture content of ~82 % in resting *E. coli* cells, the concentration of freeze-dried biocatalysts applied in the described experiment corresponds to approximately  $555 \text{ g}_{\text{WCW}} \text{ L}^{-1}$ . Compared to related biotransformations with TB-cultivated “wet” cells ( $100 \text{ g}_{\text{WCW}} \text{ L}^{-1}$ ) yielding in the formation of 2.8 mM of hydroxylated products (**Figure 17**), lyophilization seems to be unfavorable in terms of improving the light-driven biotransformations. Under optimized reaction conditions, a maximum substrate conversion of 86 % could be observed within 24 h light-driven biotransformations of indene catalyzed by CDO M232A (**Table 26**). Previous studies, exploiting the natural cofactor regeneration of *E. coli*, reported a maximum conversion of indene up to 80 %.[23] Furthermore, the determined product distribution of approximately 98% for 1,2-indanediol (**Table 29**) compared to the literature value of 44 % emphasizes the potential of the proposed light-driven approach in terms of maximum conversion and regioselectivity.[23] While this comparison highlights the superiority of the proposed light-driven approach over the concept of conventional whole-cell strategies, an accurate evaluation regarding the efficiency compared to the natural photosynthesis of autotrophs is difficult due to a lack of homologous data. However, a maximum specific activity of  $0.275 \text{ U g}_{\text{WCW}}^{-1}$  (**Table 26**) determined in the photoconversion of indene catalyzed by CDO M232A is comparable to the data obtained for oxyfunctionalization reactions catalyzed by recombinant cyanobacteria.[61] For light-driven whole-cell biotransformations of indene, an unexpected variation of the diastereomeric product ratios was observed (**Table 29**). Since the hydroxylation is catalyzed by an enzyme, the described variation of selectivity is rather unusual.[23] This behavior gives a hint that the conversion of indene to its hydroxylated products at certain conditions is not fully enzyme-driven. Control reactions without biocatalysts under light exposure revealed the occurrence of an undesired photochemical background reaction yielding in a maximum of 4.8 mM of product. (**Figure 22**). It is assumed that the occurrence of this photochemical background reaction is the result of the spontaneous oxidation of indene with ROSs formed during

incubation at 30 °C in the presence of O<sub>2</sub>. [86] However, further investigation is necessary to minimize uncertainty regarding predictable and selective photoconversion of indene. Since the electron transfer system required for the proposed artificial photosynthesis underlies an interaction between heterogeneous sacrificial electron donors and PSs providing reducing equivalents for ROs, it is suggested that the functionality is better sustained by an intact cell envelope rather than the complete vitality of the host organism. This assumption correlates with the findings obtained from growth experiments in the presence of indene. Although relatively high conversions could be determined in light-driven biotransformations with 10 mM substrate, a complete absence of cell growth due to toxicity effects (**Figure 25**) at indene concentrations exceeding 2 mM is detectable. Since the photosynthesis of autotrophs is dependent on the functionality of several intrinsic membrane proteins, [26] the current light-driven system is considered more robust concerning applications of toxic substrates. Regarding the selective hydroxylation of (*R*)-limonene, Gally *et al.* reported an almost full conversion in whole-cell biotransformations catalyzed by CDO M232A in the presence of glucose. [23] Remarkably, corresponding reactions conducted in this work yielded only in a maximum conversion of approximately 28 % (**Figure 17**). One explanation for this deviation could be the different amount of biocatalyst. While a concentration of 200 g<sub>WCW</sub> L<sup>-1</sup> of resting *E. coli* cells was applied in the previous work by Gally *et al.* [16], the half amount of biocatalyst was evaluated as most promising in the current project (**Figure 17** and **Figure 18**). It is likely that the difference in conversions can be attributed to variations in incubation times. Gally and coworkers proposed cell harvesting after two hours of incubation at 30 °C. [23] As described in the method section, cultivation was performed for 19 hours in the course of this work. Due to that, a loss of active CDO M232A during extended incubation periods can be assumed. However, for the expression of the NDO H295A variant, Halder *et al.* proposed an incubation time of 20 hours after induction. Thereby, a conversion of 77 % could be observed during biotransformations with toluene yielding benzyl alcohol. [19] Unexpectedly, control experiments conducted in the current thesis show a conversion of toluene of only 6 % catalyzed by NDO H295A and glucose supplementation. Unlike the protocol for biotransformation preparation proposed by Halder and coworkers, a temperature of 30 °C instead of 25 °C was used for enzyme expression throughout this project. Since no further

deviation to the previous work could be identified, an increased temperature during expression seems to have a negative effect on the activity of NDO H295A. In the course of whole-cell biotransformations of (*R*)-limonene and indene, undesired byproduct formation could be observed. It is proposed by previous literature that CDO M232A favors the conversion of (*R*)-limonene into its hydroxylated product (1*R*,5*S*)-carveol yielding in an almost full conversion (> 99 %).[23] In this project, the formation of (1*S*,5*S*)-carveol, (1*S*,5*R*)-carveol, (1*R*,5*R*)-carveol, and carvone could be observed in whole-cell biotransformations with CDO M232A under both light conditions and dark conditions with glucose supplementation (**Table 22**). Reactions performed with an empty vector control revealed that a background reaction catalyzed by either *E. coli* JM109 cells or the combination of light, electron donor, and PS contributes primarily to the byproduct formation. Thus, 98 % of the conversion of (*R*)-limonene can be considered to be catalyzed by CDO M232A during the light-driven biotransformations (**Table 23**). Based on previous studies, the formation of 1-indenol and indanediol can be expected by the RO-catalyzed conversion of indene.[23] The herein performed experiments show an undesired byproduct formation of quinoline and 1-indanone. The accumulation of both compounds can be observed in all light-driven biotransformations carried out in this work. However, while no byproduct formation could be detected in reactions without cells (**Figure 22**), an empty-vector control with CE and MES revealed the formation of 4.4 mM quinoline and 0.12 mM 1-indanone, respectively (**Table 26**). Remarkably, no corresponding formation of byproducts with pUC19 could be observed under dark conditions with glucose supplementation. Based on these findings, it can be assumed that the formation of quinoline is caused by *E. coli* JM109 cells stressed due to light exposure. Unfortunately, a literature search led to no proper explanation for this finding. To confirm the assumption that the desired reaction system is exclusively dependent on the presence of electron donor and PSs and also strictly light-driven, control experiments were performed. While reactions without light exposure yielded in a background conversion up to 1.5 mM, corresponding reactions in light shows a significant increase of product formation from 1.5 mM without PS up to 8.5 mM in combination with CE and MOPS (**Figure 30**). It is suggested that the background formation of the hydroxylated products is due to NAD(P)H cofactor regeneration due to residual carbon sources within the cells accumulated during

cultivation. However, the exact process behind the light-mediated electron transfer between the sacrificial electron donor and the multi-component system of the ROs is not fully understood yet. While Park and coworkers reported a reductase and cofactor-independent approach by establishing an electron transfer from TEOA via a light-excited PS directly to the prosthetic heme domain of a P450 monooxygenase,[70] no corresponding data is yet available for the herein proposed light-driven system. By the design and investigation of fusion proteins in biotransformation experiments, it was expected to gain more profound knowledge about the interaction between the electron donor, PS, and the electron transfer chain of ROs. Furthermore, fusion proteins potentially lead to an overall simplification of the Rieske multi-component system, which is favorable for the implementation in industrial applications. In this work, the construction of a His-CumA4-CumA1 fusion protein was planned in order to evaluate a possible direct electron transfer between the catalytic  $\alpha$ -subunit of the oxygenase and the reductase independent of the presence of Fd or the  $\beta$ -subunit. It was proposed to link CumA4 and CumA1 covalently without a linker sequence. For this, Gibson assembly™ was chosen as a cloning method to construct the fusion gene in a pMS470 vector backbone. However, no His-CumA4-CumA1 construct could be generated in the timeframe of this work due to a problem with either the applied Gibson master mix or low transformation efficiency of the competent *E. coli* host cells.

#### 4.2 Heterologous expression of CDO M232A and NDO H295A in *E. coli*

Although the activity of CDO M232A and NDO H295A could be confirmed by either *in vivo* biotransformation experiments or the indole assay, protein separation via SDS-PAGE revealed unequal expression of the required genes. While CumA1 and CumA2 of CDO M232A were detectable in the soluble and insoluble fractions (**Figure 11**), no detectable expression of the reductase (CumA4) or Fd (CumA3) could be seen on the SDS-PAGE gel. A similar behavior could be observed in expression studies with *E. coli* harboring NDO H295A. While low amounts of the reductase and the  $\beta$ -subunit components could be observed in the soluble fraction, Fd and the  $\alpha$ -subunit could not be determined. The issue of low or undetectable expression levels of RO genes correlates with the findings of previous studies.[16, 73] It is assumed that the expression of multiple genes under the control of a single promoter is



unfavorable regarding the formation of proteins located downstream of the transcription initiation site. [87] Thus, the overexpression of CumA1 and CumA2 of CDO can be explained since both genes are located next to the lac promoter sequence (**Figure 4**). While the CumA4 in the CDO gene cluster is remotest from the transcription site, the reductase of NDO is adjacent to the T7-promoter sequence (**Figure 5**). This correlates with the findings obtained by the performed expression studies in which no formation of CumA4 could be detected. Furthermore, a similar effect can be observed regarding the heterologous expression of the small subunits of NDO, which results in lower expression levels compared to CDO. While the large subunit of CDO can be detected in the soluble as well as in the insoluble fractions, the corresponding  $\alpha$ -subunit of the NDO was not identified on the SDS-PAGE gel. It is suggested that the use of a bidirectional promoter or gene cluster separation into two plasmids (coexpression) may improve heterologous expression.[88, 89] As indicated in previous literature, the heterologous formation of Fd in *E. coli* is commonly insufficient, which coincides with the findings obtained in the course of conducted expression studies.[90] Huang and coworkers reported the successful overexpression of clostridial and agrobacterial Fds in *E. coli* C41 (DE3) in the presence of additional iron-sulfur sources in the culture medium and coexpression of an auxiliary plasmid facilitating the proper folding of the protein.[90] Regarding the NDO H295A, basal expression of the reductase and the  $\beta$ -subunit was observed one hour before induction (**Figure 11**). Due to a lack of a *lacI* gene in the T7-promoter region, this uninduced production of the corresponding heterologous proteins could be expected. For the purpose of controlled heterologous expression and comparison with the CDO construct, subcloning of NDO into a pUC19 vector backbone under the control of a lac promoter is considered.

## 5 Conclusion

To conclude, a recently designed light-driven whole-cell approach based on the concept of artificial photosynthesis, which is proposed to circumvent the need for NAD(P)H as a cofactor for the well-studied Rieske non-heme iron oxygenases (ROs) was investigated in detail. As model enzymes the cumene dioxygenase (CDO) from *Pseudomonas fluorescens* IP01 and the

naphthalene dioxygenase (NDO) from *Pseudomonas* sp. NCIB 9816-4 have been chosen. It was assumed that by exploiting the photoexcitability of photosensitizers (PS), a light-mediated electron transfer from a sacrificial electron donor towards the multicomponent RO system within heterotrophic *E. coli* cells could be established driving the hydroxylation of the desired product. Referring to previous studies,[70, 73] the feasibility of the corresponding light-driven whole-cell approach depends on the compatibility of the reaction components required for the artificial electron transfer with the enzyme of choice. Based on the findings obtained in a proof-of-concept study reported by Wied et al. [73], this thesis aimed at a deeper characterization and optimization of the proposed system by extending the scope of electron donors and PSs for the hydroxylation of indene, (*R*)-limonene and toluene. While EDTA, MES, and MOPS were suggested as promising electron donors, CE, EY, RB, and SO were considered as potential PSs. *In vivo* biotransformation studies with resting *E. coli* JM109 cells harboring the corresponding ROs carried out in a newly designed fluorescent lamp reactor revealed the feasibility of all considered reaction systems to a variable extent. Thereby, an overall maximum conversion of 86 % could be determined for indene with CE and MOPS by the use of engineered CDO M232A after 24 h. Referring to previous findings, light-driven biotransformations with (*R*)-limonene yielded in a maximum conversion of approximately 340  $\mu$ M with CDO M232A by the use of CE and MES indicating an enhanced efficiency compared to findings revealed by Wied et al.[73] Thus, the defined goal to optimize the overall light-driven approach by varying reaction components could be confirmed. However, a photochemical background reaction could be observed in light-driven biotransformations with indene yielding in a maximum of 4.8 mM of product formation, depending on the applied light intensity. However, insufficient expression of the RO components could be observed via SDS-PAGE. Especially the heterologous production of Fd from both CDO M232A and NDO H295A could not be confirmed on an SDS-PAGE gel. However, it is assumed that an enhanced expression of Fd will contribute to an increase in product formation. The obtained results further emphasize the applicability of artificial photosynthesis for ROs by the use of sacrificial electron donors and nontoxic PSs. Due to that, a sustainable strategy to convert light energy into chemical energy within heterotrophic organisms could be established. Compared to autotrophic model organisms such as cyanobacteria, the use of *E. coli* as a host

organism is favorable due to simple cultivation and the availability of sophisticated gene engineering tools. Furthermore, experiments performed in this work revealed the feasibility of the proposed light-driven approach at high cell densities ( $\leq 300 \text{ g}_{\text{WCW}} \text{ L}^{-1}$ ), which is beneficial for upscaling at industrial scale. Since the productivity of the current light-driven system in *E. coli* is comparable to the catalytic activity of recombinant cyanobacteria, the current approach represents a promising and sustainable approach in the field of photocatalysis. Future research on the detailed characterization of the underlying electron transfer processes and the further simplification of the light-driven whole-cell approach by the construction of fusion proteins is considered. Also, the co-expression of specific chaperones facilitating the formation of the Fd protein is proposed. Furthermore, subcloning of the RO gene cluster into two distinct vectors is supposed to enhance expression levels favorable for future studies.

## 6 References

1. Sheldon, R.A. and D. Brady, *Broadening the Scope of Biocatalysis in Sustainable Organic Synthesis*. ChemSusChem, 2019. **12**(13): p. 2859-2881.
2. Choi, J.-M., S.-S. Han, and H.-S. Kim, *Industrial applications of enzyme biocatalysis: Current status and future aspects*. Biotechnol. Adv., 2015. **33**(7): p. 1443-1454.
3. Bornscheuer, U.T., *Biocatalysis: Successfully Crossing Boundaries*. Angew. Chem., Int. Ed. Engl., 2016. **55**(14): p. 4372-4373.
4. Porter, J.L., R.A. Rusli, and D.L. Ollis, *Directed Evolution of Enzymes for Industrial Biocatalysis*. ChemBioChem, 2016. **17**(3): p. 197-203.
5. Hughes, G. and J.C. Lewis, *Introduction: Biocatalysis in Industry*. Chem. Rev., 2018. **118**(1): p. 1-3.
6. Wandrey, C., A. Liese, and D. Kihumbu, *Industrial Biocatalysis: Past, Present, and Future*. Org. Process Res. Dev., 2000. **4**(4): p. 286-290.
7. D. Woodyer, R., T. Johannes, and H. Zhao, *Regeneration of Cofactors for Enzyme Biocatalysis in Enzyme Technology*, in *Enzyme Technology*. 2006. p. 83-101.
8. May, S.W., *Applications of oxidoreductases*. Curr. Opin. Biotechnol., 1999. **10**(4): p. 370-375.
9. Wang, X., et al., *Cofactor NAD(P)H Regeneration Inspired by Heterogeneous Pathways*. Chem, 2017. **2**(5): p. 621-654.
10. Singh, R., et al., *Microbial enzymes: industrial progress in 21st century*. 3 Biotech, 2016. **6**(2): p. 174.
11. Dong, J., et al., *Biocatalytic Oxidation Reactions: A Chemist's Perspective*. Angew. Chem., Int. Ed. Engl., 2018. **57**(30): p. 9238-9261.
12. Davies, H.M.L. and D. Morton, *Collective Approach to Advancing C-H Functionalization*. ACS Cent. Sci., 2017. **3**(9): p. 936-943.
13. Meunier, B., S.P. de Visser, and S. Shaik, *Mechanism of oxidation reactions catalyzed by cytochrome p450 enzymes*. Chem. Rev., 2004. **104**(9): p. 3947-3980.
14. Manikandan, P. and S. Nagini, *Cytochrome P450 Structure, Function and Clinical Significance: A Review*. Curr. Drug Targets, 2018. **19**(1): p. 38-54.

15. Aoki, H., et al., *Cloning, nucleotide sequence, and characterization of the genes encoding enzymes involved in the degradation of cumene to 2-hydroxy-6-oxo-7-methylocta-2,4-dienoic acid in Pseudomonas fluorescens IP01*. Journal of Fermentation and Bioengineering, 1996. **81**(3): p. 187-196.
16. Gally, C., *Enzymatic asymmetric dihydroxylation of alkenes*. Doctoral thesis, 2016, University of Stuttgart: Faculty of Chemistry.
17. Barry, S.M. and G.L. Challis, *Mechanism and Catalytic Diversity of Rieske Non-Heme Iron-Dependent Oxygenases*. ACS Catal., 2013. **3**(10): p. 2362-2370.
18. Ferraro, D.J., L. Gakhar, and S. Ramaswamy, *Rieske business: structure-function of Rieske non-heme oxygenases*. Biochem Biophys Res Commun, 2005. **338**(1): p. 175-90.
19. Halder, J.M., B.M. Nestl, and B. Hauer, *Semirational Engineering of the Naphthalene Dioxygenase from Pseudomonas sp. NCIB 9816-4 towards Selective Asymmetric Dihydroxylation*. ChemCatChem, 2018. **10**(1): p. 178-182.
20. Lee, S.H., et al., *Cofactor-Free, Direct Photoactivation of Enoate Reductases for the Asymmetric Reduction of C=C Bonds*. Angew Chem Int Ed Engl, 2017. **56**(30): p. 8681-8685.
21. Dong, X., et al., *Crystal structure of the terminal oxygenase component of cumene dioxygenase from Pseudomonas fluorescens IP01*. J. Bacteriol., 2005. **187**(7): p. 2483-2490.
22. Kauppi, B., et al., *Structure of an aromatic-ring-hydroxylating dioxygenase – naphthalene 1,2-dioxygenase*. Structure, 1998. **6**(5): p. 571-586.
23. Gally, C., B.M. Nestl, and B. Hauer, *Engineering Rieske Non-Heme Iron Oxygenases for the Asymmetric Dihydroxylation of Alkenes*. Angew. Chem., Int. Ed. Engl., 2015. **54**(44): p. 12952-6.
24. Pollak, N., C. Dolle, and M. Ziegler, *The power to reduce: pyridine nucleotides--small molecules with a multitude of functions*. Biochem. J., 2007. **402**(2): p. 205-18.
25. Madigan, M.T., et al., *Brock Mikrobiologie*. 2009: Pearson Studium.
26. Voet, D., et al., *Lehrbuch der Biochemie*. 2010: VCH [Imprint].
27. Chance, B. and G. Williams, *The respiratory chain and oxidative phosphorylation*. Adv. Enzymol. Relat. Areas Mol. Biol., 1956. **17**: p. 65-134.

28. Alam, K.Y. and D.P. Clark, *Anaerobic fermentation balance of Escherichia coli as observed by in vivo nuclear magnetic resonance spectroscopy*. J. Bacteriol., 1989. **171**(11): p. 6213-6217.
29. Xiao, W., et al., *NAD(H) and NADP(H) Redox Couples and Cellular Energy Metabolism*. Antioxid. Redox Signaling, 2018. **28**(3): p. 251-272.
30. Liberton, M., et al., *Organization and flexibility of cyanobacterial thylakoid membranes examined by neutron scattering*. J. Biol. Chem. , 2013. **288**(5): p. 3632-40.
31. Maxwell, K. and G.N. Johnson, *Chlorophyll fluorescence—a practical guide*. J. Exp. Bot., 2000. **51**(345): p. 659-668.
32. McEvoy, J.P. and G.W. Brudvig, *Water-splitting chemistry of photosystem II*. Chem. Rev., 2006. **106**(11): p. 4455-83.
33. Yamori, W. and T. Shikanai, *Physiological Functions of Cyclic Electron Transport Around Photosystem I in Sustaining Photosynthesis and Plant Growth*. Annu. Rev. Plant Biol., 2016. **67**: p. 81-106.
34. Barber, J., *Photosynthetic energy conversion: natural and artificial*. Chem. Soc. Rev., 2009. **38**(1): p. 185-96.
35. Cox, N., et al., *Biological water oxidation*. Acc. Chem. Res., 2013. **46**(7): p. 1588-96.
36. Nagao, R., et al., *Genetically introduced hydrogen bond interactions reveal an asymmetric charge distribution on the radical cation of the special-pair chlorophyll P680*. J. Biol. Chem. , 2017. **292**(18): p. 7474-7486.
37. Fukuyama, K., *Structure and Function of Plant-Type Ferredoxins*. Photosynth. Res., 2004. **81**(3): p. 289-301.
38. Bruschi, M. and F. Guerlesquin, *Structure, function and evolution of bacterial ferredoxins*. FEMS Microbiol. Rev., 1988. **4**(2): p. 155-175.
39. van der Donk, W.A. and H. Zhao, *Recent developments in pyridine nucleotide regeneration*. Curr. Opin. Biotechnol., 2003. **14**(4): p. 421-426.
40. Lin, B. and Y. Tao, *Whole-cell biocatalysts by design*. Microb. Cell Fact., 2017. **16**(1): p. 106.
41. Schmermund, L., et al., *Photo-Biocatalysis: Biotransformations in the Presence of Light*. ACS Catal., 2019. **9**(5): p. 4115-4144.
42. Knoot, C.J., et al., *Cyanobacteria: Promising biocatalysts for sustainable chemical production*. J. Biol. Chem. , 2018. **293**(14): p. 5044-5052.

43. Juturu, V. and J.C. Wu, *Heterologous Protein Expression in Pichia pastoris: Latest Research Progress and Applications*. ChemBioChem, 2018. **19**(1): p. 7-21.
44. Zhou, Y., et al., *Construction of engineered Saccharomyces cerevisiae strain to improve that whole-cell biocatalytic production of melibiose from raffinose*. J. Ind. Microbiol. Biotechnol., 2017. **44**(3): p. 489-501.
45. Parshikov, I.A. and J.B. Sutherland, *The use of Aspergillus niger cultures for biotransformation of terpenoids*. Process Biochem., 2014. **49**(12): p. 2086-2100.
46. Yan, N., et al., *The Potential for Microalgae as Bioreactors to Produce Pharmaceuticals*. Int. J. Mol. Sci., 2016. **17**(6).
47. Weckbecker, A., H. Gröger, and W. Hummel, *Regeneration of Nicotinamide Coenzymes: Principles and Applications for the Synthesis of Chiral Compounds*. Adv. Biochem. Eng./Biotechnol., 2010. **120**: p. 195-242.
48. Fassouane, A., et al., *Electrochemical regeneration of NAD in a plug-flow reactor*. Biotechnol. Bioeng., 1990. **35**(9): p. 935-939.
49. Wienkamp, R. and E. Steckhan, *Indirect Electrochemical Regeneration of NADH by a Bipyridinerhodium(I) Complex as Electron-Transfer Agent*. Angew. Chem., Int. Ed. Engl., 1982. **21**(10): p. 782-783.
50. Zhang, W. and F. Hollmann, *Nonconventional regeneration of redox enzymes – a practical approach for organic synthesis?* Chem. Commun., 2018. **54**(53): p. 7281-7289.
51. Taglieber, A., et al., *Light-Driven Biocatalytic Oxidation and Reduction Reactions: Scope and Limitations*. ChemBioChem, 2008. **9**(4): p. 565-572.
52. Grau, M.M., et al., *Photoenzymatic Reduction of C=C Double Bonds*. Adv. Synth. Catal., 2009. **351**(18): p. 3279-3286.
53. Ikeno, T., T. Nagano, and K. Hanaoka, *Silicon-substituted Xanthene Dyes and Their Unique Photophysical Properties for Fluorescent Probes*. Chem. Asian J., 2017. **12**(13): p. 1435-1446.
54. Hollmann, F., et al., *A Light-Driven Stereoselective Biocatalytic Oxidation*. Angew. Chem., Int. Ed. Engl., 2007. **46**(16): p. 2903-2906.
55. Mifsud, M., et al., *Photobiocatalytic chemistry of oxidoreductases using water as the electron donor*. Nat. Commun., 2014. **5**(1): p. 3145.

56. Hollmann, F., I.W.C.E. Arends, and K. Buehler, *Biocatalytic Redox Reactions for Organic Synthesis: Nonconventional Regeneration Methods*. ChemCatChem, 2010. **2**(7): p. 762-782.
57. Lee, S.H., et al., *Photobiocatalysis: Activating Redox Enzymes by Direct or Indirect Transfer of Photoinduced Electrons*. Angew. Chem., Int. Ed. Engl., 2018. **57**(27): p. 7958-7985.
58. Honda, Y., et al., *Application to Photocatalytic H<sub>2</sub> Production of a Whole-Cell Reaction by Recombinant Escherichia coli Cells Expressing [FeFe]-Hydrogenase and Maturases Genes*. Angew. Chem., Int. Ed. Engl., 2016. **55**(28): p. 8045-8048.
59. Königer, K., et al., *Recombinant Cyanobacteria for the Asymmetric Reduction of C=C Bonds Fueled by the Biocatalytic Oxidation of Water*. Angew. Chem., Int. Ed. Engl., 2016. **55**(18): p. 5582-5585.
60. Hoschek, A., et al., *Light-Dependent and Aeration-Independent Gram-Scale Hydroxylation of Cyclohexane to Cyclohexanol by CYP450 Harboring Synechocystis sp. PCC 6803*. Biotechnol. J., 2019. **14**(8): p. 1-10.
61. Hoschek, A., B. Buhler, and A. Schmid, *Overcoming the Gas-Liquid Mass Transfer of Oxygen by Coupling Photosynthetic Water Oxidation with Biocatalytic Oxyfunctionalization*. Angew. Chem., Int. Ed. Engl., 2017. **56**(47): p. 15146-15149.
62. Heidorn, T., et al., *Synthetic biology in cyanobacteria engineering and analyzing novel functions*, in *Methods in Enzymology*. 2011. p. 539-79.
63. Mazard, S., et al., *Tiny Microbes with a Big Impact: The Role of Cyanobacteria and Their Metabolites in Shaping Our Future*. Mar. Drugs, 2016. **14**(5): p. 97.
64. Sørensen, H.P. and K.K. Mortensen, *Advanced genetic strategies for recombinant protein expression in Escherichia coli*. J. Biotechnol., 2005. **115**(2): p. 113-128.
65. Hoschek, A., B. Buhler, and A. Schmid, *Stabilization and scale-up of photosynthesis-driven omega-hydroxylation of nonanoic acid methyl ester by two-liquid phase whole-cell biocatalysis*. Biotechnol. Bioeng., 2019. **116**(8): p. 1887-1900.
66. Liu, D. and H.B. Pakrasi, *Exploring native genetic elements as plug-in tools for synthetic biology in the cyanobacterium Synechocystis sp. PCC 6803*. Microb. Cell Fact., 2018. **17**(1): p. 48.
67. Jahn, M., et al., *Growth of Cyanobacteria Is Constrained by the Abundance of Light and Carbon Assimilation Proteins*. Cell Rep., 2018. **25**(2): p. 478-486.



68. Rowe, S.F., et al., *Light-Driven H<sub>2</sub>-Evolution and C=C or C=O Bond Hydrogenation by *Shewanella oneidensis*: A Versatile Strategy for Photocatalysis by Nonphotosynthetic Microorganisms*. ACS Catal., 2017. **7**: p. 7558-7566.
69. Blankenship, R.E., et al., *Comparing Photosynthetic and Photovoltaic Efficiencies and Recognizing the Potential for Improvement*. Science, 2011. **332**(6031): p. 805-809.
70. Park, J.H., et al., *Cofactor-free light-driven whole-cell cytochrome P450 catalysis*. Angew. Chem., Int. Ed. Engl., 2015. **54**(3): p. 969-73.
71. Carr, R.J., R.F. Bilton, and T. Atkinson, *Toxicity of paraquat to microorganisms*. Appl. Environ. Microbiol., 1986. **52**(5): p. 1112-1116.
72. Munro, A.W., et al., *P450 BM3: the very model of a modern flavocytochrome*. Trends Biochem. Sci., 2002. **27**(5): p. 250-257.
73. Wied, P., *Engineering Rieske Non-Heme Oxygenases for Improved Electron Transfer in Light-driven Biocatalysis*. Master thesis, 2018, Graz University of Technology Institute for Molecular Biotechnology.
74. Anastas, P.T. and J.C. Warner, *Green Chemistry: Theory and Practice*. 1998: Oxford University Press.
75. Lanfranchi, E., et al., *Exploring the Selective Demethylation of Aryl Methyl Ethers with a *Pseudomonas* Rieske Monooxygenase*. ChemBioChem, 2019. **20**(1): p. 118-125.
76. Tosstorff, A., et al., *Towards electroenzymatic processes involving old yellow enzymes and mediated cofactor regeneration*. Eng. Life Sci., 2017. **17**(1): p. 71-76.
77. Stuermer, R., et al., *Asymmetric bioreduction of activated C=C bonds using enoate reductases from the old yellow enzyme family*. Curr. Opin. Chem. Biol., 2007. **11**(2): p. 203-213.
78. Qiang, H., Y. Zarmi, and A. Richmond, *Combined effects of light intensity, light-path and culture density on output rate of *Spirulina platensis* (Cyanobacteria)*. Eur. J. Phycol., 1998. **33**(2): p. 165-171.
79. Crater, J.S. and J.C. Lievens, *Scale-up of industrial microbial processes*. FEMS Microbiol. Lett., 2018. **365**(13).
80. Melnick, J.L. and C. Wallis, *Staining and analysis of bacteria*, U.S. Patent, Editor. 1980.
81. Poullos, I., et al., *Photooxidation of eosin Y in the presence of semiconducting oxides*. Appl. Catal., B, 2003. **41**(4): p. 345-355.

82. Feenstra, R.P.G. and S.C.G. Tseng, *Comparison of Fluorescein and Rose Bengal Staining*. Am. J. Ophthalmol., 1992. **99**(4): p. 605-617.
83. Flora, S.J.S. and V. Pachauri, *Chelation in metal intoxication*. Int. J. Environ. Res. Public Health, 2010. **7**(7): p. 2745-2788.
84. Clifton, L.A., et al., *Effect of divalent cation removal on the structure of gram-negative bacterial outer membrane models*. Langmuir, 2015. **31**(1): p. 404-412.
85. Vaara, M., *Agents that increase the permeability of the outer membrane*. Microbiol. Rev., 1992. **56**(3): p. 395-411.
86. Russell, G.A., *Oxidation of Unsaturated Compunds. III. Products of the Reaction of Indene and Oxygen; Stereochemistry of the Addition of a Peroxy Radical and Oxygen to a Double Bond*. J. Am. Chem. Soc., 1956. **78**(5): p. 1035-1040.
87. Kim, K.-J., et al., *Two-promoter vector is highly efficient for overproduction of protein complexes*. Protein Sci., 2004. **13**(6): p. 1698-1703.
88. Wei, W., et al., *Functional consequences of bidirectional promoters*. Trends Genet., 2011. **27**(7): p. 267-276.
89. H Tolia, N. and L. Joshua-Tor, *Strategies for protein coexpression in Escherichia coli*. Nat. Methods, 2006. **3**: p. 55-64.
90. Huang, H., et al., *Heterologous overproduction of 2[4Fe4S]- and [2Fe2S]-type clostridial ferredoxins and [2Fe2S]-type agrobacterial ferredoxin*. Protein Expression Purif., 2016. **121**: p. 1-8.

## 7 Appendices

### Appendix A

**Table 31 Sequencing Primer for CDOv1**

Primer	DNA sequence in 5'→3'
50_pIP107D_FW_seq	GCCAATCTCCTCGGGACTTTGC
52_pIP107D_FW_seq	GGATCCTTGTGGTATGCATC
54_pIP107D_FW_seq	CTTTAGGGTCCGATTTAGTGC
60_pIP107D_cuma3	ATGACTTTTTCCAAAGTTTGTG
63_pIP107D_cuma1_Rev	GCTAGAAGTAGACCTCTTTGTGC
64_pIP107D_cuma1_FW	CTCCAAGTGGGCTGAGTTC
81_pIP107D_BB_RV	CGAGCTCGAATTCAGTGGC
pDTG141 7_fw	CGCTGGTATCTTTATAGTC

**Table 32: Sequencing Primer for NDO H295A**

Primer	DNA sequence in 5'→3'
AmpEnd_fw	CGACACGGAAATGTTGAATAC
pDTG141 1_fw	GCCGACGAAATTGCACTCAC
pDTG141 2_fw	GCGATGGTTGAAGCGTTG
pDTG141 3_fw	GGTAAGTGAATCTGGTCTGAGC
pDTG141 4_fw	GCAAATGACCTCCAAATACGG
pDTG141 5_fw	CTCCAAGTGGGCTGAGTTC
pDTG141 6_fw	GGTCTGACAGTTACCAATGCTT
pDTG141 7_fw	CGCTGGTATCTTTATAGTC

Appendix B

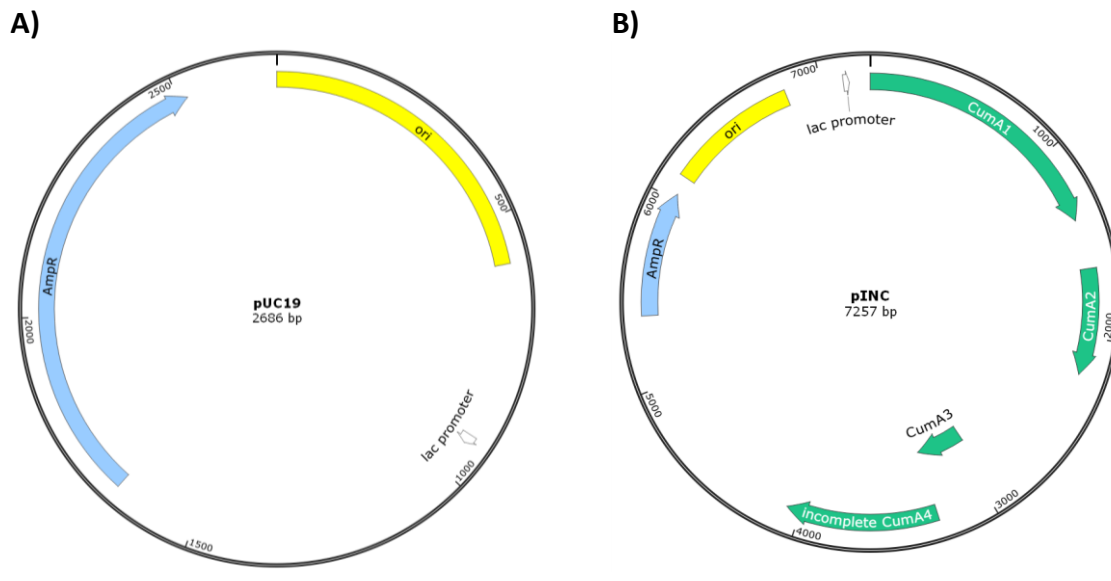


**Figure 32: Vector map of pUC19 (2686 bp) and pINC (7257 bp).** Vector map of puc19 (A): Yellow: Origin of replication (ColE1). Blue: ampicillin resistance gene (AmpR). Vector map of pINC (B): Green: CDO gene cluster; CumA1 (1380 bp), CumA2 (561 bp), CumA3 (330 bp), incomplete CumA4 (803 bp). Yellow: Origin of replication (ColE1). Blue: ampicillin resistance gene (AmpR).

Appendix C

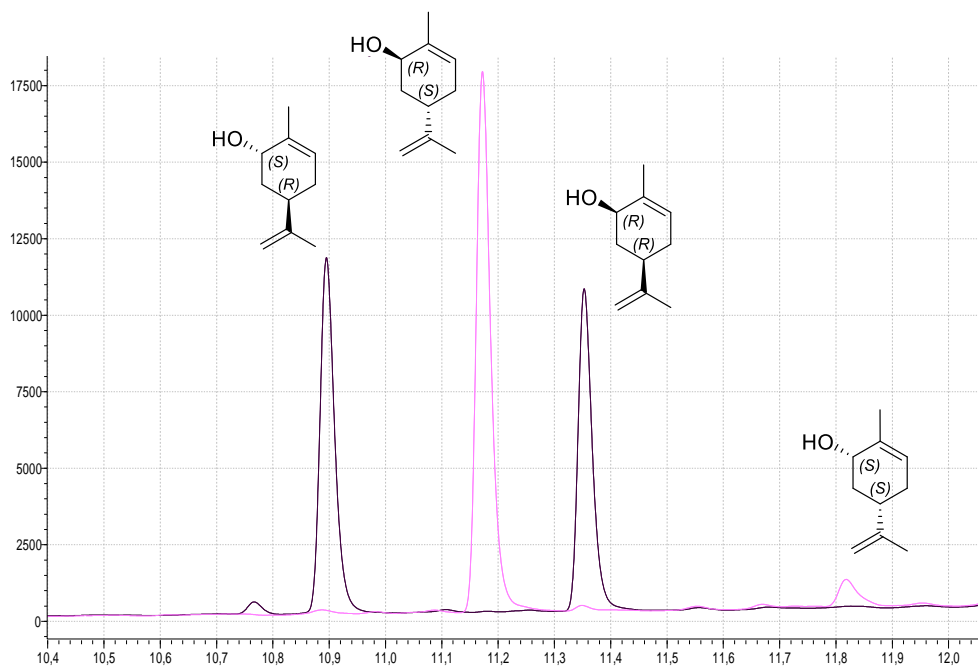


**Figure 33: Chromatogram obtained by GC-FID analysis of carveol enantiomers.** While black peaks represent a commercial racemic (-)-carveol mixture (Sigma-Aldrich), the pink peaks indicate (+)-carveols obtained by biotransformation of indene with CDO M232A. RT: (1*S*,5*R*)-carveol = 10.9 min, (1*R*,5*S*)-carveol = 11.2 min, (1*S*,5*S*)-carveol = 11.3 min, (1*S*,5*S*)-carveol = 11.8 min

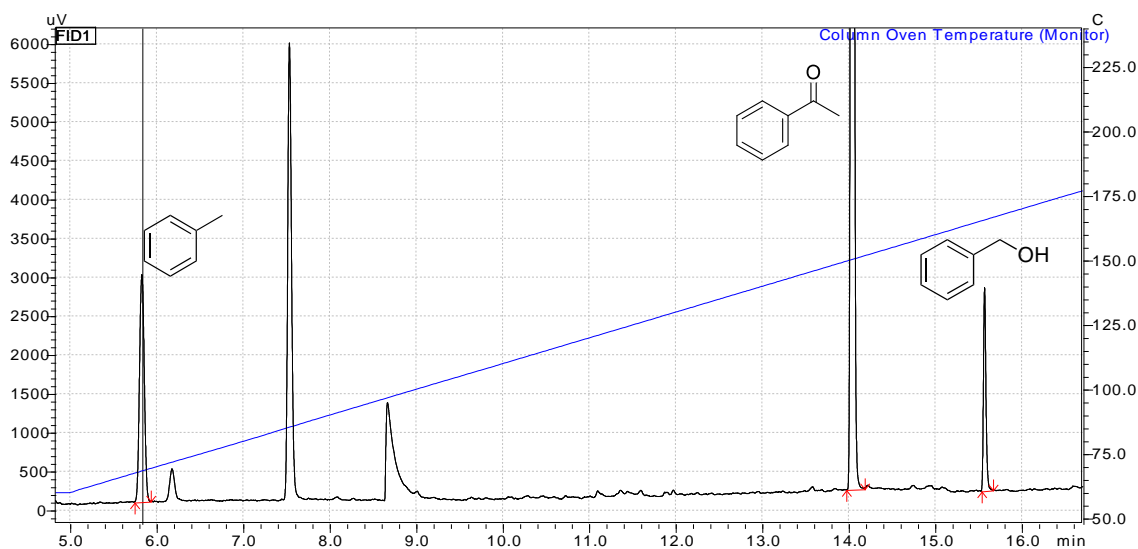


**Figure 34: Chromatogram obtained by GC-FID analysis of toluene and benzyl alcohol after 24 h light-driven-biotransformation with NDO H295A.** RT: toluene = 5.8 min, acetophenone (internal standard) = 14.1 min, benzyl alcohol = 15.6 min.

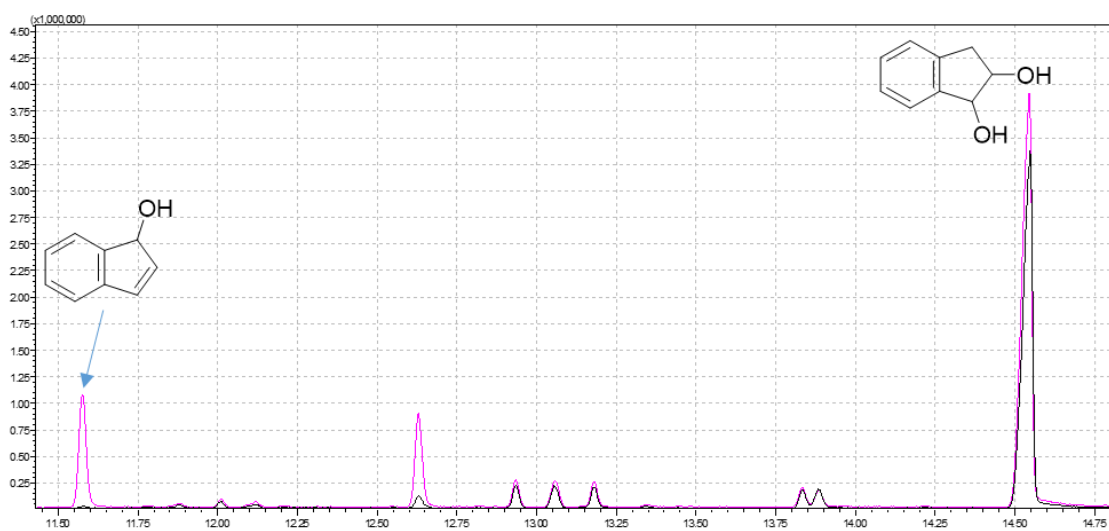


**Figure 35: Chromatogram obtained by GC-MS analysis of indenol and *cis*-1,2-indanediol after biotransformation with NDO variants. Black: products obtained with NDO WT, Pink: product distribution observed in biotransformation with NDO H295A. RT: 1-indenol = 11.6 min, 1-indanone = 12.6 min, *cis*-1,2-indanediol = 14.6 min.**

## Appendix D

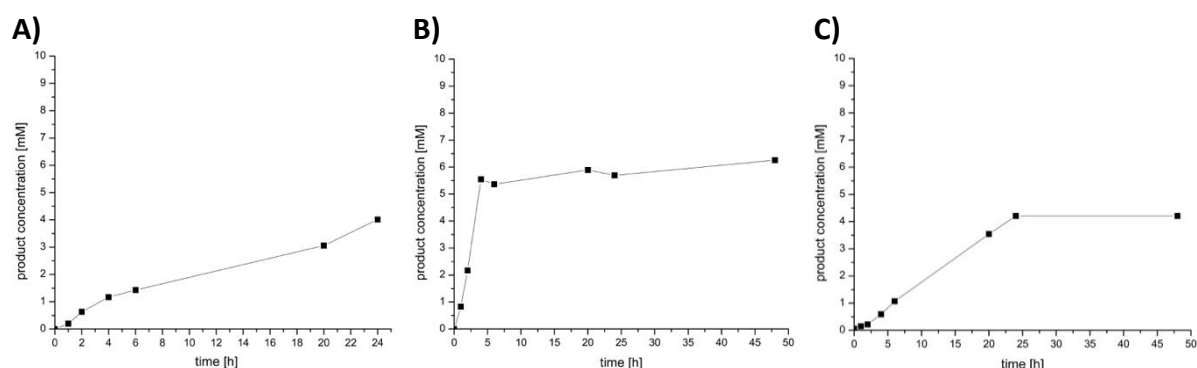


**Figure 36:** Time-courses for product concentration obtained for the light-driven whole-cell hydroxylation reaction employing CDO M232A CE (A), RB (B) and EY (C) in combination with EDTA as electron donor. Reaction conditions: 100  $\mu\text{M}$  photosensitizer, 10 mM 3, 25 mM EDTA, in 100  $\text{g}_{\text{WCW}} \text{L}^{-1}$  whole cells (19h expression), 50 mM SPB pH 7.2, white light (max. 230  $\mu\text{mol m}^{-2} \text{s}^{-1}$ ), 30°C, 140 rpm, 24-48 hours.

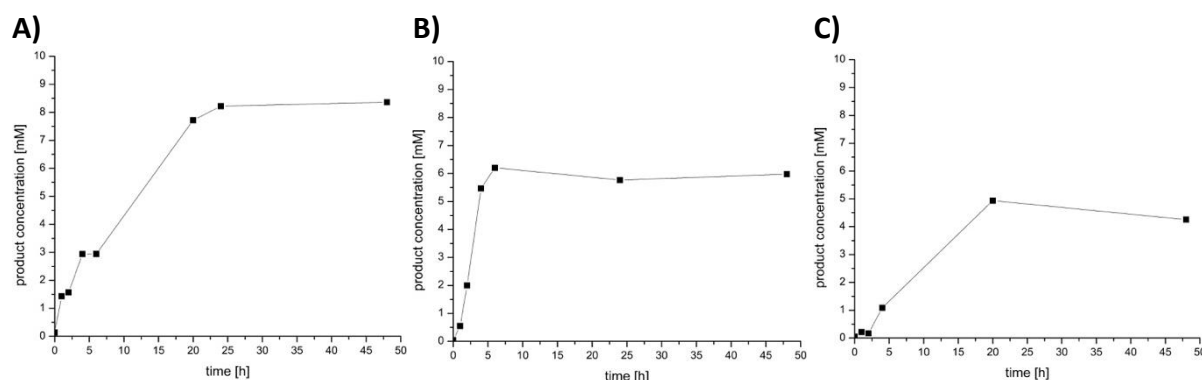


**Figure 37:** Time-courses for product concentration obtained for the light-driven whole-cell hydroxylation reaction employing CDO M232A CE (A), RB (B) and EY (C) in combination with MES as electron donor. Reaction conditions: 100  $\mu\text{M}$  photosensitizer, 10 mM 3, 50 mM MES, in 100  $\text{g}_{\text{WCW}} \text{L}^{-1}$  whole cells (19h expression), 50 mM SPB pH 7.2, white light (max. 230  $\mu\text{mol m}^{-2} \text{s}^{-1}$ ), 30°C, 140 rpm, 48 hours.

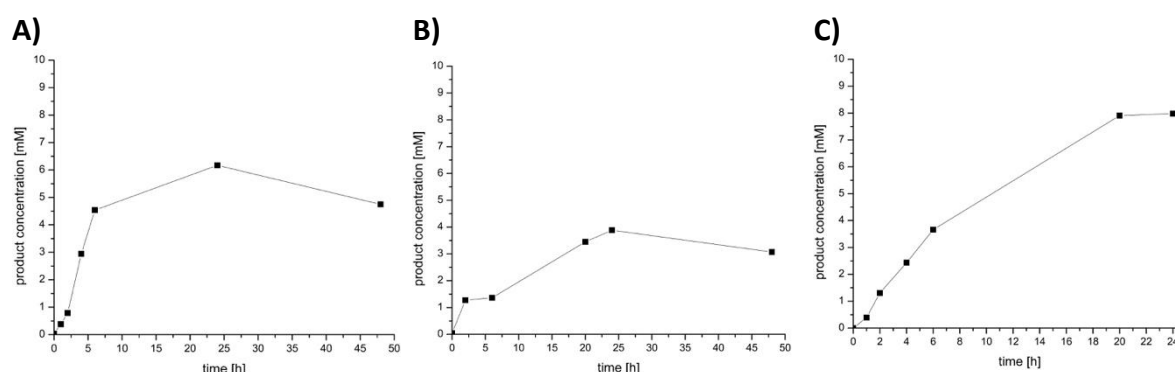


**Figure 38:** Time-courses for product concentration obtained for the light-driven whole-cell hydroxylation reaction employing CDO M232A CE (A), RB (B), and EY (C) in combination with MOPS as an electron donor. Reaction conditions: 100  $\mu\text{M}$  photosensitizer, 10 mM 3, 50 mM MOPS, in  $\text{g}_{\text{WCW}} \text{L}^{-1}$  whole cells (19h expression), 50 mM SPB pH 7.2, white light (max. 230  $\mu\text{mol m}^{-2} \text{s}^{-1}$ ), 30°C, 140 rpm, 24-48 hours.

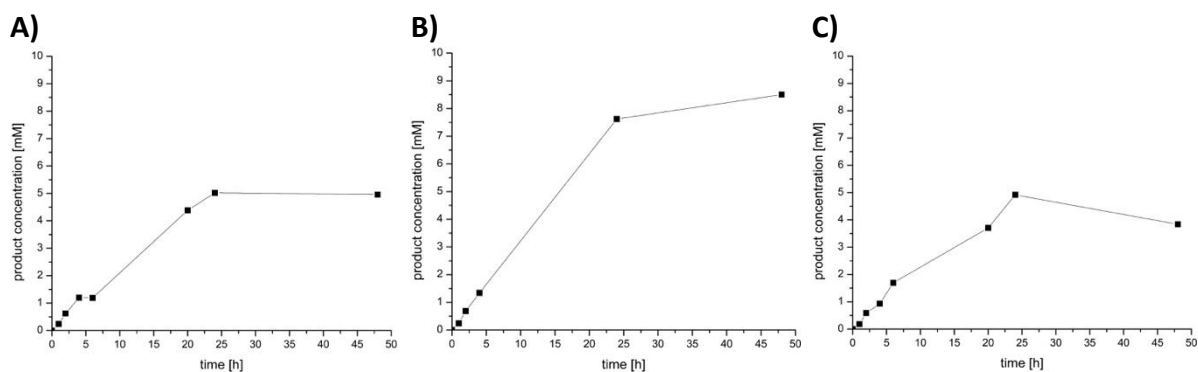


**Figure 39:** Time-courses for product concentration obtained for the light-driven whole-cell hydroxylation reaction employing NDO H295A CE (A), RB (B), and EY (C) in combination with EDTA as an electron donor. Reaction conditions: 100  $\mu\text{M}$  photosensitizer, 10 mM 3, 25 mM EDTA, in 100  $\text{g}_{\text{WCW}} \text{L}^{-1}$  whole cells (19h expression), 50 mM SPB pH 7.2, white light (max.  $230 \mu\text{mol m}^{-2} \text{s}^{-1}$ ),  $30^\circ\text{C}$ , 140 rpm, 48 hours.

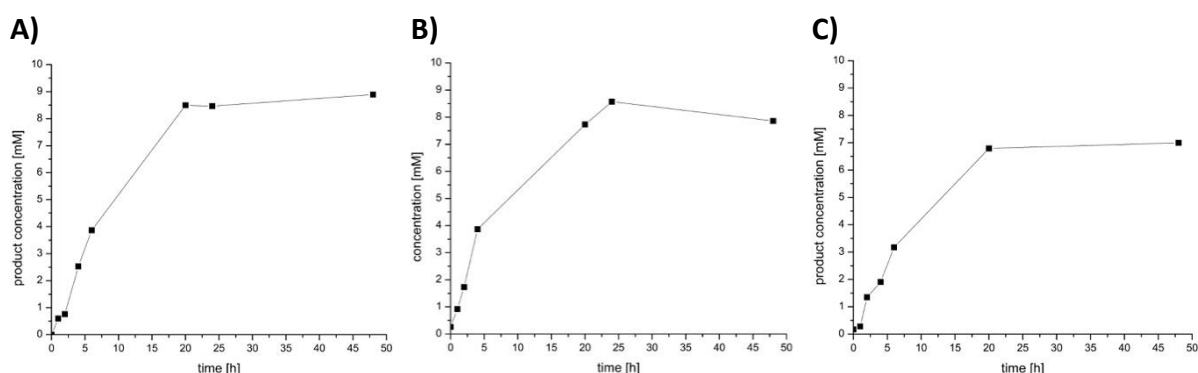


**Figure 40:** Time-courses for product concentration obtained for the light-driven whole-cell hydroxylation reaction employing NDO H295A CE (A), RB (B), and EY (C) in combination with MES as an electron donor. Reaction conditions: 100  $\mu\text{M}$  photosensitizer, 10 mM 3, 50 mM MES, in 100  $\text{g}_{\text{WCW}} \text{L}^{-1}$  whole cells (19h expression), 50 mM SPB pH 7.2, white light (max.  $230 \mu\text{mol m}^{-2} \text{s}^{-1}$ ),  $30^\circ\text{C}$ , 140 rpm, 48 hours

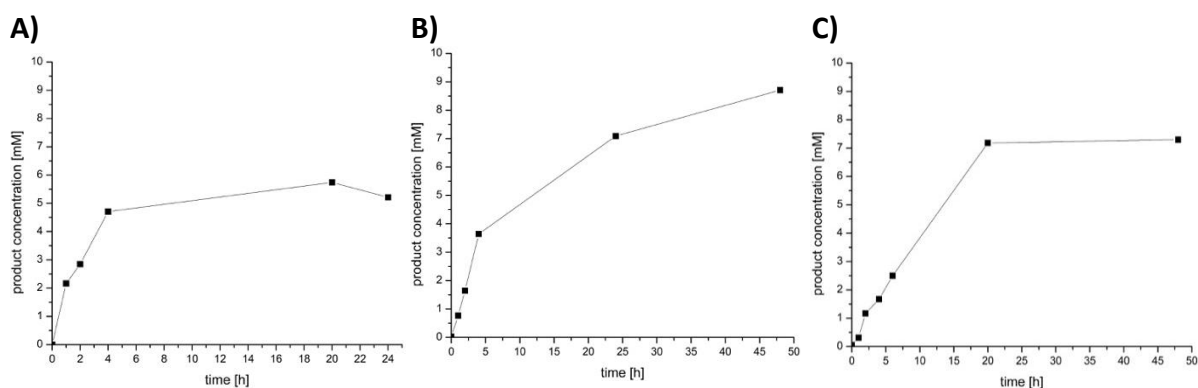


**Figure 41:** Time-courses for product concentration obtained for the light-driven whole-cell hydroxylation reaction employing NDO H295A CE (A), RB (B), and EY (C) in combination with MOPS as an electron donor. Reaction conditions: 100  $\mu\text{M}$  photosensitizer, 10 mM 3, 50 mM MOPS, in 100  $\text{g}_{\text{WCW}} \text{L}^{-1}$  whole cells (19h expression), 50 mM SPB pH 7.2, white light (max.  $230 \mu\text{mol m}^{-2} \text{s}^{-1}$ ),  $30^\circ\text{C}$ , 140 rpm, 24-48 hours.



## Appendix E

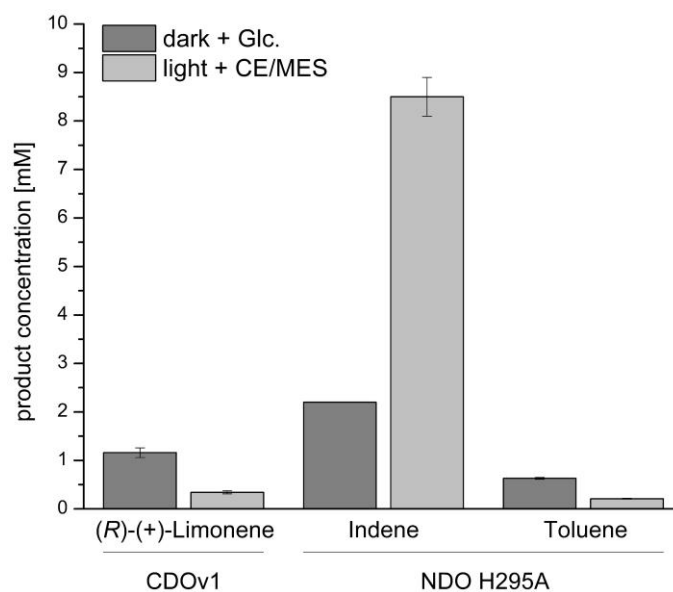


**Figure 42: Whole-cell biotransformations of various substrates catalyzed by CDO M232A or NDO H295A under light and dark conditions.** Summary of product formations determined after whole-cell biotransformations of 10 mM (*R*)-limonene, indene, or toluene as substrates with *E. coli* JM109 ( $100 \text{ g}_{\text{w/cw}} \text{ L}^{-1}$ ) cells, harboring CDO M232A or NDO H295A as biocatalysts. Dark grey bars represent reactions carried out without light exposure and glucose supplementation (20 mM). Light grey bars show experiments carried out in the presence of CE ( $100 \mu\text{M}$ ) and MES (50 mM). Reaction conditions: 30 °C at 120 rpm. Reactions were carried out in duplicates.